

# NEURO MAGNETIC STIMULATION: ENGINEERING ASPECTS

By  
Nafia Al-Mutawaly

A Thesis  
Submitted to the School of Graduate Studies  
in Partial Fulfilment of the Requirements  
for the Degree  
Doctor of Philosophy

McMaster University  
December 2002  
© Copyright by Nafia Al-Mutawaly

## **NEURO MAGNETIC STIMULATION: ENGINEERING ASPECTS**

DOCTOR OF PHILOSOPHY (2002)  
(Electrical and Computer Engineering)

McMaster University  
Hamilton, Ontario

TITLE: Neuro Magnetic Stimulation: Engineering Aspects

AUTHOR: Nafia Al-Mutawaly  
B.Eng.(University of Mosul), M.Eng. (McMaster University)

SUPERVISOR: Dr. H. de Bruin

NUMBER OF PAGES: xxiv, 169

## **Abstract**

Magnetic nerve stimulation has proven to be an effective, non-invasive technique to excite peripheral and central nervous systems. In this technique, the excitement of the neural tissue depends on exposure to a transient magnetic field generated by passing a high pulse of current through a coil. By positioning the coil in a specific orientation over the targeted tissue, the transient magnetic field will induce an electric field in the conductive milieu of the body. If this field reaches a certain threshold within a specific time period, neural depolarization is then evident.

Recently, transcranial magnetic stimulation showed promise as a novel treatment for mood disorder and other psychiatric illnesses. Considering that these sicknesses are currently one of the largest causes of disability (with a cost sometimes exceeding that of diabetes, heart disease, and hypertension) it is evident that pursuing this therapeutic approach is beneficial. However, as magnetic stimulation is relatively new, many limitations and obstacle are to be addressed before this innovative technology is approved for clinical applications.

The main limitations in applying magnetic nerve stimulation are poor field focality and inadequate strength in deep tissues (targeted area). Thus, the excitation of these regions requires very high coil currents to achieve a strong field that is capable of penetrating deep tissues. However, these fields might activate adjacent tissues as well as the targeted area. Further, the high currents will result in coil heating, especially for a high rate of repetition.

Another limitation, especially in transcranial stimulation, is the lack of knowledge of precisely which area of neural tissue is being affected since no immediate behavioral effects are apparent. As well, current literature on the effects of current reversal in the coils and the virtual cathode of the coil suggests conflicting results.

The primary objective of this thesis is the development and testing of new coil designs that can focus the magnetic field more effectively. Two such coils have been built. The first coil has an air core, while the other has a magnetic core. The magnetic fields of these coils, applied to the human upper limb, have been determined theoretically, and the results compared to the field generated by the most common commercial coil, the Figure-8 coil. To design these coils and to test them experimentally, a current pulse generator has been designed and built. Further, a novel measurement system using surface mount inductances and a computer based data acquisition system has been designed and built. The experimental results confirm the theoretical findings, that the air core coil is slightly better than the Figure-8, as far as field strength and focality are concerned. In addition, the experimental results, prove that the coil with the ferromagnetic core, is superior.

The second objective is to investigate the effect of stimulus waveforms theoretically, experimentally, and through *in vivo* study. The goals of the study are to establish a quantitative relationship among various waveforms and to investigate the effect of these waveforms in determining the site of stimulation. Accordingly, a multi subject trial was conducted: a Figure-8 coil was applied to the median nerve of ten subjects at the upper limb. The motor responses of the thenar muscle were then recorded. The study results show that the biphasic stimulating pulse is more effective than the monophasic pulse, as has been concluded by other researchers.

However, the effective stimulating point, or virtual cathode of the coil, was found to be not simply 3 to 4 cm from the coil center as had been reported. In fact, the study shows that the site of the virtual cathode is affected by the current amplitude and the degree of inhomogeneity of the tissues surrounding the nerve. Furthermore, reversing the coil current direction results in a different level of stimulation but does not affect the virtual cathode position.

In summary, the research presented in this thesis covers theoretical concepts, experimental aspects, and human studies related to neuro magnetic stimulation. The results of the experiment and the study are consistent with the theoretical analysis. The proposed coil design is novel and offers promise for a better coil system for magnetic nerve stimulation.

**This Work is Dedicated to My Dear Mother**

## **Acknowledgements**

I would like first to thank the mighty God for blessing me with the guidance to complete this task.

Next, I would like to express my gratitude to my supervisor Dr. Hubert de Bruin for his support throughout the course of this thesis. Many thanks to the other members of my supervisory committee, Dr. Raymond Findlay, Dr. Joseph Dableh, and Dr. Gary Hasey for their helpful discussions and advice throughout this work.

I greatly appreciate the assistance of Mr. Ed Padgett of the biomedical technology department at McMaster university medical centre. I also would like to thank other staff members for their help, Mrs Fennell, Mr. Kewon, Mr. Suchecki, Mr. Boyes, and Mr. Fick.



## Table of Contents

### Chapter 1 Introduction

1.1 History Preview	Page 1
1.2 Clinical Applications of Magnetic Nerve Stimulation	Page 2
1.3 Advantages and Current Limitations of MNS and rTMS	Page 6
1.4 Justification and Scope of this Thesis	Page 9
1.5 Thesis Structure	Page 11

### Chapter 2 Stimulation of Nerve Fibers

2.1 Anatomy of the Nervous System	Page 14
2.2 The Sodium-Potassium Pump	Page 17
2.3 Mechanisms of Neuron Excitation	Page 18
2.4 The Equivalent Circuit of the Myelinated Nerve	Page 19
2.5 The Cable Equation	Page 23
2.6 Roth and Basser Cable Model	Page 24
2.7 General Formulation for estimating the Electric Field during Magnetic Stimulation	Page 27
2.8 Estimation of the Induced Electric Field - Roth's Analysis	Page 28

## **Chapter 3 Design Aspects and Computer Simulations for Magnetic Coils**

<b>3.1 Introduction</b>	<b>Page 33</b>
<b>3.2 Previous Coil Designs</b>	<b>Page 33</b>
<b>3.3 The Proposed Coils</b>	<b>Page 38</b>
<b>3.4 Modeling the Proposed Coils</b>	<b>Page 41</b>
<b>3.5 Estimation of the Induced Electric Field using a Numerical Method</b>	<b>Page 43</b>
<b>3.6 Calculations of the Magnetic Vector Potential <math>\vec{A}</math></b>	<b>Page 45</b>
<b>3.7 Problem Definition and Simulations</b>	<b>Page 46</b>
<b>3.8 Results</b>	<b>Page 51</b>
<b>3.9 The Effects of Pulse Configuration</b>	<b>Page 54</b>
<b>3.1 A Comparison between the Proposed Coils and Other Coils</b>	<b>Page 56</b>

## **Chapter 4 Design and Construction of Magnetic Stimulators and Measuring Apparatus**

<b>4.1 The Design and Construction of a Magnetic Stimulator</b>	<b>Page 60</b>
<b>4.1.1 The Selection of Main Components</b>	<b>Page 60</b>
<b>4.1.2 Construction of an Advanced Stimulator</b>	<b>Page 62</b>
<b>4.1.3 Construction of a Simple Stimulator</b>	<b>Page 68</b>
<b>4.1.4 Critical Issues, Safety Considerations and Future Designs</b>	<b>Page 69</b>
<b>4.2 Measuring the Induced Electrical Fields in 3-Dimensions</b>	<b>Page 71</b>
<b>4.2.1 Previous Studies</b>	<b>Page 71</b>
<b>4.2.2 Design of a Measurement Apparatus</b>	<b>Page 73</b>

<b>4.2.3 Experimental Hardware and Software</b>	Page 75
<b>4.2.4 Evaluating the Testing Apparatus</b>	Page 77
<b>4.2.5 Discussion of the Experimental Results</b>	Page 79

## **Chapter 5 Experimental Results**

<b>5.1 Calculating the Induced electric field</b>	Page 81
<b>5.2 Measuring the Induced electric field</b>	Page 84
<b>5.3 Testing and Evaluating the Stimulating Coils</b>	Page 86
<b>5.4 Experimental Results</b>	Page 88
<b>5.5 Discussion of the Experimental Results</b>	Page 91
<b>5.6 Measuring the Induced electric field within various media</b>	Page 92
<b>5.7 Method and Results</b>	Page 94
<b>5.8 Discussion of the Experimental Results</b>	Page 97

## **Chapter 6 Magnetic Stimulation: The Effects of Pulse Configuration**

<b>6.1 Introduction</b>	Page 100
<b>6.2 The Organization and Function of Skeletal Muscle Tissues</b>	Page 101
<b>6.3 Modeling the M-wave</b>	Page 103
<b>6.4 The Effect of Pulse Shape on Neural Stimulation</b>	Page 106
<b>6.5 Experimental Study</b>	Page 108
<b>6.6 Experiment Hardware and Software</b>	Page 109
<b>6.7 Method</b>	Page 111
<b>6.8 Results</b>	Page 112
<b>6.9 Analyses of the Results</b>	Page 118
<b>6.1 Discussion</b>	Page 124

## **Chapter 7 Conclusions and Future Investigation**

**7.1 Conclusions** Page 129

**7.2 Future Investigations** Page 134

**Appendix A ECT vs rTMS** Page 137

**Appendix B rTMS: Risks and Safety Guidelines** Page 142

### **Appendix C Mono-phasic and Bi-phasic Pulses in Magnetic Stimulation**

**C.1 The effect of L, R, C on current pulse configuration** Page 149

**C.2 The current pulses during magnetic stimulation** Page 150

**Appendix D Simple Magnetic Stimulator** Page 154

**References** Page 157

**List of Publications** Page 168

## List of Figures

### Chapter 1

- Figure 1.1** Page 5  
Different clinical applications for magnetic nerve stimulation.

### Chapter 2

- Figure 2.1** Page 15  
A typical nerve cell (neuron) within the peripheral nervous system.
- Figure 2.2** Page 19  
A circuit model representing a unit area of a nerve cell membrane.
- Figure 2.3** Page 20  
Equivalent circuit model of a myelinated axon.

### Chapter 3

- Figure 3.1** Pages 36, 37  
Various types of magnetic stimulation coils.
- Figure 3.2** Page 38  
The proposed air core coil.

<b>Figure 3.3</b>	Page 38
The proposed magnetic core coil.	
<b>Figure 3.4</b>	Page 46
A model representing a cross section of the upper limb at the junction of the proximal and middle thirds of the humerus.	
<b>Figure 3.5</b>	Page 47
A model representing a Figure-8 coil (Dantec Company) projected above a section of the upper limb.	
<b>Figure 3.6</b>	Page 47
A model representing the proposed magnetic core coil projected above a section of the upper limb.	
<b>Figure 3.7</b>	Page 49
Bi-phasic current pulses generated to supply Figure-8, air core, and magnetic core coils.	
<b>Figure 3.8</b>	Page 51
Magnetic flux density along the Y-axis (depth of field penetration).	
<b>Figure 3.9</b>	Page 52
Magnetic flux density along the X-axis (field focality).	
<b>Figure 3.10</b>	Page 52
Magnetic flux density along the Z-axis (field focality).	
<b>Figure 3.11</b>	Page 53
The induced electric fields resulting from the application of bi-phasic current pulses.	
<b>Figure 3.12</b>	Page 55
Mono-phasic current pulses used to supply Figure-8, air core, and magnetic core coils.	
<b>Figure 3.13</b>	Page 55
The induced electric fields resulting from the application of mono-phasic current pulses.	

## **Chapter 4**

<b>Figure 4.1</b>	Page 60
A simple equivalent circuit of a magnetic stimulator.	
<b>Figure 4.2</b>	Page 63
A block diagram of the different stages of a magnetic stimulator.	
<b>Figure 4.3</b>	Page 67
An Advanced Magnetic Stimulator.	
<b>Figure 4.4</b>	Page 68
A Simple Magnetic Stimulator.	
<b>Figure 4.5</b>	Page 72
Experiment set up by Maccabee et al..	
<b>Figure 4.6</b>	Page 72
The measurement apparatus used by Lin et al..	
<b>Figure 4.7</b>	Page 74
Experiment setup - spherical volume.	
<b>Figure 4.8</b>	Page 74
Experiment setup - cartesian volume.	
<b>Figure 4.9</b>	Page 76
Front panel display of the software showing the induced voltages in the inductors.	
<b>Figure 4.10</b>	Page 77
Induced voltages generated by a circular coil when using bi-phasic waveforms.	
<b>Figure 4.11</b>	Page 78
Induced voltages generated by a circular coil when using mono-phasic waveforms.	
<b>Figure 4.12</b>	Page 78
The areas of the induced voltages for circular and Figure-8 coils using two waveforms.	

## Chapter 5

<b>Figure 5.1</b>	Page 82
Plane wave entering conducting medium at normal incidence.	
<b>Figure 5.2</b>	Page 84
A model illustrating the measurement of electric field using an inductor.	
<b>Figure 5.3</b>	Page 87
Various types of assembled coils.	
<b>Figure 5.4</b>	Page 89
Induced fields generated by various coils captured at 2cm below the coil centers.	
<b>Figure 5.5</b>	Page 89
The measured electric field (normalized) along the X-axis (field focality).	
<b>Figure 5.6</b>	Page 90
The measured electric field along the Y-axis (depth of field penetration).	
<b>Figure 5.7</b>	Page 90
The measured electric field along the Z-axis (field focality).	
<b>Figure 5.8</b>	Page 92
Two probes insulated and enclosed by a medium.	
<b>Figure 5.9</b>	Page 93
Experiment setup - Top: homogeneous medium, Bottom: heterogeneous medium.	
<b>Figure 5.10</b>	Page 95
Normalized electric fields captured by insulated inductors.	
<b>Figure 5.11</b>	Page 96
Normalized electric fields captured in homogeneous medium.	
<b>Figure 5.12</b>	Page 96
Normalized electric fields captured in heterogeneous medium.	



## Chapter 6

- Figure 6.1** Page 101  
An anatomical structure of a motor unit.
- Figure 6.2** Page 105  
A model illustrating the generation of the M-wave from superimposed motor unit action potentials.
- Figure 6.3** Page 109  
The positions of the recording electrodes and the sites of stimulation.
- Figure 6.4** Page 110  
Front panel display of the software capturing the M-wave of a subject.
- Figure 6.5** Page 112  
M-wave responses using electrical stimulation.
- Figure 6.6** Page 113  
M-wave responses for bi-phasic pulses using a Figure-8 coil at the elbow.
- Figure 6.7** Page 114  
M-wave responses for mono-phasic pulses using a Figure-8 coil at the elbow.
- Figure 6.8** Page 115  
M-wave responses for various waveforms and current directions using a Figure-8 coil.
- Figure 6.9** Page 119  
Normalized M-wave amplitudes (mean  $\pm$  S.D.) for bi and mono pulses (10 subjects, Figure-8 coil, elbow).
- Figure 6.10** Page 122  
Shift (mean  $\pm$  S.D.) in the virtual cathode due to bi and mono waveforms (9 subjects, Figure-8 coil, elbow).

## **Appendix A**

**Figure A.1** Page 138

An illustration of various placement of unilateral electrodes with the reference electrode being at the vertex.

**Figure A.2** Page 138

An illustration of the coil placement during TMS.

**Figure A.3** Page 140

Different waveforms used in ECT.

**Figure A.4** Page 140

Different waveforms used in rTMS.

## **Appendix C**

**Figure C.1** Page 150

A circuit model of a typical magnetic stimulator.

**Figure C.2** Page 152

Waveforms generated for Figure-8 and air core coils.

**Figure C.3** Page 153

Waveforms generated for a magnetic core coil.

## **Appendix D**

**Figure D.1** Page 154

A schematic diagram of the simple magnetic stimulator.

**Figure D.2**

Page 155

The high voltage capacitor bank.

**Figure D.3**

Page 156

The hardware circuitry of the simple magnetic stimulator.

## List of Tables

### Chapter 3

<b>Table 3.1</b>	Page 48
Tissue conductivities at 10 kHz.	

### Chapter 6

<b>Table 6.1</b>	Page 118
Summary of the M-waves resulting from using different coils at the elbow.	

<b>Table 6.2</b>	Page 120
Summary of the shift in the virtual cathode position.	

<b>Table 6.3</b>	Page 121
Shift of the virtual cathode when using bi-phasic and mono-phasic pulses.	

<b>Table 6.4</b>	Page 123
Averaged M-wave responses as a function of current direction.	

<b>Table 6.5</b>	Page 123
Averaged shifts of the virtual cathode as a function of current direction.	

### Appendix A

<b>Table A.1</b>	Pages 137-141
A comparison between ECT and rTMS.	

## **Appendix B**

### **Table B.1**

Page 147

Maximum safe duration for single trains of rTMS based on the National Institute of Neurological Disorders and Stroke Experience.

### **Table B.2**

Page 148

Current rTMS safety guidelines: safe intertrain intervals.

## List of Symbols

$A_1, A_2$	Constants applied to solve 2 <sup>nd</sup> order differential equation
$\bar{A}_0$	Magnetic vector potential (Wb/m)
$\bar{A}_1$	Magnetic vector potential (Wb/m)
$\bar{A}_n$	Instantaneous magnetic vector potential (Wb/m)
$\bar{A}_{n-1}$	Previous value of Magnetic vector potential (Wb/m)
$B$	Magnetic flux density (Tesla)
$C$	Capacitance of the magnetic stimulator high voltage circuitry (F)
$C_m$	Membrane Capacitance (F)
$c_m$	Membrane Capacitance Per Unit Area (F/m <sup>2</sup> )
$CV$	Nerve conduction velocity (m/s)
$D$	Electric flux density (C/m <sup>2</sup> )
$d$	Axon diameter (m)
$d$	Dimensional constant = 1 (m <sup>-1</sup> ) (page 25)
$d$	Distance separating the inductor from the stimulating coil (m) (page 85)
$\partial A/\partial t$	Contribution of the electric field from magnetic induction (V/m)
$d_i$	Axon internal diameter (m)
$d_o$	Axon outer diameter (m)
$di/dt$	Coil current rate of change (A/ $\mu$ s)
$d_j/d_i$	Ratio of outer to inner axon diameter (1.333)
$dl'$	A segment of the stimulating coil (m)
$d_{elbow}$	Distance from the measuring electrodes to the site of stimulation-elbow (cm)
$d_{wrist}$	Distance from the measuring electrodes and the site of stimulation-wrist (cm)
$E$	Electric field intensity (V/m)
$E_{Cl}^-$	Chloride ion potential ("Nernst Potentials" @ 37 °C) (V)
$E_K^+$	Potassium ion potential ("Nernst Potentials" @ 37 °C) (V)
$E_{Na}^+$	Sodium ion potential ("Nernst Potentials" @ 37 °C) (V)
$F$	Faraday's Constant (C/mol)
$f$	Frequency (Hz)
$G_c$	Cytoplasmic Conductance (S)
$G_m$	Membrane Conductance (S)
$g_m$	Membrane Conductance Per Unit Area (S/m <sup>2</sup> )
$g_{Cl}^-$	Chloride ion conductance (S)
$g_K^+$	Potassium ion conductance (S)
$g_{Na}^+$	Sodium ion conductance (S)
$H$	Magnetic field strength (A/m)

$h_i(t)$	Transfer function
$i$	Current of the stimulating coil (A)
$i$	Index of an electric pulse (page 116)
$i$	Index of a magnetic pulses (page 117)
$J$	Current Density ( $A/m^2$ )
$\sigma E_y$	Conduction current density ( $A/m^2$ )
$j\omega\epsilon E_y$	Displacement current density ( $A/m^2$ )
$K$	Dielectric constant of nerve myelin
$K_e$	Total number of electrical pulses
$K_m$	Total number of magnetic pulses
$k$	Dimensional constant = 1 (Wb/(A.t.m)) (page 30)
$k$	Scaling factor (page 85)
$L$	Inductance of the stimulating coil (H)
$\ell$	Length (m)
$\ell$	The shortest distance separating the $j$ th node from the $n$ th node (m)
$M(t)$	Functional Representation of M-Wave (V)
$m_n(t)$	Motor Unit Action Potential (V)
$N$	Number of coil turns
$N$	Total number of subjects
$n$	Index of a subject
$n$	Index of a node of Ranvier
$P_{Cl}^-$	Membrane permeability of the Chloride ion
$P_K^+$	Membrane permeability of the Potassium ion
$P_{Na}^+$	Membrane permeability of the Sodium ion
$R$	Gas Constant (J/(K mol) (page 17)
$R$	Distance (m) (page 29)
$R$	Tissue resistive component ( $\Omega$ )
$R$	Equivalent resistance of the magnetic stimulator-high voltage circuitry ( $\Omega$ )
$R_f$	Resistance of the current pathway flowing from the capacitor to the coil ( $\Omega$ )
$R_r$	Resistance of the current pathway flowing from the coil to the capacitor ( $\Omega$ )
$s_1, s_2$	Quadratic roots applied to solve 2 <sup>nd</sup> order differential equation
$T$	Absolute Temperature (K)
$t$	Time (s)
$t_{delay(n)}$	Motor Unit Latency (s)
$V_e$	Extracellular Potential (V)
$V_i$	Intracellular potential (V)
$V_i$	Induced voltage (V) (page 85)
$V_m$	Transmembrane potential (V)
$V_r$	Resting Membrane Potential (V)
$V_{e,n}$	External nodal voltage (V)
$V_{i,n}$	Internal nodal voltage (V)
$w$	length of the surface mount inductor (m)
$x$	Distance along the axon (m)

$X_c$	Tissue capacitive reactance ( $\Omega$ )
$\Delta x$	Internodal length (m)
$\nabla$	Divergence
$\nabla \times$	Curl operator
$\nabla \Phi$	Electrostatic field (electric scalar potential) (V/m)
$\Phi$	Representation of charge accumulation (C)
$\Delta x$	Distance between adjacent Nodes of Ranvier (m)
$a$	Damping factor (1/s)
$\epsilon$	Electrical permittivity (F/m)
$\epsilon_0$	Dielectric constant for a vacuum ( $8.85 \times 10^{-12}$ ) (F/m)
$\epsilon_r$	Relative dielectric constant
$\delta$	Width of Node of Ranvier (m)
$\delta(t)$	Dirac Delta function
$\delta_n(t)$	Functional representation of motor nerve action potential
$\lambda_{mye}$	Space constant for the myelinated axon (m)
$\mu$	Magnetic permeability (H/m)
$\mu_0$	Permeability of free space ( $4\pi \times 10^{-7}$ ) (H/m)
$\mu_r$	Relative permeability
$\zeta$	Electric field intensity (V/m)
$\zeta_A$	Transient electric field component (V/m)
$\zeta_{Total}$	Total electric field (V/m)
$\zeta_x$	Electric field component along the axon (x axis) (V/m)
$\zeta_\phi$	Static electric field component (V/m)
$\rho_{mye}$	Resistivity of myelin ( $7.4 \times 10^5$ k $\Omega$ cm)
$\rho_a$	Resistivity of axoplasm ( $5.47 \times 10^{-2}$ k $\Omega$ cm)
$\rho_c$	Resistivity of cytoplasm (intracellular) ( $\Omega$ m)
$\sigma$	Tissue conductivity (S/m)
$\sigma_l$	Longitudinal tissue conductivity (S/m)
$\sigma_t$	Transverse tissue conductivity (S/m)
$\tau_{mye}$	Time constant for the myelinated axon (s)
$\tau_{electric}$	Latency due to electric stimulation (s)
$\tau_{magnetic}$	Latency due to magnetic stimulation (s)
$\tau_{elbow}$	M-wave latency when stimulating the elbow (s)
$\tau_{wrist}$	M-wave latency when stimulating the wrist (s)
$\omega$	Radian frequency (rad/s)
$\omega_0$	Resonant frequency (rad/s)
$\omega_r$	Ringling frequency (rad/s)



## List of Abbreviations

<b>ALS</b>	Amyotrophic lateral sclerosis
<b>ANOVA</b>	Analysis of variance
<b>BD</b>	Bipolar disorder
<b>CMAP</b>	Compound muscle action potential
<b>CMMR</b>	Common mode rejection ratio
<b>ECS</b>	Electroconvulsive shock
<b>ECT</b>	Electroconvulsive therapy
<b>FEM</b>	Finite element method
<b>FDI</b>	First dorsal interosseus
<b>EMG</b>	Electromyography
<b>FMS</b>	Functional magnetic stimulation
<b>ISTS</b>	International Society of Transcranial Magnetic Stimulation
<b>MEP</b>	Motor evoked potential
<b>MNS</b>	Magnetic nerve stimulation
<b>rTMS</b>	Repetitive transcranial magnetic stimulation
<b>SCR</b>	Silicon-controlled rectifier
<b>TMS</b>	Transcranial magnetic stimulation

## Chapter 1 Introduction

### 1.1 History Preview

By the end of the eighteenth century, the notion that animal tissue responds to electricity was reasonably well established. As reviewed by Rattay [1], Galvani and Volta demonstrated in the 1790s that electric currents could affect the activities of muscles and nerves. However, this knowledge was not used effectively in psychiatry until April 1938, when Cerletti and Bini first described electroconvulsive therapy (ECT) [2].

In 1831 Michael Faraday described the magnetically induced current. Faraday wound two coils on an iron ring and found that whenever the coil on one side was connected or disconnected from a battery, an electrical current passed through the coil on the other side. His theory was that the iron ring acted as a channel linking the magnetic field of both coils such that any change in the magnetic field of the first coil would result in an induced current in the second.

The earliest scientific attempts to use magnetic energy to alter brain activity were conducted by D'Arsonval in 1896 and Thompson in 1910 [3]. Placing a large coil carrying substantial alternating current near the head of a human volunteer, D'Arsonval stated that the subject perceived bright spots, or "phosphenes" in the visual field [3].

Using currents with frequencies of 60Hz and 1kHz, Kolin et al. reported selective

nerve stimulation in 1959 [3]. The group achieved these stimulations by wrapping a frog sciatic nerve around an electrical pole.

In 1965 Bickford and Freeming introduced magnetic nerve stimulation (MNS) by discharging a capacitor into a skin-surface coil [3]. They applied this method to the peripheral nerves of humans and animals.

In the late 1970s and early 1980s, Barker et al. conducted many experiments with the objective of stimulating deep nerves [3]. This group reported their first success in stimulating the human motor cortex in 1985 [4]. By this event the modern era of transcranial magnetic stimulation (TMS) started. With the availability of equipment that can generate up to 50 pulses per second, the therapeutic potential of repetitive transcranial magnetic stimulation (rTMS) was introduced in the 1990s [5].

The concept of MNS is based on Faraday's experiment with the stimulating coil representing that connected to a power supply, the targeted nerve representing the second coil and the tissues representing the medium linking the magnetic field between both coils [3]. Establishing an alternating current in the stimulating coil produces an alternating magnetic field that links the two coils. This field results in an induced electric field in the nerve. If the electric field gradient reaches a certain threshold, nerve stimulation becomes evident.

## **1.2 Clinical Applications of Magnetic Nerve Stimulation**

The therapeutic potential of magnetic energy has been a subject of long debate in both conventional and alternative medical practices. Numerous devices using magnetic fields, ranging from the questionable to the truly innovative, have claimed a wide variety of

clinical benefits. Nevertheless, many of these devices proved to be effective in numerous clinical applications and hold great promise for further advancements. These applications cover several areas with the most critical listed below.

#### 1. Diagnosing disease and mapping the upper motor neuron

Diagnosis of some neurological dysfunction, such as Amyotrophic Lateral Sclerosis (ALS), depends on the evaluation of upper and lower motor neurons. While the lower motor neuron involvement may be examined with electromyography (EMG), the involvement of the upper motor neuron may be elusive and difficult to test. Studies conducted by Triggs et al.[6] and Miscio et al. [7] investigated the effectiveness of TMS to identify abnormal upper motor neurons in patients suffering from ALS. Both groups confirmed that TMS showed a high sensitivity to any abnormality and improved the diagnosis. Further, both group findings agreed that TMS provides important diagnostic information for an early prediction of ALS.

More investigations to evaluate the effectiveness of TMS as a diagnostic tool were performed by Cicinelli et al. [8]. In their study, TMS was employed for mapping the motor cortex of both hemispheres. The conclusion of this study was: TMS can offer a new tool in diagnosing neurological disorders that affect the central nervous system.

Although the above studies were applied to map upper motor neurons, it should be noted that the measured responses were collected from the lower motor neurons. However, if the lower motor neurons are severely dysfunctional, then quantifying the abnormality of upper motor neurons will be complicated. In these cases, an alternative diagnostic tool, such as an MRI, could be used to evaluate the brain and spinal cord conditions.

## 2. Rehabilitation and therapeutic treatments

In the past few years, functional magnetic stimulation (FMS) has been shown to be an attractive and promising field for rehabilitation purposes. Recently, many researchers have used this non-invasive technology as a new therapeutic tool to stimulate various organs such as bladder, colon, abdominal and respiratory muscles.

By stimulating the sacral nerves within the suprapubic region, Lin et al. [9,10] studied the effectiveness of FMS in activating bladder contraction and improving bowel movements in patients suffering from spinal cord injury. For bladder stimulation, their results showed that FMS can be helpful to patients with neurogenic bladders [9]. Further, this group was successful in stimulating the colon and concluded that FMS reduces the total and segmental colonic transit times [10]. By stimulating the roots of the sacral nerves, Yamanishi et al. [11] and Fujishiro et al. [12] studied the feasibility of using FMS to control urinary incontinence. Their conclusions found that FMS was effective in urethral closure and bladder inhibition, and evidently as a treatment of urinary incontinence.

Another application of FMS is to improve respiratory pacing in patients unable to activate the abdominal muscles due to spinal cord injury. Polkey et al. [13] and Singh et al. [14], applied FMS to the spinal cord (between T8 and L5) with the aim of stimulating the roots of the thoracic and lumbar nerves. They confirmed that FMS of the abdominal and expiratory muscles can generate a substantially positive intra-abdominal and intrathoracic pressures and consequently can enhance the expiratory pressures, volumes, and flow. Their conclusions are: FMS can be a valuable technique for restoring cough in patients in critical care or peri-operative settings.

### 3. Evaluation of motor pathways and monitoring neural surgeries

As magnetic fields have the capability of penetrating deep anatomical structures, TMS can be used to excite neural fibers embedded within deep tissues or covered by bones. From this perspective, TMS can be used to monitor the integrity of the spinal cord during surgery [15]. Figure 1.1 displays various clinical applications for magnetic nerve stimulation.

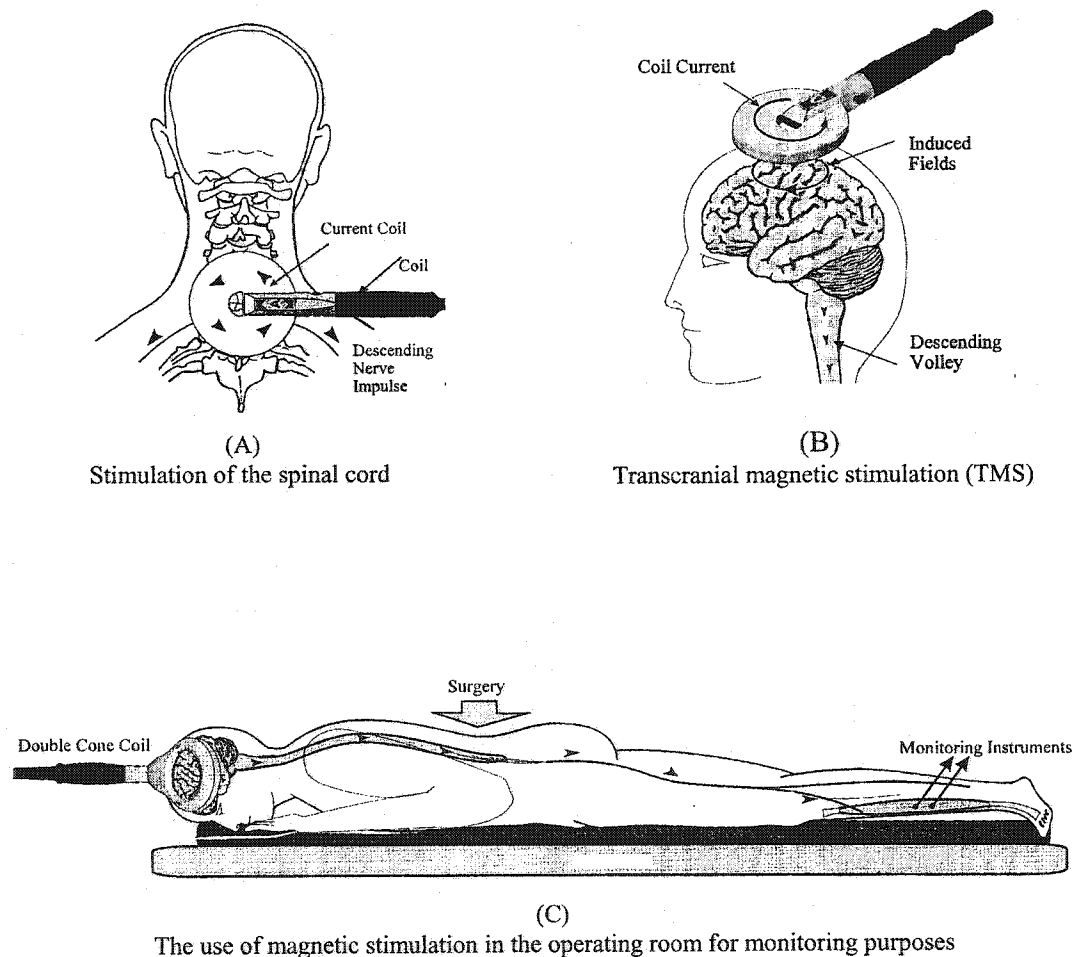


**Figure 1.1**  
Different clinical applications for magnetic nerve stimulation (taken from [15]).

#### 4. Treatment of Mood Disorders

In most cases, the symptoms of mood disorders are controlled with pharmacological treatment. However, despite the various types of medications available, there are many side effects associated with their use. Pharmacological treatment, particularly among elderly patients, is more complicated due to the medical comorbidity, polypharmacy, and patient's greater vulnerability to medication toxicity [16,17]. Further, large numbers of patients (as many as 1 in 5 ) may not respond to any of the drugs (antidepressant medication-resistant patients) [18]. An alternative to treat these patients is the use of electroconvulsive therapy (ECT) [19]. However, despite the advantages of ECT, there are many cognitive side effects as well as the problem of general anaesthesia, therefore, a new therapeutic approach is needed. The new approach that was recently adopted by some members of the psychiatric community is repetitive transcranial magnetic stimulation ( rTMS). This novel non-invasive technology has shown great promise as a treatment for depression, even in antidepressant medication-resistant patients [20,21]. A detailed comparison between the mechanisms and application aspects of ECT and rTMS can be found in Appendix A.

Since its early development as a new therapeutic tool, the possibility that rTMS may replace ECT has been frequently suggested in the clinical research community [22,23]. Studies in animals indicate that rTMS can produce behavioral and biological effects which are qualitatively similar to those seen after electroconvulsive shock (ECS) [24-26]. Grunhaus et al. [27], and Pridmore et al. [28] have recently completed two well designed studies in which patients were randomly assigned to ECT and rTMS with the objective of comparing the effectiveness of rTMS to that of ECT. Both groups observed marked improvements in

non-psychotic patients. In agreement with the findings of references 27 and 28, other researchers predict that rTMS therapy may ultimately find a crucial role in the list of treatment options for patients suffering from major depression or other neuropsychiatric illnesses [29,30]. However, before this materializes two critical issues must be clarified:

1. The outcomes of all the studies investigating rTMS have been realized despite the fact that rTMS treatment settings are still not fully determined. Needless to say that a better understanding of rTMS mechanisms and functionality combined with improved instruments will accelerate the realization of its therapeutic potential.
2. Comparing results of trials in which rTMS was used for depression treatment, is complicated due to the variations in rTMS methodology, diagnostic heterogeneity, the differences in equipment output, and lack of knowledge regarding dose-response relationships. As has been suggested by many researchers, following precise and well defined guidelines will simplify the task and ensure valid comparison.

### **1.3 Advantages and Current Limitations of MNS and rTMS**

The potential advantages of MNS over electrical stimulation are:

1. Reduction or sometimes elimination of pain.
2. Access to tissues covered by poorly conductive structures.
3. Stimulation of neural tissues lying deep in the body without requiring an invasive technique or high energy pulses [3,15].

As for rTMS when compared with ECT, the advantages are as follows:

1. Selectivity of discrete brain regions for stimulation in a more controlled manner [31].



2. Reduction of unwanted side effects associated with ECT such as seizures.
3. General anaesthesia is not required when applying rTMS [31].
4. From a cost perspective, rTMS treatment can be administered by a single operator in an outpatient setting. This leads to tremendous savings when compared to the cost of providing ECT.

Despite these advantages, the current clinical use of rTMS for treatment is considered experimental and requires regulatory agency approval in Canada and the USA (see Appendix B for more details regarding rTMS risks and safety guidelines).

In order to realize the full therapeutic potential of rTMS, the following key points must be addressed.

#### 1. Coil Design

The clinical coils currently used produce effective magnetic fields only for a limited penetration depth of 1-2 cm into the brain [32,33]. At this level of penetration most regions in the brain are not activated by magnetic stimulation. Some of these unaffected regions include the basal ganglia, the cingulate gyrus, and the thalamus, all of which are believed to be related to depression [34,35]. Accordingly, the stimulation of these deep structures requires new coil designs with greater depths of penetration and improved field focality.

#### 2. Pulse configuration, current direction, coil orientation, and stimulating site

It is well established that pulse shape influences the neurophysiological responses during MNS [36-38]. Also, it has been shown that current reversal in the coils changes the site of stimulation or stimulates other neural structures at the same site [39,40]. Further, it has been demonstrated that coil position and orientation are critical factors [41].

Considerable controversy still exists regarding the stimulation site (position of the virtual cathode) with respect to the coil, especially when stimulating inhomogeneous tissue structures. These are significant issues for determining optimum cortical stimulation strategies, yet no criteria have been established to define the most effective values for these parameters.

### 3. Consistency in coil placement

Coil positioning is an important but relatively unstudied issue. In most clinics, the current practice is to place the coil on the head 5 cm anterior to the site of the motor cortex for activation of the abductor pollicis brevis muscle, irrespective of the size and shape of the subject's head. This technique results in coil positioning over widely different brain regions across subjects with different head sizes. Recently, in a few advanced research facilities digital cameras were utilized to ensure precise and consistent coil positioning. However, due to the significant costs involved, these systems are limited to only a few research centers.

### 4. Other issues

The rate of repetition, the total number of pulses per session, and the relationship between dose of stimulation and antidepressant response are still under investigation.

## **1.4 Justification and Scope of this Thesis**

Mood disorder is currently one of the largest causes of disability with its cost sometimes exceeding those of diabetes, heart disease, and hypertension [43,44]. Further, if the symptoms are not managed effectively, the cost of the treatment increases tremendously. For example, the mean cost of a well controlled patient suffering from Bipolar Disorder (BD)

per life-time is \$11,720 US, yet this cost may rise precipitously to \$624,785 US, when the symptoms are not managed effectively [42].

The goal of the work presented in this thesis is to improve the current technology of rTMS. From an engineering perspective, the following issues were addressed in this work:

### 1. Coil Design

The main limitations in using rTMS are poor field focality and inadequate strength in deep tissues (targeted area). Excitation of these regions requires very high coil currents to achieve a strong field that is capable of penetrating deep tissues, however, these fields might activate adjacent tissues as well as the targeted area. Further, the high currents will result in coil heating, especially for a high rate of repetition. In this work, two new coil designs are proposed: air core and magnetic core coils. Both coils include a third vertical winding in addition to the two horizontal windings. Adding a third winding will improve field focality and will help control the depth of penetration. Moreover, the addition of the magnetic core will enhance the field strength as well as the depth of penetration. This enhancement will minimize the current required to generate the magnetic field, and consequently, reduces the generated heat within the windings and improves the coil thermal performance. However, there is concern that a more powerful coil could inadvertently induce seizures. It should be noted that seizures have been intentionally induced in depressed patients with the advantage of fewer cognitive side effects compared with ECT.

### 2. Pulse configuration, current direction, stimulating site and coil orientation

A number of studies have addressed the effectiveness of pulse configuration (mono-phasic, bi-phasic) during magnetic stimulation. Using the compound muscle action potential

(CMAPs) of a selected muscle, bi-phasic pulses appear to stimulate more motor neurons than mono-phasic pulses with the same energy content.

In this thesis, the effectiveness of different waveforms and the reversal of current direction will be quantified through simulations and experiments including a study in vivo. As well, the site of stimulation (virtual cathode) will be investigated with the objective of optimizing coil placement and its orientation precisely over the targeted area.

### **1.5 Thesis Structure**

Chapter 1 presented a history preview of MNS, its advantages, and limitations. A brief description of the state-of-the-art in the clinical use of MNS in diagnosing and therapeutic applications was included with a special focus on rTMS in treating mood disorders. The advantages of MNS and rTMS as well as the limitations of the latter (compared to ECT) were outlined. The scope of this thesis and the justification for the work were also addressed.

Chapter 2 provides background information regarding the neural system structure and function as well as the relationship between nerve stimulation and an applied magnetic field. A model representing a stimulated peripheral nerve axon (cable model) is mathematically described and analyzed. A mathematical field analysis of nerve stimulation, Roth's model, is presented with the main focus on the static component of the induced electric field.

Chapter 3 addresses the outstanding problems associated with coil design such as the lack of field focality and coil over-heating. The advantages and limitations of commercial coils, new coils proposed by other researchers, and our coils are presented. With the

objective of building a coil that is effective in rTMS, numerical simulations were performed on the previously used coils (circular, figure-8) as well as the proposed coils (air core, magnetic core). These simulations were conducted using the Finite Element Method in three dimensions combined with a transient analysis. An outline describing the software that was used to perform the simulations including problem description and post processing results are presented. Key results from these simulations and the advantages of the proposed coil designs are summarized.

Chapter 4 , which is divided into two sections, presents the hardware development aspects of this thesis. The first section outlines design principles and component selection that were implemented in building two magnetic stimulators (simple, advanced). The second section describes a new technique used to evaluate the stimulating coils by measuring the induced electric fields in three dimensions. In addition, this section covers the software and hardware used to construct two measuring apparatuses. A brief overview of the previous researchers' work as well as the evaluation results from the new apparatus are presented.

Chapter 5 summarizes the experimental results of this work and groups them in two parts. The first part covers the testing and evaluation of various coils (commercial vs. proposed), while the second part addresses the effect of changing the medium, on the induced electric field, during magnetic stimulation. The main objective of the second part is to test and evaluate Roth's hypothesis using different models with heterogeneous conductivities.

Chapter 6 addresses the effects of pulse configuration on stimulating lower motor neurons by measuring the compound muscle action potential (CMAPs) of a specific muscle (thenar muscle). It also covers the concept of action potential and its role in muscle

excitation. The results of a study, investigating the effect of pulse configuration, are presented and compared with that of other researchers.

Chapter 7 presents the conclusions that were drawn, recommendations, and an outline for possible future work in this area. The suggested future work identifies problems that have not been resolved and summarizes recommendations for further improvements to the current rTMS technology.

## Chapter 2      Stimulation of Nerve Fibers

To facilitate a better understanding of nerve interaction with external magnetic fields, a brief background of the nervous system physiology and functionality is presented in this chapter. This includes an overview of the nerve anatomical structure and its functions with an emphasis on peripheral nerves. Also, this chapter discusses the most accepted model, the “cable model,” to represent the excited nerve fiber during magnetic stimulation. As well, a numerical field analysis of nerve stimulation, Roth’s model, is discussed with the main focus on the static component of the induced electric field.

### 2.1 Anatomy of the Nervous System

The basic unit of the nervous system anatomy is the neuron. The human nervous system is a collection of about  $10^{11+1}$  neurons arranged in a highly structured manner [45]. The neurons are responsible for coding, transmitting, transforming, and decoding information. The morphology of neurons varies greatly, however, they have certain common features. Figure 2.1 shows the structure of a typical neuron including its major components: a cell body (soma) which contains a nucleus, dendrites, and a long thread-like fibre called an axon [45].

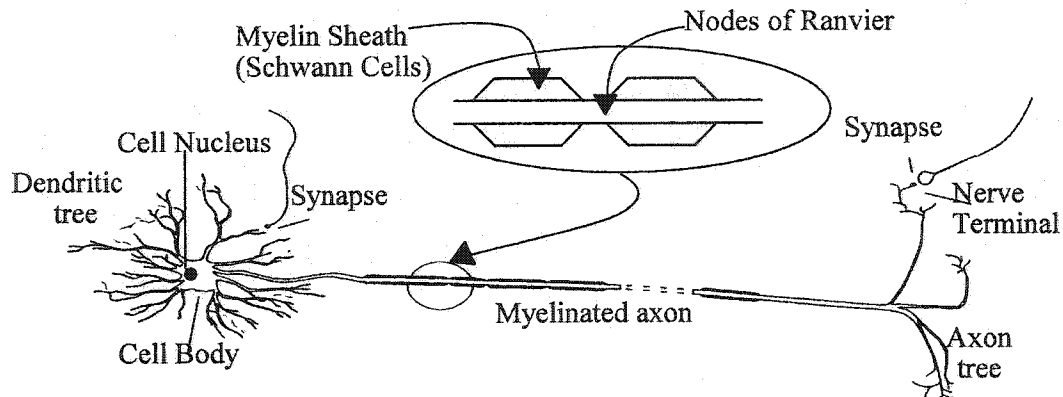


Figure 2.1 (after [45])

A typical nerve cell (neuron) within the peripheral nervous system. The drawing is not to scale and the dashed lines on the axon emphasize that the length of the axon is much greater than that of the cell body and may extend for several tens of centimeters.

Surrounding the neuron is a cell membrane, a boundary that separates the cytoplasm intracellular fluid from the interstitial fluid. This boundary consists of a phospholipid bi-layer in which transmembrane proteins are embedded [46]. Inputs to a neuron, which may vary from one to thousands, occur at the cell body and the synaptic sites (which are scattered over the surfaces of the dendrites). The axon of a neuron may reach a length of up to a meter and can have diameters that range between  $0.3 \mu\text{m}$  and  $20 \mu\text{m}$  (average  $10 \mu\text{m}$ ) [47,48]. Typically, the axon terminates in branches (synapse) that connect with other neurons or with skeletal muscle fibers as in the case of a motor unit.

Depending on the type of axons, the nerves can be divided into two major categories: myelinated and unmyelinated. If the axon is surrounded by a layer of myelin sheath, the nerve is called myelinated. In contrast, if the axon is bare the nerve is called unmyelinated [46]. The focus for the remainder of this chapter is on the myelinated nerves, as the targeted nerve considered in this thesis (for both modeling and experimenting) is the median nerve.



A myelinated fibre consists of an axon sheathed by a cylindrical sleeve of myelin. At regular intervals, the myelin sheath is segmented by  $2.5 \mu\text{m}$  gaps called the Nodes of Ranvier [45]. These gaps are the only points of contact which link the cell membrane with the extracellular tissues. It is at the Nodes of Ranvier that the neuron signals are generated and regenerated as they propagate down the length of the axon. The length of the segment between the Nodes of Ranvier depends on the fiber size and is estimated to be 100 times the fiber diameter [49]. Each of these segments, which may be referred to as internodal or internode, is formed by a supporting cell. The supporting cells associated with the peripheral nervous system are called Schwann cells. A variety of functions are ascribed to the supporting cells, including providing mechanical support for neurons, buffering extracellular solution composition, maintaining insulation for the electrical signal (as it propagates along the axon) from the highly conductive extracellular fluid, guiding the migration of neurons during development of the nervous system, nourishing neurons, participating in the formation of the blood-brain barrier, and disposing of cellular waste [45].

Most researchers agree that the axon internodes play a major role in peripheral nerve stimulation as they have noted that larger fibers are more readily excited than smaller ones [50,51]. Their interpretation is based on the fact that axons with larger diameters have longer internodes which result in higher voltage gradients between adjacent nodes and consequently, lower effective thresholds for nerve excitation.

## 2.2 The Sodium-Potassium Pump

For nerve fibers, the concentration of ions in the extracellular fluids is different from that in the cell internal cytoplasm. This difference in concentration generates an equilibrium transmembrane potential  $V_m$  which can be attributed to the contributions of the three most significant ions: Potassium  $K^+$ , Sodium  $Na^+$ , and Chloride  $Cl^-$ . The effects of these ions can be modeled as DC voltage sources that supply ionic currents through their respective gates. From a mathematical perspective, the transmembrane potential  $V_m$  can be calculated using the Nernst relationship or the Goldman constant-field equation (equation 2.1), which is an extension of the Nernst equation [52].

$$V_m = \left( \frac{RT}{F} \right) \ln \left( \frac{P_{K^+} [K^+]_o + P_{Na^+} [Na^+]_o + P_{Cl^-} [Cl^-]_i}{P_{K^+} [K^+]_i + P_{Na^+} [Na^+]_i + P_{Cl^-} [Cl^-]_o} \right) \quad (2.1)$$

where  $V_m$  is the membrane potential,  $R$  is the gas constant,  $T$  is the absolute temperature,  $F$  is the Faraday constant, and  $P_K, P_{Na}, P_{Cl}$  are the membrane permeabilities of the ions  $K^+, Na^+, Cl^-$  respectively.

Since the above ions have different concentrations across the cell membrane, their influx and efflux are not in equilibrium. As  $Na^+$  has a higher concentration outside the cell while  $K^+$  is higher inside the cell, the  $Na^+$  will have the tendency to flow into the cell while the  $K^+$  will flow in the opposite direction. To maintain the balance in ion concentrations as well as the cell resting potential, a set of proteins embedded within the cell membrane play a major role. These proteins, which can be defined as the Sodium-Potassium pump, force the extra  $Na^+$  from the cell interior to its exterior and pump the  $K^+$  in the opposite direction. As

the process of moving ions against their concentration gradient requires energy to “fuel” the Sodium-Potassium pump, chemical energy is supplied from cleaving adenosine triphosphate molecules [46].

### 2.3 Mechanisms of Neuron Excitation

The concept of neuronal or axonal excitation involves the alteration of the transmembrane potential ( $V_m$ ) from its resting potential (approximately -90 mV) to a higher level [46]. If  $V_m$  increases to -60 mV, the Sodium gates will open (increase their conductance) allowing more  $Na^+$  to flow into the cell. This will trigger an increase in the transmembrane potential, hence increasing the flow of the  $Na^+$ . The accumulated  $Na^+$  inside the cell will initiate positive feedback that will change the transmembrane potential from -60 mV to approximately 30 mV. This momentary change in the membrane potential is defined as neuron excitation or firing and it can be considered as the initiation of the “Action Potential” [46]. After the neuronal firing, the Sodium gates, which are time dependent, will begin to close, blocking the influx of  $Na^+$ . Simultaneously, the Potassium gates will open allowing  $K^+$  to flow from the cell interior to its exterior. This process will bring the cell membrane back to its resting potential [46].

It is well accepted that the ionic activities described above can be modeled as an electrical circuit representing the ionic currents and the membrane electrical properties. As charges accumulate across the membrane due its dielectric property (phospholipid bilayer), the membrane can be modeled as a capacitor. Further, depending on the gate’s ionic permeability, these gates can be modeled as variable selective conductances. Figure 2.2 is

a graphical interpretation of the above and it outlines an electric circuit model of a cell membrane where:  $E_{Na}$  and  $E_K$ , represent the  $Na^+$  and  $K^+$  equilibrium potentials (“Nernst Potentials”) respectively,  $g_{Na}$  and  $g_K$  denote the Sodium and Potassium conductances respectively, while  $C_m$  and  $V_m$  are the membrane capacitance and potential [53]. Although the chloride ions were included in equation (2.1), they have been eliminated from the equivalent circuit as they have a minute effect relative to the other currents.

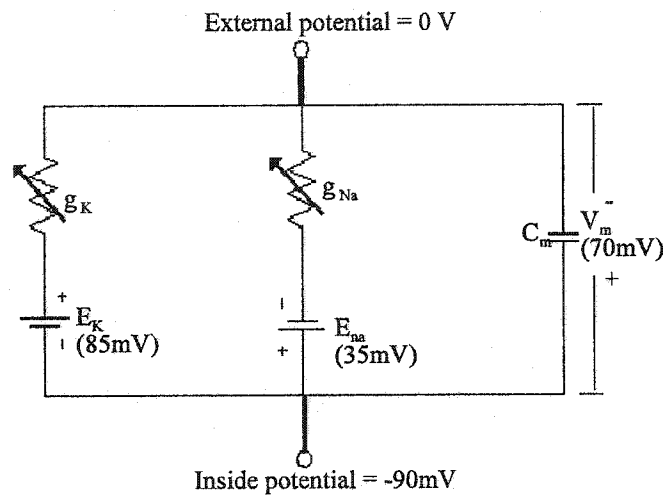


**Figure 2.2**  
A circuit model representing a unit area of a nerve cell membrane.

## 2.4 The Equivalent Circuit of the Myelinated Nerve

Many models have been developed over the last 50 years to represent the nervous system and its physiological activities. In these models, it has been clearly established that any neuron activity is the result of a sequence of chemical diffusions between the neuron and its surroundings through the cell membrane. To model these effects, a simplified equivalent circuit model, which consists of passive conductances and capacitances, was implemented.

Figure 2.3 illustrates a circuit model of the myelinated nerve axon and its associated elements as it was originally formulated by McNeal [49].

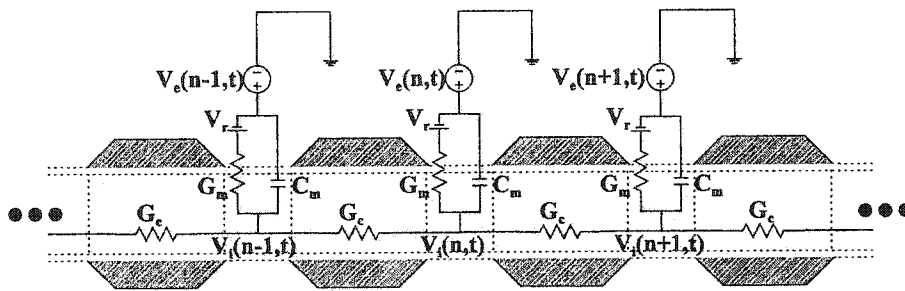


Figure 2.3

Equivalent circuit model of a myelinated axon. The circuit is superimposed on the axial cross section of the fiber in an attempt to relate the equivalent circuit components to the physical structure of the axon. The parameters  $G_m$  and  $C_m$  represent the conductance and the capacitance associated with the exposed section of the membrane. As the cytoplasm is considered to be predominantly resistive, it is denoted by the conductance  $G_c$ . The term  $V_r$  represents resting potential, while the terms  $V_i$ ,  $V_e$ , and  $V_m$  denote intracellular, extracellular, and transmembrane potentials, respectively. The potentials  $V_i$ ,  $V_e$ , and  $V_m$  are discrete variables as they are indexed by the parameter  $n$  which assigns a specific number for each Node of Ranvier. By applying Kirchhoff's voltage law, the transmembrane potential  $V_m$  can be calculated using the relation  $V_m = V_i - V_e - V_r$ . The axon shown above is assumed to extend in both directions.

The purpose of the above model is to relate the physical structure of the myelinated axon to the equivalent circuit components. As was illustrated earlier, the Nodes of Ranvier are the membrane's only contact points with the extracellular environment as the intervening areas between them are insulated by Schwann cells. Considering that Schwann cells have an extremely high impedance relative to the bare membrane [45], it can be assumed that these cells are effectively non-conducting. This assumption has been implemented in virtually all models presented in the literature.

By applying Kirchhoff's current law at the intracellular nodes, the currents flowing from the  $n$ th node of Ranvier can be described by the following differential equation:

$$C_m \frac{dV_m(n,t)}{dt} + G_m V_m(n,t) + G_c [[V_e(n-1,t) + V_m(n-1,t)] - [V_e(n,t) + V_m(n,t)]] + G_c [[V_e(n+1,t) + V_m(n+1,t)] - [V_e(n,t) + V_m(n,t)]] = 0 \quad (2.2)$$

Re-arranging the terms in equation (2.2) results:

$$C_m \frac{dV_m(n,t)}{dt} + G_m V_m(n,t) - G_c [V_m(n-1,t) - 2V_m(n,t) + V_m(n+1,t)] = G_c [V_e(n-1,t) - 2V_e(n,t) + V_e(n+1,t)] \quad (2.3)$$

In equations (2.2, 2.3),  $V_m$  represents the transmembrane potential while  $V_e$ , which is a discrete term for each Node of Ranvier, denotes the node extracellular potential. The terms  $G_m$  and  $G_c$  are the conductances of the membrane and the cytoplasm respectively. The parameter  $C_m$  represents the capacitance associated with the exposed section of the membrane. It should be noted that the terms representing the extracellular and transmembrane potentials in equations (2.2, 2.3) are functions of both the node position, as indexed through the parameter  $n$ , and time represented by the variable  $t$ .

To solve equation (2.3), the equivalent circuit components  $C_m$ ,  $G_m$  and  $G_c$  must be known. To compute these parameters is a simple task considering they are based on an idealized geometry and linear electrical properties of the axon membrane and the cytoplasm. The segmental capacitance  $C_m$ , which represents the capacitance of the cell membrane exposed to the extracellular medium at each node, can be calculated using equation (2.4)

$$C_m = c_m \pi d \delta \quad (2.4)$$

where  $c_m$  is the distributed capacitance per unit area of a cell membrane,  $d$  is the axon diameter, and  $\delta$  is the width of the Node of Ranvier. In a similar manner, equation (2.5) can be used to calculate the membrane conductance  $G_m$  at the Node of Ranvier.

$$G_m = g_m \pi d \delta \quad (2.5)$$

where  $g_m$  is the distributed conductance per unit area of a cell membrane,  $d$  and  $\delta$  are the same variables used in equation (2.4). Considering that the resistivity of the cytoplasm  $\rho_c$  is known, the calculation of the segmental axial conductance  $G_c$  can be implemented using the following equation:

$$G_c = \frac{\pi d^2}{4 \rho_c \Delta x} \quad (2.6)$$

where  $\rho_c$  is the cytoplasm resistivity (intracellular),  $\Delta x$  is the length from center to center between adjacent Nodes of Ranvier, and  $d$  is the variable used in equations (2.4, 2.5).

## 2.5 The Cable Equation

Equation (2.3) can be re-arranged as follows:

$$\begin{aligned} & \left[ \left[ \frac{G_c}{G_m} \right] [V_m(n-1,t) - 2V_m(n,t) + V_m(n+1,t)] - [V_m(n,t)] - \left[ \frac{C_m}{G_m} \right] \frac{dV_m(n,t)}{dt} \right] \\ & = - \left[ \left[ \frac{G_c}{G_m} \right] [V_e(n-1,t) - 2V_e(n,t) + V_e(n+1,t)] \right] \end{aligned} \quad (2.7)$$

Equation (2.7) can be analogously expressed in a continuous form as:

$$\lambda^2 \frac{\partial^2 V_m}{\partial x^2} - V_m - \tau_m \frac{\partial V_m}{\partial t} = \lambda^2 \frac{\partial \zeta_x}{\partial x} \quad (2.8)$$

where  $\zeta_x$  is the electric field along the axon (x axis),  $\lambda$  and  $\tau_m$  are the axon space and time constants respectively and can be described by:

$$\lambda = \sqrt{\frac{G_c}{G_m}} ; \tau_m = \frac{C_m}{G_m} \quad (2.9)$$

Equation (2.8), also known as the “cable equation<sup>1</sup>”, represents a general formula for the transfer of the action potential along the axon. This equation has been implemented by many researchers, who modeled axonal fibers during magnetic stimulation, with the

---

<sup>1</sup>

This equation is called the “cable equation” due to its similarities with that solved first by William Thompson (also known as Lord Kelvin) in 1855. The original equation was describing a model of an Atlantic submarine cable to be used for intercontinental telegraphy. The similarity here is the leaky jacket for that model relative to the leaky membrane [45].



objective of defining the optimum parameters required to achieve nerve excitation.

## 2.6 Roth and Basser Cable Model

Roth and Basser modified the cable equation in order to calculate the threshold of the magnetic field needed to achieve stimulation [54,55]. They defined the transmembrane potential for a myelinated nerve (which is governed by the cable equation) and linked it with the induced electric field (which results from the transient magnetic field) by the following equation [55]:

$$\lambda_{mye}^2 \frac{\partial^2 V_m}{\partial x^2} - V_m - \tau_{mye} \frac{\partial V_m}{\partial t} = \lambda_{mye}^2 \frac{\partial \zeta_x(x,t)}{\partial x} \quad (2.10)$$

where  $V_m$  is the transmembrane potential,  $\lambda_{mye}$  and  $\tau_{mye}$  are the space and time constants for the myelinated axon respectively, and  $\zeta_x$  is the electric field (V/m) induced in the nerve (due to the transient magnetic field) with  $x$  being the direction of the axon. The terms  $\lambda_{mye}$  and  $\tau_{mye}$  can be represented as [55]:

$$\lambda_{mye} = d_i \sqrt{\frac{\rho_{mye}}{8\rho_a} \ln\left(\frac{d_o}{d_i}\right)} \quad ; \quad \tau_{mye} = \epsilon_o K \rho_{mye} \quad (2.11)$$

where  $\epsilon_o$  is the permittivity of vacuum ( $8.85 \times 10^{-8} \mu\text{F cm}^{-1}$ ),  $K$  is the dielectric constant of myelin (7),  $\rho_{mye}$  is the resistivity of myelin ( $7.4 \times 10^5 \text{ k}\Omega \text{ cm}$ ),  $\rho_a$  is the resistivity of axoplasm ( $5.47 \times 10^{-2} \text{ k}\Omega \text{ cm}$ ),  $d_i$  is a variable that depends on the fiber size, and  $d_o/d_i$  is the ratio of outer to inner axon diameter (1.333) [55].

It should be noted that equation (2.10) has been derived to calculate the threshold of the electric field (resulting from magnetic stimulation) required to achieve nerve excitation for a straight long axon. However, if the axon (at node  $n$ ) is terminated or bent with respect to the field lines, then the cable equation must be modified to accommodate these changes. The modified equation is:

$$\lambda_{mye}^2 \frac{\partial^2 V_m}{\partial x^2} - V_m - \tau_{mye} \frac{\partial V_m}{\partial t} = \lambda_{mye}^2 d \frac{(V_e(n,t) - V_e(j,t))}{\ell} \quad (2.12)$$

where  $d$  is a dimensional constant ( $1/m$ ),  $j$  is the index of the node inducing the stimulation due to its proximity to the  $n$ th node, and  $\ell$  is the shortest distance separating the  $j$ th node from the  $n$ th node. Equation (2.12) shows that the excitation of a bent nerve does not depend on the electric field's first spatial derivative but rather on the electric field itself.

As indicated earlier, many researchers applied the cable equation to their models, with the main objective of defining the threshold of the electric field required to induce nerve excitation. Their key findings can be summarized as follows:

1. The term on the right hand side of the cable equations (2.8,2.10), represents the axial component of the electric field gradient and they characterize the effect of the induced electric field on the transmembrane potential along the axon. This analogous "driving function" [56] can be considered equivalent to Rattay's "activation function"[1] during electrical stimulation.
2. Nerve excitation depends on the electric field first derivative along the nerve axis or equivalently on the second spatial derivative of voltage. However, some researchers

suggest that stimulation depends mainly on the electric field magnitude (peak) rather than its spatial distribution [54-57]. This can be attributed to the high local electric field resulting when the fiber is terminated or bent as the effect of this scenario is parallel to that of a spatial derivative of the applied field (see equation 2.12).

3. With respect to the effect of nerve size, all researchers agree that nerve excitation during magnetic stimulation is dependent on the axon diameter and length. Their conclusions indicate that axons with larger diameters require lower thresholds to reach excitation [55-57]. This is also applicable for short axons (less than 9 cm) [56].
4. In regard to defining the site of stimulation (virtual cathode), controversy still exists due to the problem complexity which can be attributed to the variation in coil parameters (shape, placement, orientation, current waveform), nerve parameters (size, length, bent, termination), and the conductive tissue environment.
5. In addition to the variables included in the cable equation, another critical parameter that should be considered is the rate of change of the generated magnetic field as it defines the induced electric field. It has been confirmed by Nagarajan [56] and Reilly [57], that bi-phasic waveforms (compared to mono-phasic) require lower thresholds to stimulate nerve fibers. Interestingly, these findings contradict that of Gorman and Mortimer [50], who reported a reduction in the thresholds when the waveform is changed from bi-phasic to mono-phasic during electrical stimulation.

Finally, it should be noted, that there are more complex models to represent nerve fibers. These models, which may include non-linear parameters, have not been considered as they result in more complex problems, especially with the addition of the magnetic field.

## 2.7 General Formulation for estimating the Electric Field during Magnetic Stimulation

It is well known that the electric field vector is governed by Maxwell's equation [58] and can be described as:

$$\nabla \times \bar{\zeta} = -\frac{\partial \bar{B}}{\partial t} \quad (2.13)$$

where  $\zeta$  is the electric field,  $B$  is the magnetic flux density, and  $\nabla \times$  is the curl operator. In order to minimize the number of unknown variables and render more manageable numerical calculations, it is customary to represent the magnetic field by a vector potential [59]. Assume that the vector potential ( $A$ ) was chosen, such that:

$$\bar{B} = \nabla \times \bar{A} \quad (2.14)$$

However, equation (2.14) does not fully define ( $A$ ), since *a vector is uniquely defined if and only if its curl, divergence, and value at one space point are known (Helmholtz theorem)*. Substituting equation (2.14) into equation (2.13) results in:

$$\nabla \times \left( \bar{\zeta} + \frac{\partial \bar{A}}{\partial t} \right) = 0 \quad (2.15)$$

Applying the vector theory (*the curl of any gradient vanishes*) to equation (2.15) results in:

$$\nabla \times \nabla \Phi = 0 \quad (2.16)$$

where  $\nabla \Phi$  represents electrostatic potential (electric scalar potential). By combining equations (2.15, 2.16):

$$\bar{\zeta} = -\nabla\Phi - \frac{\partial\bar{A}}{\partial t} \quad (2.17)$$

Equation (2.17) presents a formula that can be used to estimate the electric field that is generated by a magnetic field. It shows that the electric field generally consists of two sources and can be written as:

$$\bar{\zeta}_{Total} = \bar{\zeta}_{\phi} + \bar{\zeta}_A \quad (2.18)$$

where  $\bar{\zeta}_{Total}$  is the total electric field,  $\bar{\zeta}_{\phi}$  is the electrostatic potential (electric scalar potential) that arises from fixed electric charges ( $-\nabla\Phi$ ), while  $\bar{\zeta}_A$  represents the contribution of the induced electric field due to the transient magnetic field ( $-\partial\bar{A}/\partial t$ ). It should be noted that the effect of the  $\bar{\zeta}_{\phi}$  component is critical as it opposes the  $\bar{\zeta}_A$  component and consequently decreases the total electric field induced.

## 2.8 Estimation of the Induced Electric Field - Roth's Analysis

To estimate the electric field induced by magnetic stimulation, Roth et al. [60] computed  $\bar{\zeta}_{\phi}$  and  $\bar{\zeta}_A$  and added their effects. Their analysis can be summarized as follows:

When a circular coil is placed above the skin in a vertical position (current is normal), an electric field will be induced due to the coil transient current. This field will result in ion movement in the tissue and ultimately charges build up along the electric lines. As the skin conductivity is low, and the time required for the charge buildup is shorter than the rise time of the coil current, these charges will accumulate and create the static component of the

electric field. Similar fields would be generated at the interfaces between regions with different tissue conductivities.

To calculate  $\zeta_{\phi}$ , it is essential to determine  $(-\nabla\Phi)$  first. However, this is a difficult task as the source of  $\Phi$  (the accumulated charge) is not known. Roth et al. [60] determined  $\Phi$  by assuming that the tissue scalar potential obeys Poisson's equation:

$$\nabla^2\Phi = 0 \quad (2.19)$$

By applying the finite difference method (including suitable boundary conditions) equation (2.19) was solved.

To calculate  $\zeta_A$ , this group approximated the circular coil to a polygon shape and summed the induced electric field produced by each line segment [60]. This was achieved by using the coil geometry in conjunction with Amperes' law and calculating the vector potential  $\bar{A}$  at one point in space:

$$A = \frac{\mu_0 N i}{4\pi} \int \frac{dl'}{R} \quad (2.20)$$

where  $\mu_0$  is the permeability of free space and is equivalent to that of biological tissues [58],  $N$  is the number of coil turns,  $i$  is the coil current,  $dl'$  is a vector representing a small length of the coil (pointing in the direction of the current), and  $R$  is the distance from  $dl'$  to the point where  $\bar{A}$  is calculated. The electric field resulting from the transient field becomes:

$$\zeta_A = -\frac{\partial \bar{A}}{\partial t} = -\frac{\mu_0 N}{4\pi} \frac{\partial i}{\partial t} \int \frac{dl'}{R} \quad (2.21)$$

For distances equivalent to the coil size, the integral in equation (2.20) was approximated to one. Therefore, equation (2.21) can be represented as:

$$|\zeta_A| = N \frac{k}{10} \frac{\partial i}{\partial t} \quad (2.22)$$

where  $\zeta_A$  is in V/m,  $k=1$  and is in Wb/(A.t.m), and  $\partial i/\partial t$  is in A/ $\mu$ s.

For the above analysis, a few critical points must be addressed:

1. Despite the obvious influence of the static field component  $\zeta_\phi$  on the total field  $\zeta_{Total}$  (see equation 2.18), a literature search surprisingly revealed that no study has been conducted (in vitro or vivo) to measure the  $\zeta_\phi$  component or to quantify its physiological effects. In fact, Roth's paper was the primary document which discussed this issue in detail and it has been referred to by all other publications with no attempt to verify or contradict the findings.
2. Based on Roth's model, the  $\zeta_\phi$  component becomes significant especially when a coil is positioned normal to regions with different conductivities. Consequently, other researchers assumed that this component could be neglected if the coil flat surface is placed parallel and close to such regions [56,61,62]. This assumption applies for both Figure-8 and circular coils.
3. Roth's analysis showed that the static field  $\zeta_\phi$  has a subtractive effect on the total field  $\zeta_{Total}$  as it opposes the induced field  $\zeta_A$ . Subsequently, it can be concluded that, if the region of interest is composed of conductively heterogenous tissues, the total electric field will become rapidly weak as the magnetic lines penetrate each

successive layer.

4. In conjunction with the point above, Roth et al. [63] illustrated that the contribution of the static field  $\zeta_\phi$  is significant when the magnetic lines flow from a medium with higher conductivity to one with lower conductivity and it is negligible when the magnetic lines flow in the opposite direction.
5. Finally, it should be noted that equation (2.22) cannot be applied to calculate the electric field generated by coils with more complex geometry. This is due to the difficulties involved in solving the integral in equation (2.21). The alternative is to apply a numerical method.



## **Chapter 3      Design Aspects and Computer Simulations for Magnetic Coils**

It is well established that the stimulating coil represents the main component in magnetic stimulation as it determines field spatial distribution and consequently the resulting stimulation. This chapter discusses the design aspects of two new proposed coils and compares their performance to that of commercial coils. To provide the reader with a background of the coils used for magnetic stimulation, a history preview is presented covering a brief description of commercial coils as well as coils suggested by other researchers. To evaluate the proposed coils two sets of computer simulations using the Finite Element Method (FEM) in three dimensions combined with a transient solver, were implemented. The first set of simulations compared the proposed coils' field focality, depth of penetration, and strength to those of the commercial coils, while the second set quantified the effects of changing pulse configurations (mono-phasic, bi-phasic). As the software **MagNet** was used for these simulations, an outline describing the software, including problem description and solver selection, is illustrated. The key results from the simulations, including magnetic field densities and electric field gradients, are presented and discussed. Finally, a comparison covering potentials and limitations, between the commercial coils, coils suggested by other researchers, and the proposed coils, is provided.

### **3.1 Introduction**

Magnetic nerve stimulation is a non-invasive technique that can be used to excite both the peripheral and central nervous systems [3]. The major limitation in this technique is the lack of a focused field. At sufficiently high magnetic pulses the field diffuses stimulating the target population of neurons as well as adjacent tissues. This diffusion reduces the efficiency of the transferred energy from the stimulating coil to the targeted nerve and makes controlling the field inside the body extremely difficult. To compensate for this diffusion, excessively high amplitude currents are required to supply the coil with adequate energy to excite deep tissues, as is the case in transcranial magnetic stimulation (TMS). These high currents result in excessive heating of the stimulating coils especially in repetitive transcranial magnetic stimulation (rTMS). Considering the above limitations, this thesis presents two new coil designs with the objective of enhancing field focalty, increasing the depth of penetration, and improving the coil thermal performance.

### **3.2 Previous Coil Designs**

The first practical coil used for transcranial magnetic stimulation (TMS), a circular coil, was developed by Barker at the University of Sheffield [4]. Ueno et al. joined pairs of circular coils to form the “Figure-8” coil (also known as the “butterfly”coil) [64]. Compared to the circular coil, the advantages of the Figure-8 coil include an increase in the coupling of energy between the coil and the tissue as well as an enhancement in the field focality below the coil joint. Based on these advantages, and with an attempt to stimulate the heart, Mouchawar et al. and Hosono et al. developed and tested large Figure-8 coils that were

capable of delivering several Kilo joules per pulse [65,66].

Epstein et al. constructed a quadruple-loop coil with the objective of precise stimulation of upper motor units [32]. Their coil consisted of four loops which were curved to adopt the shape of the skull. The four loops were united at a central segment resulting in a stronger field below this segment (similar to that of the Figure-8 or butterfly coil). In conjunction with an MRI machine, three coils with various central segment lengths were superimposed on MRI images to map the stimulation sites within the brain. Assuming that the coils can produce the same electric field at one point, the site of stimulation was defined as the intersection of the electric fields generated by the three coils.

To improve field focality, Roth et al. suggested a four leaf magnetic coil [67] which consisted of four sets of (nearly) circular windings. According to their hypothesis, this coil provides a well defined site of stimulation under the coil center (the junction of the windings). This hypothesis was confirmed by *in vitro* experiments in which mammalian peripheral nerves were stimulated [68].

In the mid 1990's some researchers attempted further improvements to the conventional coils. Ren et al. modified the Figure-8 coil producing the "slinky" coil which consisted of multiple circular loops joined together at one point [69]. Using different numbers of loops (3,5,7), several versions of the slinky coil were constructed and tested with the objective of determining the most effective (focal) coil. In a similar effort to enhance the field focality, Knaulein and Weyh decentralized the turns of the butterfly coil producing an "eccentric coil" [70].

In the past two years the efforts of designing new coils resulted in magnetic core coils

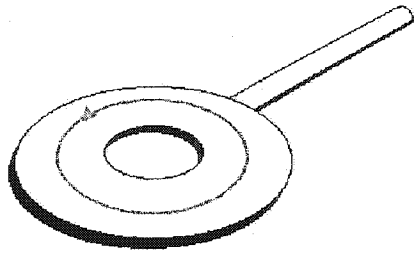
and coils consisting of multiple loops placed in different orientations.

With respect to the magnetic core coils, Davey and Epstein proposed a half toroid magnetic core coil made of Supermendur material [71]. They suggested that the introduction of the magnetic material improved field strength, focality and consequently enhanced the coil performance during TMS. In parallel, Carbutaru and Durand proposed a coil with a full toroid core made of Supermendur material [72]. According to their theory, the immersion of the coil in a conducting medium, which is in contact with the skin, results in induced electric fields both perpendicular and parallel to the skin.

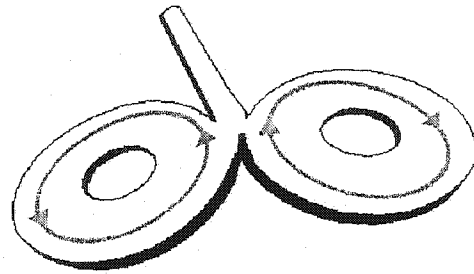
Regarding coils with multiple loops, Lin et al. constructed various versions of the slinky coil [73]. In an effort to achieve maximum field focality during functional magnetic stimulation (FMS), this group varied the coil turns number, distribution, orientation, and shape. Further improvements to the coils used in FMS were attempted by Hsiao and Lin as they proposed and constructed the spiral coil which they used to improve the stimulation of expiratory muscles [74].

Recently, Hsu and Durand proposed a novel coil with the objective of improving the localization of magnetic stimulation [75]. Their coil consisted of five loops: two loops, resembling a butterfly coil, were positioned in one plane, a third loop was positioned normal to the joint of the butterfly coil, while the fourth and fifth loops were placed on each side of the third loop. The addition of the central normal loop enhances field depth of penetration while the combination of the fourth and fifth normal loops (one on each side) minimizes the stimulating field outside the region of interest.

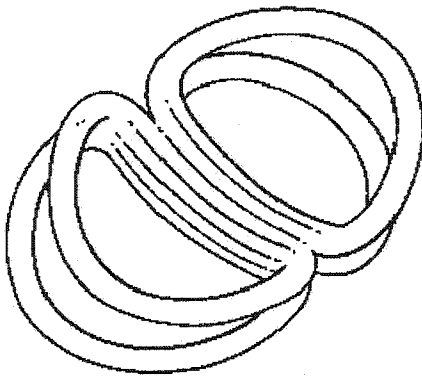
Figure 3.1 illustrates the various coils described above.



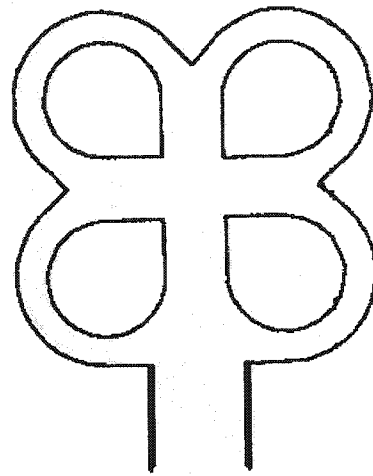
(a)  
Basic circular coil (after 4)



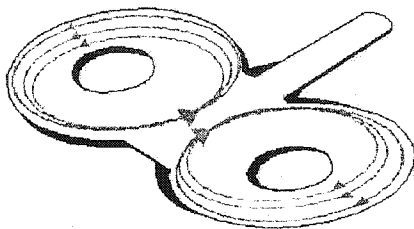
(b)  
Figure "eight" coil (after 64)



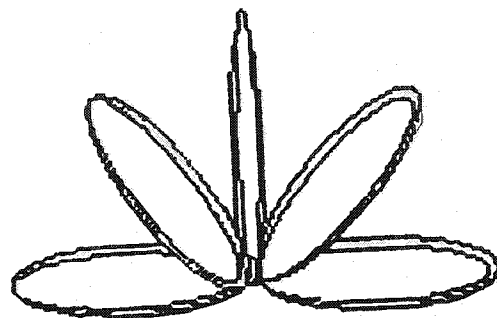
(c)  
Quadruple-loop coil (taken from 32)



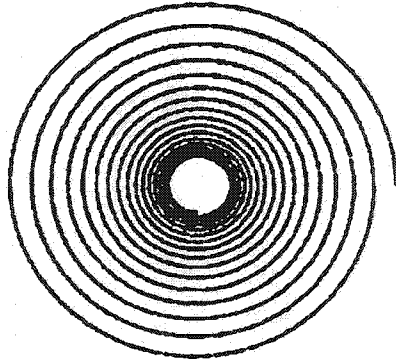
(d)  
Four leaf coil (taken from 68)



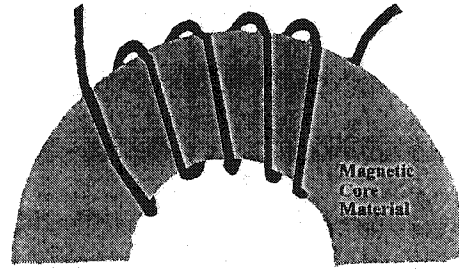
(e)  
Eccentric coil (after 70)



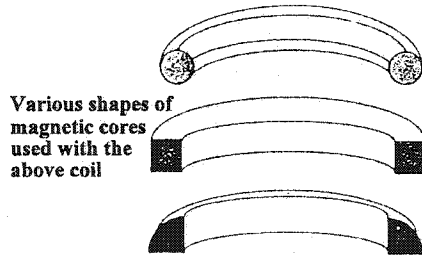
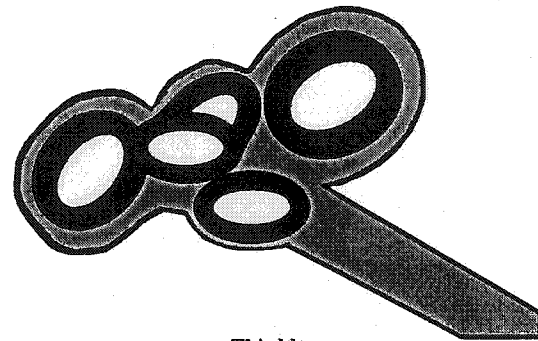
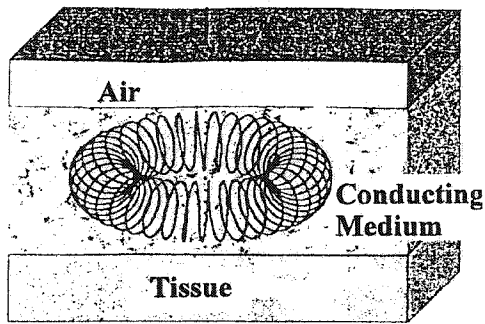
(f)  
Slinky coil (taken from 73)



(g)  
Spiral coil (taken from 74)

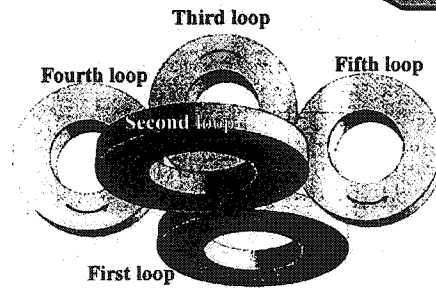


(h)  
Magnetic core coil (taken from 71)



Various shapes of magnetic cores used with the above coil

(i)  
Full toroid core coil (taken from 72)



(k)  
Multiple loops coil (taken from 75)

**Figure 3.1**  
Various types of magnetic stimulation coils.

### 3.3 The Proposed Coils

In previous work two types of stimulating coils were proposed: an air core and a magnetic core [76]. The primary objective of the proposed coils was to obtain a focused magnetic field which can be adjusted according to the nerve depth and the required level of excitation. Figures 3.2 and 3.3 show the proposed coils.

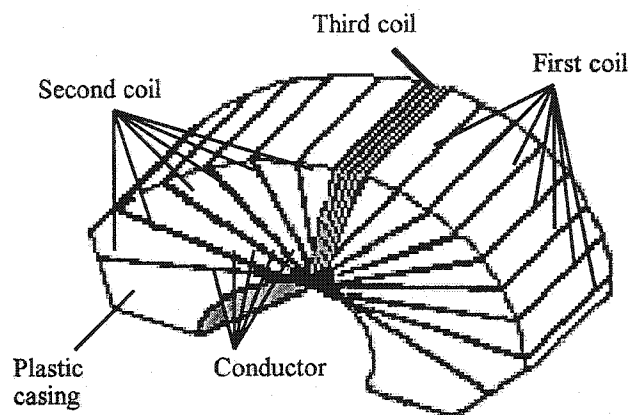


Figure 3.2  
The proposed air core coil.

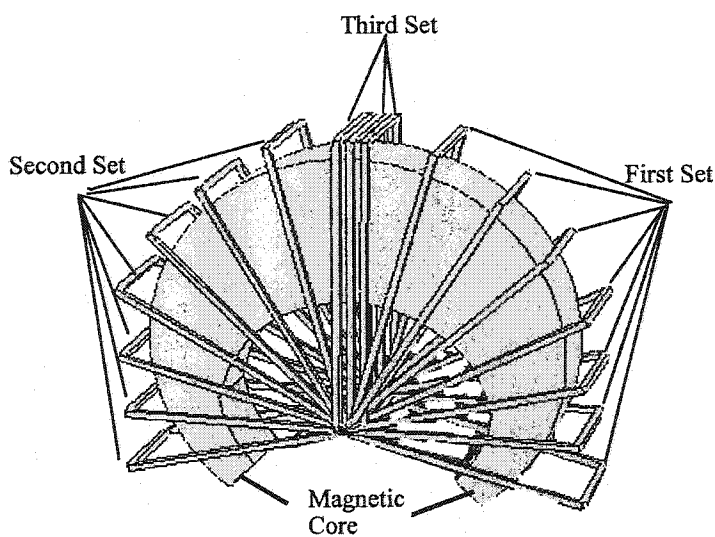


Figure 3.3  
The proposed magnetic core coil.

The design aspects of the proposed coils were based on modifying Ren et al.'s slinky coil [69]. The modifications were introduced in three stages. First, the number of coil turns was increased to 14 turns, which were divided into two sets and uniformly distributed along an arc. Second, a third set of windings was added and positioned normal to the plane of interest. Third, a core with magnetic properties was introduced to the coil. The combination of the first and second modifications resulted in the proposed air core coil, while the combination of all three modifications created the proposed magnetic core coil. Other than the difference in the core material, both coils are similar in shape, size, number of turns, and type of conductors.

At this stage, it is critical to discuss the theoretical aspects, implications, and contributions of the above modifications to the proposed coils. These can be summarized by the following:

1. As has been suggested by Ren et al. [69] and confirmed by Lin et al. [73], increasing the number of loops in the slinky coil resulted in improving the field strength. This is based on the concept that the summation of magnetic lines for a tightly wound coil is higher than that of a coil with split windings (due to the subtractive cross field). Accordingly, for the slinky coil, a stronger field is expected below its joint (assuming it to be the region of interest) and a weaker field elsewhere. In a similar manner, and with the objective of increasing the effect of the cross field in the proposed coils, it was decided to increase the number of windings to 14. This number was selected to meet two objectives. First, to generate uniform flux density within both coils which consequently enhance their performance and minimize the



(hysteresis) losses associated with the magnetic core coil. Second, to ensure that the resultant inductances of both coils are within the range of standard stimulating coils (10-30 $\mu$ H). More details regarding the role of the coil inductance are outlined in the following section and in Chapter 4.

2. The addition of the third set of windings was deduced on the basis of work by previous researchers investigating the impact of coil orientation [61,77,78]. When supplied by a separate source of current, which can be independently varied, the third set of windings provides the flexibility to control the level of field penetration. Further, the placement of this set normal to the joint of the other windings will maximize the field below the joint (across the targeted nerve) and weaken it elsewhere as the flux lines generated by the third set cancel that of other windings.
3. The introduction of the magnetic core to the coil creates an enclosed path within the coil for the magnetic lines to follow resulting in a more controlled (focused) field. The forms of control include directing the field to the region of interest and minimizing its diffusion within the surrounding tissues. In addition, the magnetic core minimizes the pulsing currents needed to achieve the required stimulations. This reduction in currents will decrease heat build up and consequently will improve coil thermal performance.

### 3.4 Modeling the Proposed Coils

When modeling the proposed coils the following key points were addressed:

#### A. Coil conductor: type, layout, and number of turns

The coil conductor considered for the simulations was a solid, square copper wire (size 12) with a conductivity of  $5.7 \times 10^7$  S/m. For each modeled coil, three sets of windings were defined for a total of 17 turns (7 turns per set for each side and 3 turns for the perpendicular set). The three sets were considered to be connected in parallel with the side turns distributed across arcs of  $-15^\circ$  to  $75^\circ$  and  $105^\circ$  to  $195^\circ$  respectively ( $15^\circ$  separation between consecutive turns) with the perpendicular turns tightly wound. This winding arrangement generates the required field strength and results in an acceptable coil inductance (12 to 15  $\mu\text{H}$  for an air core coil and 20 to 25  $\mu\text{H}$  for a magnetic core coil). It should be noted that the coil inductance represents an extremely critical parameter in magnetic stimulation as it determines coil current peak and defines pulse configuration (see details in Chapter 4).

#### B. Magnetic core geometry

It is evident that the field distribution for an air core coil is defined by the geometric layout of its conductors while the core shape of a magnetic coil determines its field distribution. Based on this concept, it was decided to model the magnetic core such that it intensifies the field within the targeted area while maintaining the flux density below core saturation. To meet the above criteria the following adjustments were incorporated:

1. Since a large number of turns covers the middle section of the core (higher current

density), this section was designed wider than the remainder of the core.

2. The distance between the two core ends was designed to be the shortest distance between each end and any point on its opposite side. This critical length will ensure that the flux lines will travel through a well defined path (starting from one core end through the target area and ending at the other core end).
3. Due to the air gap between the core ends, these ends were modeled to be the narrowest sections of the core. This increases the flux density delivered to the target and subsequently improves the volumetric coupled magnetic energy.

### C. Magnetic core material

The coils currently used for magnetic stimulation are primarily air core coils (circular, Figure-8, butterfly) which are capable of producing high magnetic pulses (1-2.5 Tesla) with short duration ( $200\mu\text{s}$ -1ms) [15]. For a magnetic core coil, a Supermendur material (which operates linearly with a flux density up to 2.2 Tesla) represents an excellent choice for this application [71]. Other materials that can be considered for this application, although costly, are cobalt alloys (which operate with a maximum linear range of 1.8-1.95 Tesla) [76]. It should be stated that severe magnetic losses (eddy currents losses) will result if the above materials were fabricated from standard laminations (200 to  $400\mu\text{m}$ ). This is due to the fact that the magnetic losses associated with these materials increase tremendously as the operating frequency increases. To overcome this problem, thin laminations (25 to  $50\mu\text{m}$ ) must be used when fabricating the core.

### **3.5 Estimation of the Induced Electric Field using a Numerical Method**

In magnetic stimulation, the calculation (estimation) of the electric field induced within the tissue is critical as it determines the stimulation area and the level of excitation. However, for the proposed coils, this estimation is not an easy task due to many constraints and difficulties which include: coil complex shapes, the non-linear behavior of the magnetic core, the transient state of the supply, and the heterogenous nature of tissues. Considering these factors, it becomes difficult to solve this problem with precise results using an analytical method. Alternatively, a numerical method is recommended. There are various numerical methods available with the most commonly being: finite difference, integral formulation, circuit models, and finite elements. From these options, the finite element method (FEM) was selected to solve this problem as:

1. FEM can be applied to a problem with complex geometry that may include various types of boundaries. This problem has a complex shape and is composed of many boundaries.
2. FEM can be applied to a problem that consists of regions with heterogeneous electrical characteristics, as is applicable to this problem.
3. In FEM, the mesh (grid) can be refined according to the solution requirements. This is compatible with this problem as the area of interest (the nerve) is very small relative to the remainder of the region.

To have a tractable FEM solution, it is necessary to introduce the following assumptions and approximations:

1. As the operating frequency for magnetic stimulation ranges between 2-10 kHz, the corresponding wave lengths are much longer than any distance associated with the human body. Accordingly, it can be assumed that the associated fields are primarily governed by their first time derivative and are independent of the second derivative.
2. The skin depth effect is negligible as the magnetic field produced by the induced current in the tissue is much smaller than that produced by the coil current.
3. At a frequency of 10 kHz, the capacitive effect of all tissues can be neglected and they can be considered purely resistive (see appendix A for more details).
4. The targeted tissues are homogeneous, isotropic and have volume conductors with simple geometry. This is the least valid assumption, since all biological tissues are quite inhomogeneous and many are anisotropic. However, this assumption has been accepted for modeling and calculating electromagnetic fields of this type.

### 3.6 Calculations of the Magnetic Vector Potential $\bar{A}$

Recalling equation (2.18):

$$\bar{\zeta}_{Total} = \bar{\zeta}_{\Phi} + \bar{\zeta}_A$$

From the above equation, considering that the effect of  $\zeta_{\phi}$  is minimal and can be neglected (details in Chapter 5), the total electric field ( $\zeta_{Total}$ ) can be determined using  $\zeta_A$  only. To calculate  $\zeta_A$ , the software **MagNet** (which is based on the FEM) will be used [79].

Since the function responsible for stimulation is transient, a time stepping procedure, such as the Crank- Nicolson scheme, is required to obtain the value of the magnetic vector potential over different periods of time. When applying this technique, it is assumed that the initial value of the magnetic vector potential to be  $\bar{A}_0$ , while the new value  $\bar{A}_1$  can be calculated after a short time step. As time progresses, the value  $\bar{A}_n$  is defined according to the field instantaneous value as well as the value of  $\bar{A}_{n-1}$  from the previous time step. The advantage in using the Crank-Nicolson method for this analysis is that it provides a solution with unconditional stability [80]<sup>1</sup>. However, during the initial time steps, an oscillation may occur within the calculations. The amplitude of this oscillation depends on the size of the element, the time step, the material properties and the calculations' initial step. To reduce the severity of this oscillation, it is critical to select a small element size and a short time step.

---

<sup>1</sup>

Unconditional stability may be taken to mean that if the magnetic vector potential distribution at time  $t$  is transformed to the frequency domain using a Fourier transform, the amplification for every frequency component decays with time.

### 3.7 Problem Definition and Simulations

The analyses conducted in this study, with the objective of evaluating the proposed coils, used the median nerve as the targeted area. Since the median nerve is well defined, a model with distinctive boundaries that represents it can be developed. The alternative choice is a model that represents the cranial region. However, using a cranial model results in a problem that is difficult to solve or requires tremendous simplifications which leads to unrealistic results. The simulations applied to model the median nerve, using the software **MagNet**, involves pre-processing of the problem, solving the problem, and post processing of the results. A summary of the steps followed in these simulations is listed below.

#### 1. Describing and constructing the problem geometry

The process of assembling the problem geometry involves two steps. In the first step the problem is defined within a set of two dimensional planes, while in the second step, the two dimensional planes are combined creating a three dimensional model. Figure 3.4 illustrates a simplified model representing the median nerve within the upper limb.

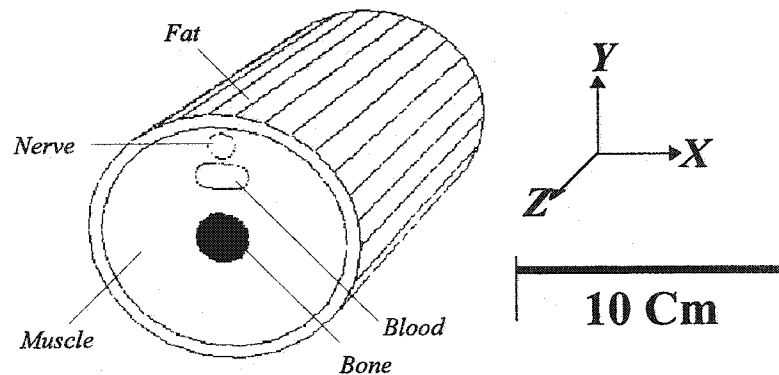


**Figure 3.4**  
A model representing a cross section of the upper limb at the junction of the proximal and middle thirds of the humerus (outside diameter 10cm, length 20cm).

Figures 3.5 and 3.6 illustrate a combination of the upper limb with the Figure-8 and the magnetic core coil respectively.

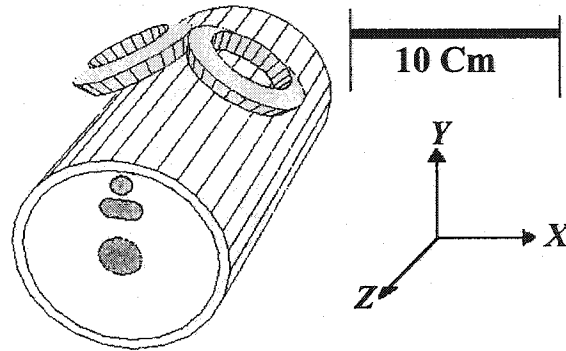


**Figure 3.5**

A model representing a Figure-8 coil projected above a section of the upper limb. The outer diameter of this coil, 10cm (X-axis), was implemented based on the size of a clinical coil (Dantec Company).

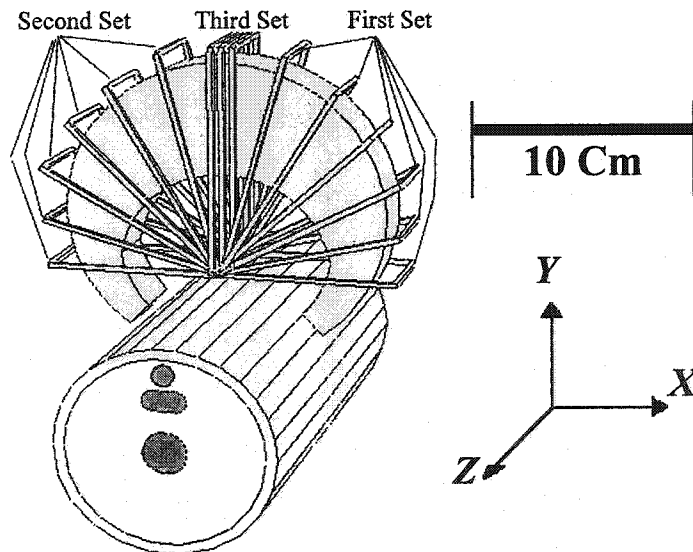


**Figure 3.6**

A model representing a magnetic core coil projected above a section of the upper limb. The thickness (depth-Z axis) of this coil is 5cm.



## 2. Introducing nodes/elements to create a suitable mesh

For this problem, careful mesh distribution was considered. To ensure minimum error when estimating the field, high node densities were applied especially across the nerve region and at the coil- arm interface. Using the mesh tool box provided by **MagNet**, the total mesh generated for these analyses included 101,805 nodes and 175,070 elements.

## 3. Defining the regions (materials) properties

After applying the mesh, the electrical conductivities of the heterogeneous tissues included in this model were assigned according to Table 3.1 [81]. For the magnetic characteristics, the relative permeabilities of the various regions were considered to be similar or equal to that of free space ( $\mu_r=1$ ) [58].

Tissue	Transverse Conductivity $\sigma_t$ S/m	Longitudinal Conductivity $\sigma_l$ S/m
Skin	0.5	0.5
Fat	0.045	0.045
Muscle	0.085	0.55
Bone	0.013	0.013
Nerve	0.05	0.5
Blood	0.68	0.68

Table 3.1  
Tissue conductivities at 10 kHz (after 81)

## 4. Implementing appropriate boundary conditions

The boundary in the XY-plane for this problem was defined as a circle with a radius of 50 cm from the center of the arm, while the boundary in the Z-axis (depth) was defined

20 cm away from the front and the back cross sections of the arm. Assuming that the magnetic flux diminishes at the boundary, Dirichlet's boundary conditions were considered.

5. Applying the forcing function (voltages, currents)

An algorithm was written, using the software **Matlab** to generate the pulsing currents (forcing function) required to supply the coils. Figure 3.7 shows a bi-phasic decayed sinusoid wave (which will be referred to in this thesis as a pulse) generated to supply Figure-8, air core, and magnetic core coils (for details regarding the circuit parameters, see Appendix C).

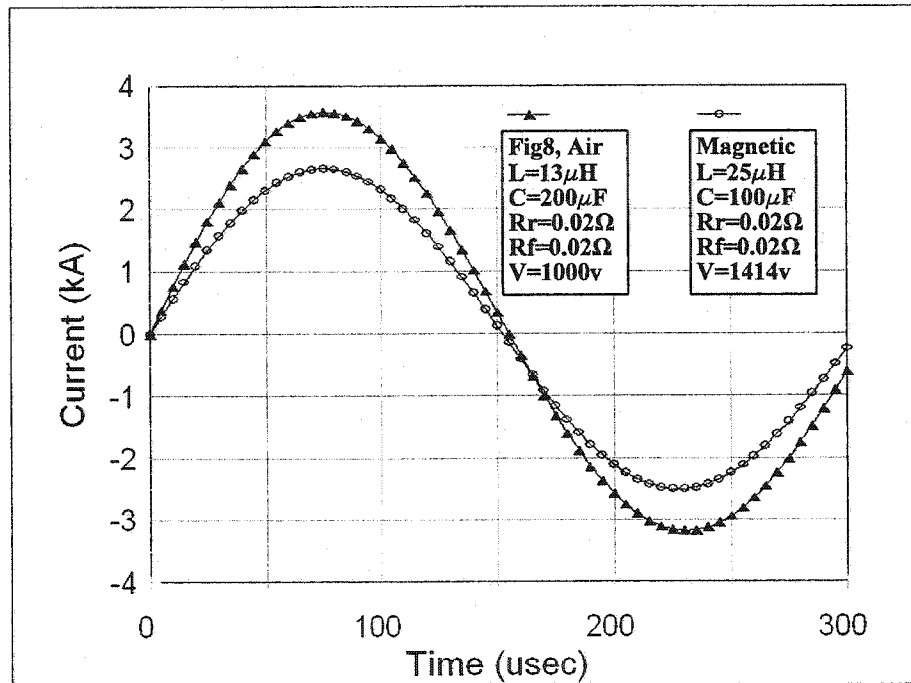


Figure 3.7  
Bi-phasic current pulses generated to supply Figure-8, air core, and magnetic core coils.

The corresponding current, for the Figure-8 coil, is divided into two equal parts, while the currents for the proposed coils are divided into three equal parts: two parts were

divided among 14 turns, while the third part was divided among the 3 windings of the third perpendicular set. Two key points must be stated regarding the above waveforms: first, these waveforms were constructed based on monitoring the current pulses generated by a commercial system (Dantec Magpro), second, as the Figure-8 and air core coils have the same inductance ( $13\mu\text{H}$ ), the same current waveform was applied to each of them.

#### 6. Solver selection

The primary objective of the computer simulations is to determine the most effective parameters that govern the proposed coils, such as, coil configuration, size, shape, number of turns and windings distribution. To simplify the evaluation process of these parameters, a static solver was used in the preliminary simulations. Due to its simplicity and short running time, this solver can be used as a quick evaluation for any change in the problem parameters and consequently, improve the designs within a relatively short period of time. As the problem critical parameters were established, a transient solver was applied to evaluate the proposed coils. After a few trials using the transient solver, it was concluded that a time step which ranges between  $2\text{-}5\mu\text{s}$  is a practical choice for this problem as it provides solution stability and enables reasonable execution time. Considering that the longest pulse period is  $350\mu\text{s}$ , it was decided to define the duration of the time window for all analyses to be equal to  $400\mu\text{s}$ .

#### 7. Post processing the data

The post processor stage in **MagNet**, which is based on a stack mechanism, is responsible for extracting the variables of interest from the results. Three stacks are included in this stage: the *field stack* which stores the geometry and the solution, the *curve stack*

which stores field values along a contour defined over the solution, and the *numeric stack* which stores simple numbers or constants. These stacks provide the user with all the functions needed (mathematical and algebraic) to calculate various variables such as: flux density, current density, inductance, stored energy, forces, torque, etc.

### 3.8 Results

Figure 3.8 shows the magnetic flux density along the Y-axis (see Figure 3.4) starting from the coil interface with the arm and penetrating through the tissues to the bone center.

Figure 3.9 shows the magnetic flux density along the perimeter of a cylinder having a radius of 3.75 cm (X-axis). With its center defined at the center of the arm, the cylinder radius represents the distance between the center of the arm and that of the nerve ( $r = [x^2 + y^2]^{0.5}$ ).

Figure 3.10 illustrates the magnetic flux density along the Z-axis of the above cylinder.

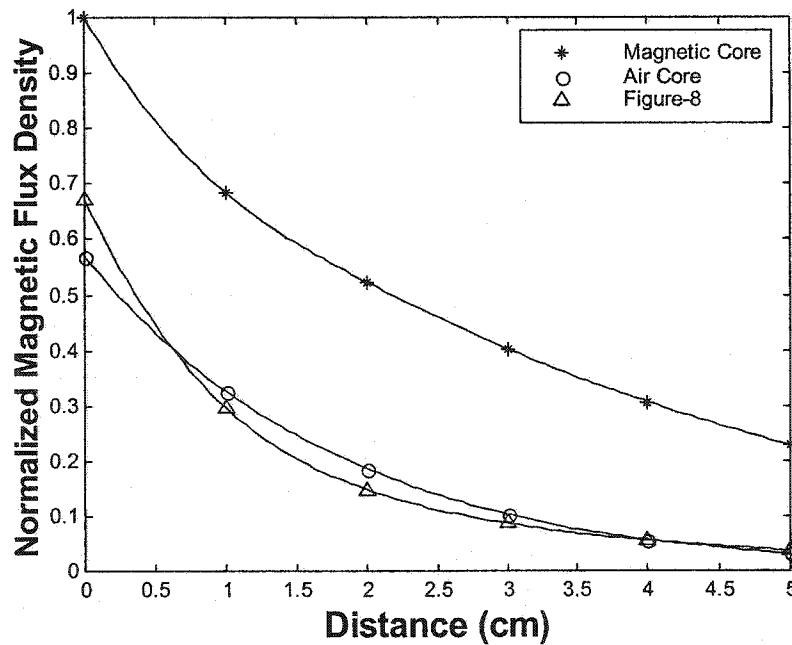


Figure 3.8  
Magnetic flux density along the Y-axis (depth of field penetration).

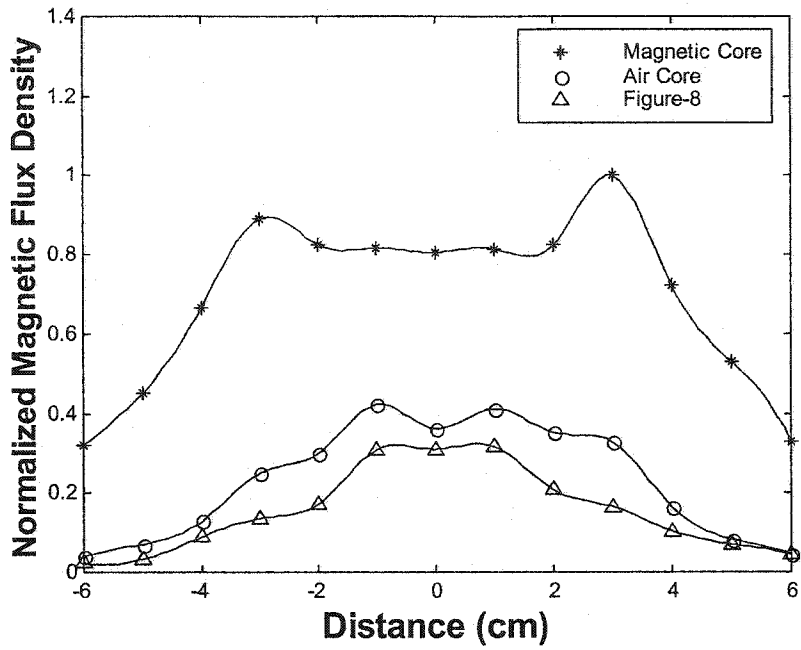


Figure 3.9  
Magnetic flux density along the X-axis (field focality).

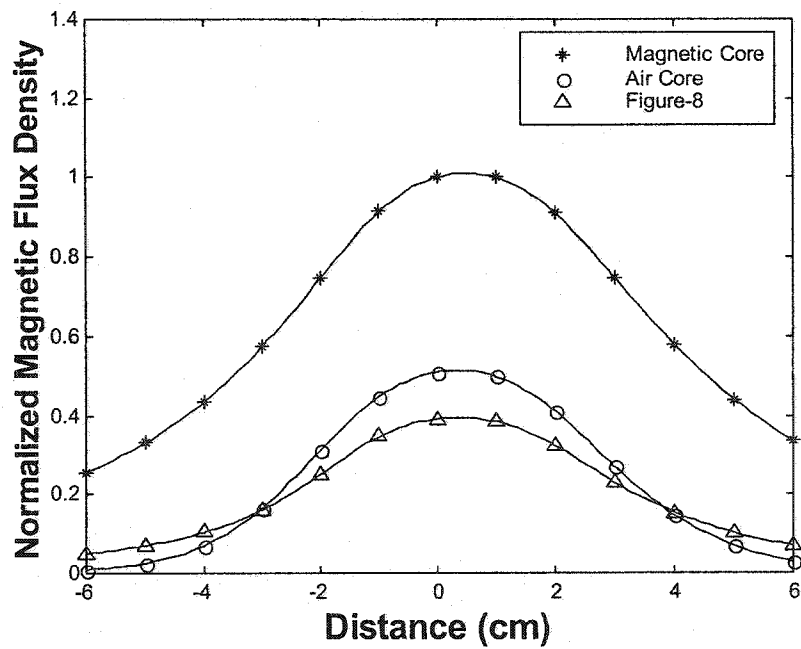
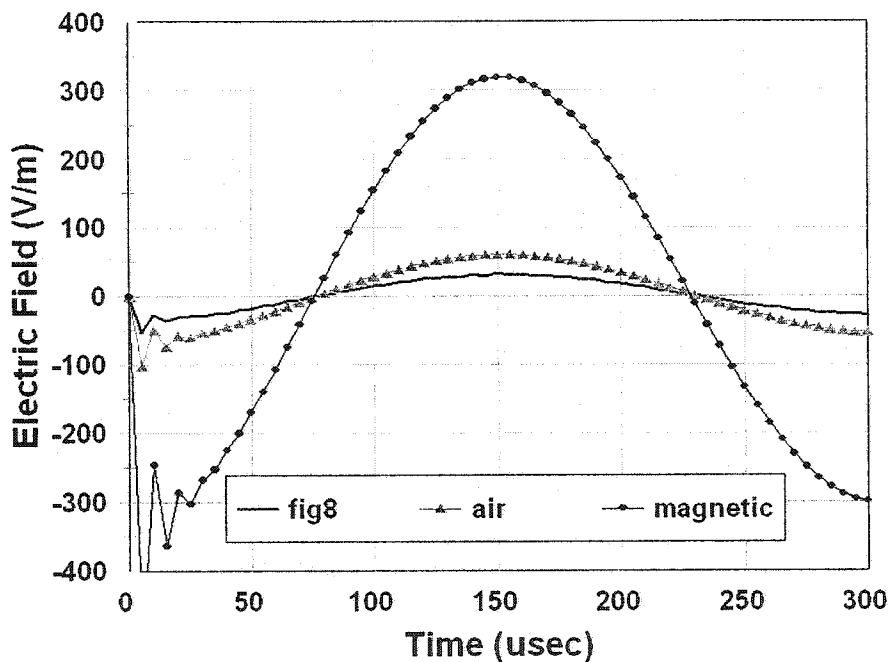


Figure 3.10  
Magnetic flux density along the Z-axis (field focality).

From Figure 3.10, it can be seen that the magnetic field gradient (along the Z-axis) of the air core coil is higher than that of the Figure-8, hence better stimulation is expected. Also, from the above figures, it can be seen that the flux density and the field gradients produced by the magnetic core coil are higher than those generated by the air core or Figure-8 coil (almost double). These findings agree with the work done by Ren et al.[69], Davey et al. [71], and Lin et al.[73] and are consistent with the previous 2-dimensional analysis [76]. However, the advantage in using the 3-dimensional analysis is that it generates a more realistic magnetic field distribution for the stimulating coil and the surrounding regions.



**Figure 3.11**  
The induced electric fields resulting from the application of bi-phasic current pulses.

Figure 3.11 shows the electric fields induced in the nerve as produced by the three coils. From this figure it can be seen that the air core coil generated an electric field that was

twice as high as the Figure-8 coil. This result agrees with the work done by Lin et al.[73] as they confirmed that this type of windings distribution enhances both field focality and strength. From the same figure, it can be seen that the magnetic core coil generated an electric field five times higher than that of the air core coil. This result was expected as the energy coupled between the arm and the magnetic core coil is higher than the energy coupled by the other two coils. Also, these findings agree with Davey et al. [71] who suggested that the introduction of a magnetic core improves field strength.

### **3.9 The Effects of Pulse Configuration**

To investigate the effects of pulse configuration (bi-phasic vs mono-phasic), it was decided to run another set of simulations using a mono-phasic pulse with its initial phase identical to that of bi-phasic (see Appendix C). These simulations were conducted by implementing the same problems described in the previous section (Figure-8 coil and the two proposed coils). As the current waveform is the only difference between the two sets of simulations, an algorithm was written using the software **MatLab** to generate the current pulses required. Figure 3.12 shows the mono-phasic current pulses generated to supply the Figure-8, air core, and magnetic coils (for more details regarding the waveform and the circuit parameters listed in this figure, see Chapter 4 and Appendix C). The simulations for this section were conducted by following the same steps outlined in the previous section. Figure 3.13 illustrates the electric fields induced at the nerve by the three coils when using a mono-phasic pulse. With respect to the flux densities, linearly proportional results comparable to that described in the previous section were obtained.

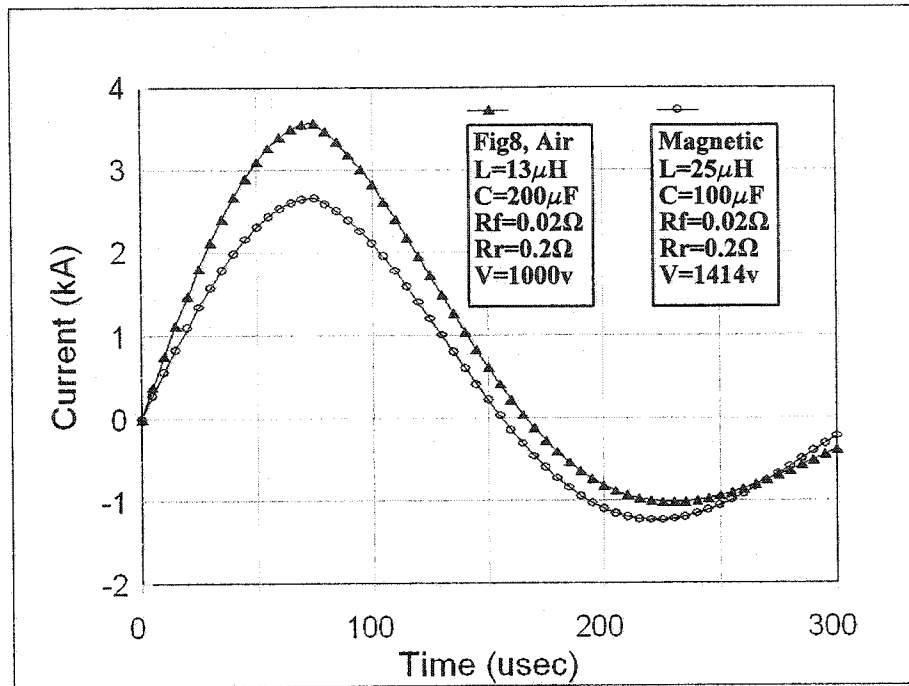


Figure 3.12  
Mono-phasic current pulses used to supply Figure-8, air core, and magnetic core coils.

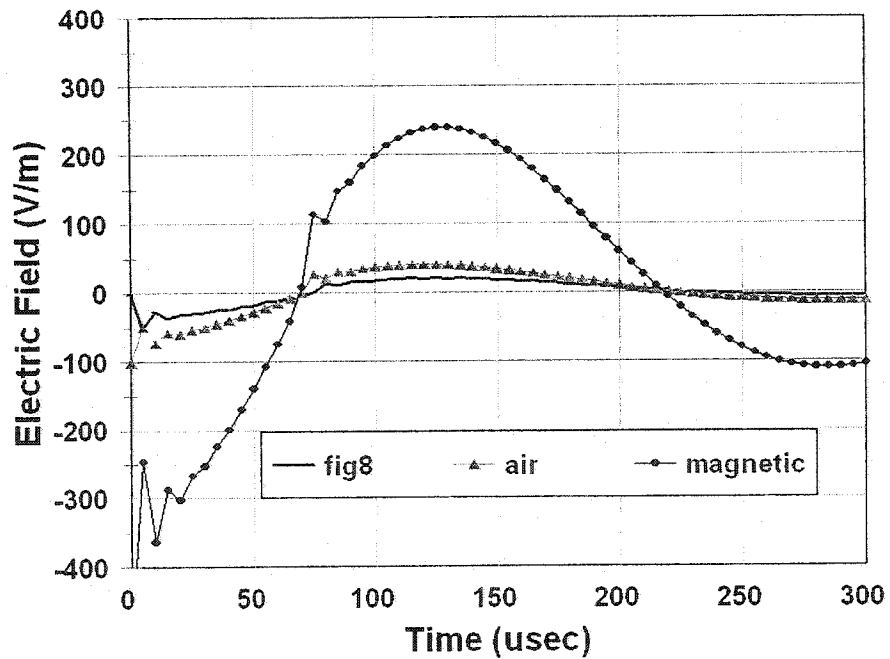


Figure 3.13  
The induced electric fields resulting from the application of mono-phasic current pulses.



From Figure 3.13, distortions can be noticed in the induced electric field waveforms as they change polarity from negative to positive. These irregularities are attributed to the instantaneous change in the current damping ratio (see Appendix C). To minimize this effect, a smaller time step (less than  $2 \mu\text{s}$ ) must be adopted by the transient solver. However, the use of such a small time step was avoided as it results in a tremendous increase in the time required by the solver to accomplish its task.

Comparing the waveform in Figure 3.13 to that in Figure 3.11, it is obvious that the induced electric fields for bi-phasic waveforms are higher than mono-phasic ones. Also, it can be noted, from both figures, that the area under the curve of the proposed magnetic core coil is larger than that for the other two coils due to the energy stored in the magnetic core.

In conclusion, the results obtained from both analyses clearly indicate that a bi-phasic waveform is more effective than a mono-phasic waveform.

### **3.10 A Comparison between the Proposed Coils and Other Coils**

Thus far, it is critical to compare the proposed coils with those described earlier. In addition to being used in many clinical applications, the coils considered for the comparison were selected due to the similarity of their designs with that of the proposed coils.

1. Figure-8 coil (Uno et al. [64]): It is well established that the Figure-8 coil is the most commonly used in clinical applications due to its field focality, practical size and relatively light weight. Compared to this coil, the simulation results revealed that both proposed coils provide higher induced electric fields as well as better focality.

From a practical perspective, the only limitation in replacing the Figure-8 coil is the additional weight introduced by the magnetic core material.

2. Slinky coil (Ren et al. [69]): It has been shown that the performance of the slinky coil (field focality and strength) is better than that of Figure-8 [69]. Lin et al. confirmed these findings and suggested the use of this coil for Functional Magnetic Stimulation (FMS) [73]. When comparing the induced field of the proposed air coil (slinky-type) to that of Figure-8, the simulation results show an agreement with the above investigations as the air coil generated higher and more focused induced fields.
3. Half toroid magnetic core coil (Davey et al. [71]): The simulation results showed that the magnetic core material enhances the coil performance. These results agree with the conclusions of Davey et al. who recently added magnetic material (partial toroid core) to the stimulating coil[71]. According to their design, which was implemented commercially by Neotonus Inc., the addition of the magnetic material improved field strength and focality. The main difference between their design and the proposed magnetic coil is its unique core geometry which adapts and controls the flux lines more effectively. Further, the suggested core shape results in minimum magnetic reluctance (losses) as well as an acceptable coil's size and weight.
4. Multi-loop coil (Hsu et al. [75]): Although this coil is not readily used commercially, it has been included in this comparison due to its similarity to the proposed air coil. The main difference between this coil and the air coil (assuming that the first, second and third loops of both coils are matching each other as they generate the same field pattern) is the introduction of the fourth and fifth loop. Nevertheless, in the proposed

air core coil, the function of the fourth and fifth loops (generating cross field<sup>2</sup>) was accommodated through the distribution of the multi-side turns.

In addition, comparing this coil to the magnetic core coil, the introduction of the magnetic core minimizes the field outside the region of interest which consequently enhances the field focality.

In summary, the simulation results in conjunction with the above comparison confirm that the design of the proposed coils enhances the induced field strength and focality. Clearly, the use of the ferromagnetic material plays a major role in improving the field delivered by the stimulating coil to the targeted area. Further, the addition of the third set of windings provides flexibility in delivering the required stimulus. For instance, if deep penetration is required, the current supplied to the first and second coils should be higher than the third (perpendicular) coil. However, if the target is not deep, effective stimulation can be achieved by supplying current to the third coil only [76].

Finally, it is critical to mention that the design of the proposed coils was suggested [76] prior to and in parallel with the work published by other researchers (see history preview).

---

2

Due to insulation, placement, etc; gaps occur between the coil turns. These gaps result in a variation in the magnetic field around each coil turn when compared to other turns. Consequently, non-linear field, current, and voltage distributions across the coil turns are expected.

## **Chapter 4      Design and Construction of Magnetic Stimulators and Measuring Apparatus**

This chapter covers the design and fabrication procedures for the systems used during the experimental phase of this thesis. These systems have been grouped into two sections. In the first section the general guidelines for designing and constructing a magnetic stimulator are presented. These guidelines cover theoretical concepts, hardware aspects and components required to build a stimulator. The critical points discussed in this section are based on key findings and difficulties encountered during the process of building two units. Some suggestions to improve future designs are also provided.

There is a discussion in the second section of this chapter of coil testing apparatuses used by previous researchers as well as two new prototypes developed for this thesis. In both prototypes the induced voltages are measured and subsequently mapped to their respective electric fields. The first prototype maps the induced fields within a spherical volume (resembling the head), while the second captures the fields within a two dimensional plane. Finally, the advantages of using the proposed measuring apparatuses are outlined.

## 4.1 The Design and Construction of a Magnetic Stimulator

To effectively compare the performance of the proposed coils to coils that are currently used, a stimulator capable of withstanding a range of testing conditions is required. Because such a device is not available, modification of an existing system or acquiring a custom built unit were identified as two possible options. However, modified or custom built clinical equipment are extremely expensive in terms of capital cost and maintenance and have limited warranties. Hence, it was decided to build a new system that can be used for the experimental phase of this work.

### 4.1.1 The Selection of Main Components

Magnetic stimulators employ two main elements: a pulse generator and a stimulating coil that couples the energy to the target nerve via a magnetic field. A typical pulse generator used in these systems consists of a high voltage power supply and a capacitor. Using switching circuitry, the capacitor is usually charged to a high voltage and discharged into the stimulating coil. Figure 4.1 illustrates this concept.

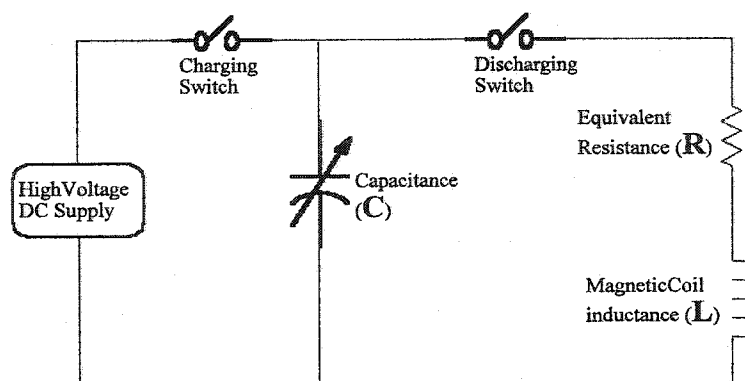


**Figure 4.1**  
A simple equivalent circuit of a magnetic stimulator.

In Figure 4.1,  $L$  is the inductance of the stimulating coil,  $R$  and  $C$  are the discharging circuit resistance and capacitance respectively. These three elements are the main parameters that determine the current pulse during magnetic stimulation. To achieve the required stimulation, this current pulse should have sufficient magnitude and duration. For such a pulse, the amplitude is defined by the electric field required to initiate neuro-excitation while its duration is bounded by the nerve depolarization time and the fundamental law of excitation embodied in the strength duration relation (S-D curve)<sup>1</sup>. The peak of typical current pulses ranges between 1 and 10 kA. The rate of change varies from 30 to 150 A/ $\mu$ sec.

As the time required for nerve depolarization ranges between 0.1-0.5msec, the circuit components ( $L$ ,  $R$ ,  $C$ ) should be selected carefully to ensure an operating frequency that ranges between 2-10 kHz. Of the three components, the coil inductance  $L$  cannot be changed as its value is predetermined by the coil design. Typical values of commercial coil inductances range between 10-30 $\mu$ H.

To realize the desired output (high pulsing current) while maintaining minimum losses, the circuit equivalent resistance  $R$  should be kept low. Nevertheless, an external resistance may be added to the discharging circuit with the objective of generating a monophasic waveform (see Appendix C). An alternative to the above is to increase the circuit capacitance, however, due to the weight, size, and cost of these capacitors, the addition of resistance is preferable. In addition, this option is practical since monophasic stimulation requires limited energy consumption as it is primarily used for single-pulse investigation and

---

<sup>1</sup> An S-D curve represents the relationship between the threshold amplitude of a stimulus and the first phase duration for which that stimulus must be applied to elicit a tissue response [82].

rarely for repetitive stimulation. Typical values of  $R$  range between 0.1-0.2  $\Omega$ .

The charging capacitor  $C$  is a pulse charge-discharge type capacitor that is especially designed for such applications and it is relatively expensive when compared to typical ac or dc capacitors with equivalent ratings. This capacitor represents the main component that can be used to vary the circuit current and operating frequency. For instance, if the capacitor value is increased, then the pulsing frequency will decrease. This decreases the rate of flux change in the stimulating coil to a point where it may not be able to excite the nerve. Conversely, decreasing the capacitor increases the pulsing frequency to a point where the excitation field is faster than the depolarization time constant of the neuron. Equation (4.1) can be used to calculate the (approximate) value of the capacitor required for the stimulating system (assuming the equivalent circuit resistance  $R$  is negligible):

$$C = \frac{1}{L(2\pi f)^2} \quad (4.1)$$

where:  $C$  is the circuit capacitance,  $L$  is the coil inductance, and  $f$  is the circuit pulsing frequency. Considering the range of operating frequencies listed above (2-10 kHz), typical values for the capacitor vary between 50-400 $\mu$ F with rated voltages up to 3kV.

#### 4.1.2 Construction of an Advanced Stimulator

From the previous section, it can be concluded, that a magnetic stimulator is comparable to a current pulse generator. The criteria defining such a pulse are: pulse type, peak value, duty cycle, rise and fall times, and rate of repetition. Based on these criteria, a

magnetic stimulator was designed and constructed to test and evaluate the proposed coils. This stimulator is considered to be an “advanced” system as it can be driven by a computer and includes all the functions required for a clinical system. Figure 4.2 shows a block diagram representing the different stages of this system.

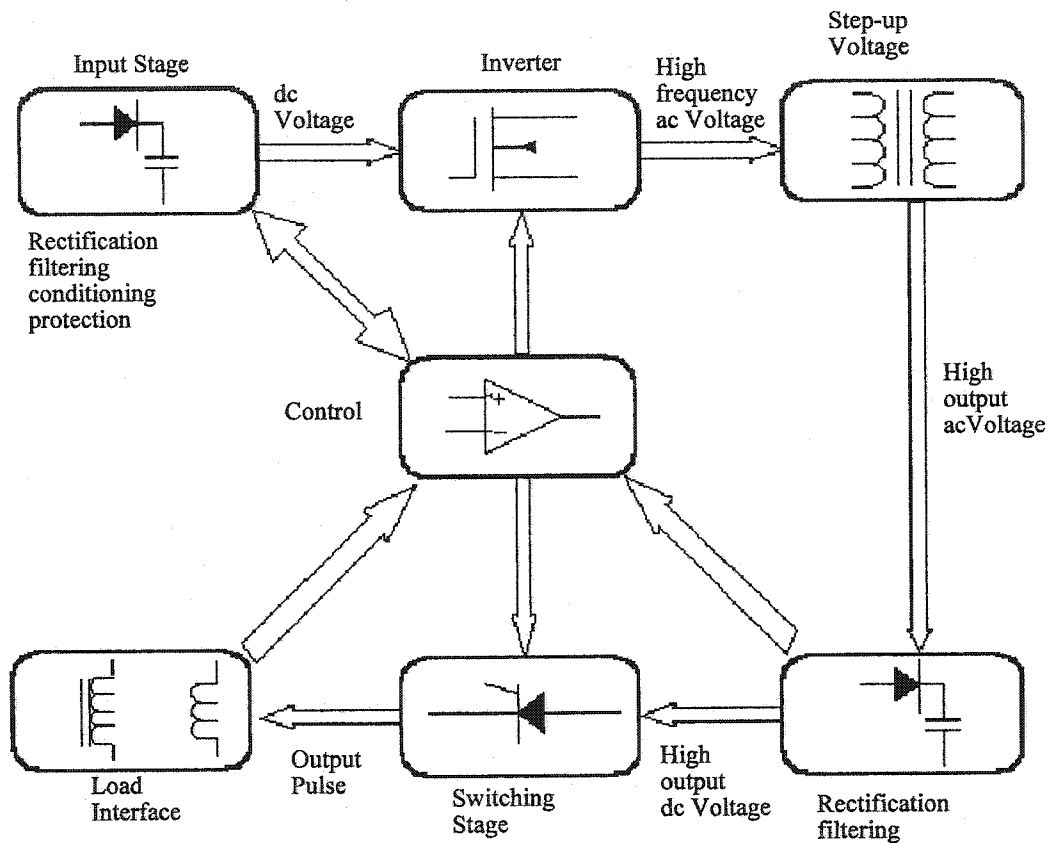


**Figure 4.2**  
A block diagram of the different stages of a magnetic stimulator.

The stages in the above figure can be grouped into the following clusters:



#### A. Input stage

This stage provides the system with the DC biases and the driving voltage that supplies the inverter stage. In addition to system protection, other functions are handled by this stage such as: rectification, filtering, and conditioning of the input voltages. For the advanced system, a custom built 3kVA transformer with 4 kV isolation, was constructed to supply the input stage. Using an optional input voltage of 120 or 240V, this transformer supplies the following voltages: 17V, 25V, 400V. These voltages are rectified and filtered to generate the system biases ( $\pm 5V$ ,  $\pm 12V$ ,  $\pm 15V$ ) as well as the main driving voltage (400V).

#### B. Inverter stage

The inverter stage converts the DC voltage (provided by the input stage) to a high frequency AC voltage. The advantages of switching to a high frequency are: decreasing the charging time of the high voltage capacitor and reducing the size and weight of the step up transformer (which is supplied by this stage). In the advanced system, this stage is implemented by four MOSFETs resembling an H-bridge with an operating frequency of 100 kHz.

#### C. Step-up voltage stage

The main component of this stage is a high frequency step-up transformer. Due to its high operating frequency (100 kHz) the core of this transformer should be constructed from a ferrite material. Furthermore, compared to conventional 60Hz transformers, special considerations should be given to the design and fabrication process. For instance, in addition

to the typical parameters that are normally addressed (volts/turn ratings, layer to layer insulating ratings, type of insulating material, and thermal dissipation), careful attention should be given to leakage flux, winding geometry, and parasitic leakage capacitance.

For the advanced system, a 1kVA step-up transformer was fabricated using a “U” shape ferrite core. With 4kV isolation, the turns ratio of this transformer is set to 1:5 while its input voltage is rated for 400V. The primary coil (input) of this transformer is connected across the H-bridge arms while its secondary (output) is directed to the high voltage stage. To minimize the leakage capacitance between the transformer windings (resulting from the high frequency), multi strand wires were used. It should be noted that constructing this transformer was challenging due to its transient voltages.

#### D. High voltage stage

The input of this stage is a high frequency AC voltage supplied by the step-up transformer while its output (after rectification and filtering) is a DC voltage used to charge the high voltage capacitor ( $200\mu\text{F}$  rated for 3kV). Through opto-coupling feedback circuitry, the capacitor voltage is continuously monitored and ultimately regulated by the control stage. This regulation process is based on acquiring the capacitor voltage by the control stage and comparing it to the desired voltage (set by the user). A charge/discharge command is then sent to the capacitor to adjust its voltage (energy). In both constructed systems, a readout of the high voltage is displayed on the front panel via an LCD (that operates on a 9 volt battery). To ensure full isolation and to avoid any voltage breakdown (arcing), all the components of this stage are isolated.

#### E. High voltage switching circuit

The primary objective of this stage is to deliver the DC voltage stored in the main capacitor to the stimulating coil. For practical purposes (pulse ratings and device cost), an SCR represents an excellent choice to deliver the required pulses. When selecting an SCR for such an application, its rated peak reverse voltage must be twice the system maximum high voltage and its rushing current must be 10 kA or higher. For the advanced system, the SCR used was rated for 4 kV peak reverse voltage and 15kA rushing current. These ratings are higher than the system maximum ratings and consequently ensure safe SCR operation.

In addition to choosing the proper SCR, selecting a suitable triggering device (a pulse transformer or a photo-trigger circuit) is critical. This device must ensure complete isolation between this stage and the control stage. For the advanced system, the triggering circuit is implemented using a combination of opto-coupler and fiber optic cable. The fiber optic cable (which carries the triggering signal) was implemented to provide adequate distance between the high voltage stage and the control stage.

#### F. Load interface

This stage, which represents the interface between the unit and the coil assembly, provides the control stage with various feedback signals such as verifying coil connection and monitoring coil temperature. For the advanced system, two micro-switches are used to ensure proper connection between the coil terminal and the unit. With respect to the coil temperature, a small thermistor is embedded in the coil assembly to monitor its temperature. If the coil is not connected properly or its temperature exceeds the desired limit the

associated warning lights, which are attached to the system front panel, are activated.

#### G. Control stage

The control stage, which may range from a few ICs to a microprocessor, represents the link to all of the above stages. This stage handles various tasks such as: system monitoring, decision making, and displaying the variables of interest. The performance of this stage is based on acquiring various variables (pulse intensity, duration, configuration, and rate of repetition) and comparing them to the desired settings (defined by the user). Depending on the system status and the desired output, a corresponding command is issued by this stage. Figure 4.3 displays the advanced system.

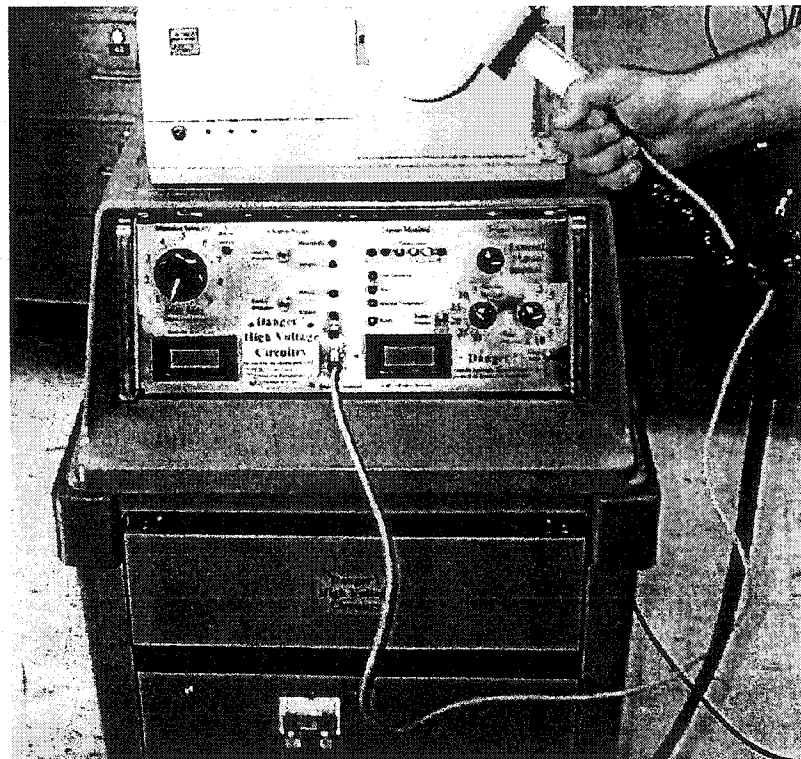


**Figure 4.3**  
An Advanced Magnetic Stimulator.

### 4.1.3 Construction of a Simple Stimulator

Although, the structure of the advanced system was completed successfully, hardware constraints prevented its use in a fully experimental setting. These constraints are primarily attributed to the high frequency step up transformer which was manually constructed. Despite passing a 4 kV isolation test, arcs were noticed across the transformer windings when fast repetitive rate or high stimulation intensity was applied (higher than 15 Hz or 70% of the system output). The arcing, which is a result of the transient signals discharging, could not be rectified despite all of the attempts in rewinding and re-fabricating the transformer. Accordingly, it was decided to replace the advanced system (due to safety concerns) with a simple unit to complete the experimental phase of this thesis within the time constraints. Figures 4.4 displays the simple system. More details regarding this system can be found in Appendix D.

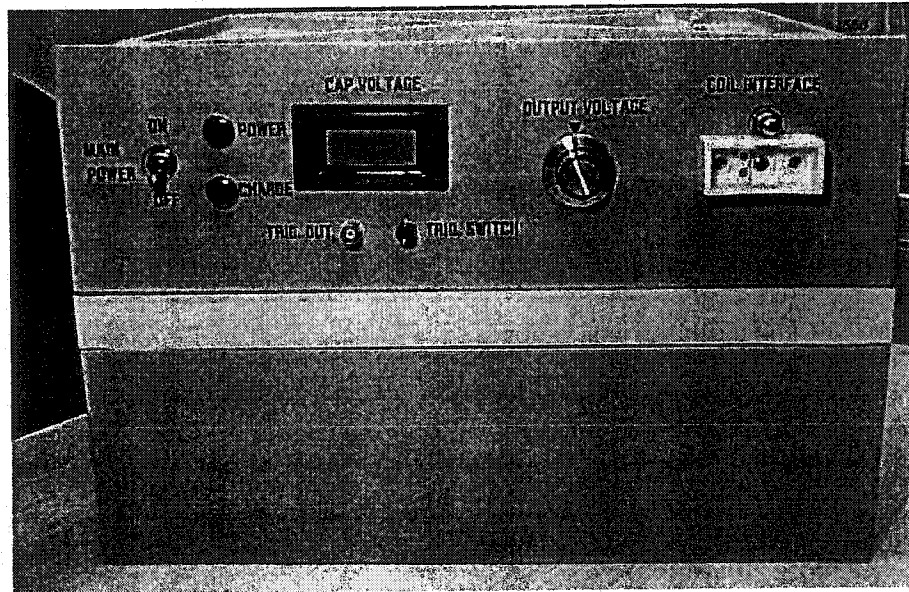


**Figure 4.4**  
A Simple Magnetic Stimulator.

#### 4.1.4 Critical Issues, Safety Considerations and Future Designs

- 1) For a magnetic stimulator, preventing noise from interfering with the signals processed by the control stage represents the most critical issue. This noise is the result of high  $di/dt$  and  $dv/dt$  created during switching. For such an application, the best approach to reduce the noise is to have a resonant switching topology. This can be achieved by adding inductors to the input of the stages that handle high power signals. For the advanced system various inductors have been designed, constructed, and added to the stimulator. The values and types of these inductors were calculated to provide the required AC and DC filtering and to meet the circuit ratings (current and voltage). Two software packages (supplied by Micrometals Inc. and Magnetics Inc.) were used to define and calculate the inductor parameters (core type and size, number of turns, thermal dissipation and losses, etc.). In addition, good shielding practices (for both components and wires) and maintaining a low ripple on the bias voltage are implemented in both systems. The latter was accomplished by adding filtering capacitors and maintaining proper references (grounds).
- 2) As there are many feedback circuits utilized by a stimulator (such as current and potential transformers, shunt and voltage divider resistors) reliable isolation is essential to ensure a safe operating system. To meet the above criteria in both systems, opto-couplers and transformers are used to separate the high voltage circuitry from the low voltage. These opto-couplers and transformers are rated/tested and approved for 4kV isolation.
- 3) As described earlier, magnetic stimulation (mainly repetitive) results in heat build up

within the coil and the system components. Typically, this thermal accumulation affects the system performance (resulting in the use of more than one coil per session) and in extreme cases, causes coil or system failure. Accordingly, continuous thermal dissipation and monitoring of the system are essential for safe operation. In the advanced system, heat sinks combined with fans and thermal fuses were used to ensure proper thermal dissipation. In addition, thermistors were embedded in the coil windings to monitor and maintain the coil temperature within a range of 15-50°C. An LED graph bar, displaying the coil temperature, is attached to the unit front panel.

- 4) When applying magnetic stimulation, patient and operator safety are critical concerns due to the high energy transferred by the system. In particular, coil failure is the main concern due to the coil proximity to both the patient and the operator. Therefore, when designing these coils special attention should be given to electrical hazards (coil malfunctioning). It should be noted that the coils constructed for this work are intended for experimental use only and not for clinical studies.
- 5) When selecting subjects/patients for stimulation, special attention must be given to those with implants (pacemaker, metal pins) as unexpected responses may occur. These conditions were followed in the study conducted for this work (see Chapter 6).
- 6) Suggestions for future designs include: using a variable capacitor (capacitor bank) as it provides better control of the waveform shape and energy, and adding a micro processor which translates to a software driven system that is easily upgraded.

## **4.2 Measuring the Induced Electrical Fields in 3-Dimensions**

The induced electric fields during magnetic stimulation are critical variables in evaluating and quantifying the effectiveness of the equipment. A precise measure of these fields in three dimensions is the first step to map and define their spatial distributions. However, measuring these fields is a tedious task due to the field transient pattern and dependence on many variables such as: coil type, pulse configuration, media conductivity, and target shape. Further, these fields are extremely sensitive to coil position and orientation especially within biological tissues. In this section, a practical approach is presented to map the induced electrical fields in three dimensions within spherical and cartesian volumes.

### **4.2.1 Previous Studies**

Previous researchers conducted many experiments to measure and map the electrical fields in both homogeneous and inhomogeneous media. Their measuring apparatus generally consisted of: a positioning device, a tank of saline solution, various types of probes, and an oscilloscope. Figures 4.5 and 4.6 illustrate some of these experiment setups. Based on these setups, the voltage gradients between the probe(s) tips, assuming that the distance between the tips is negligible, was approximated to represent the electric field as a point source. However, the experimental procedures were time consuming and required considerable attention to ensure valid measurements. Further, the collected data could not be retrieved since they were captured only by a multi channel oscilloscope and not stored on a computer. As well, most of the experiments utilized flat surfaces and did not accurately model transcranial stimulation which requires spherical volume. Weissman et al. [83] conducted



a study using multi spherical targets; however, their measurements were limited to specific points and did not map the induced fields throughout the entire targeted region.

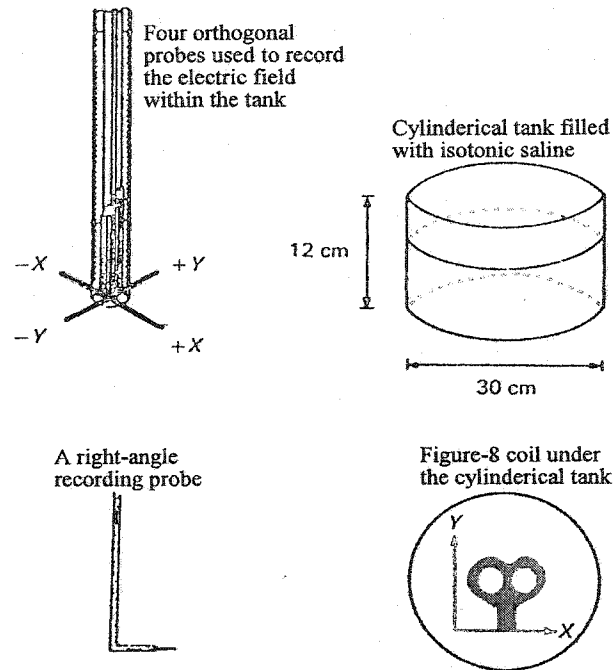


Figure 4.5  
Experiment set up by Maccabee et al. (taken from [37]).

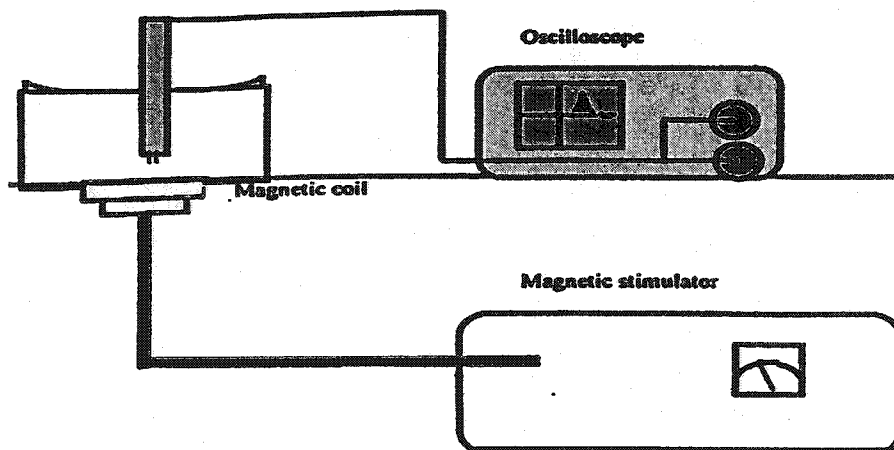


Figure 4.6  
The measurement apparatus used by Lin et al. (taken from [73]).

#### 4.2.2 Design of a Measurement Apparatus

Considering the previous work, two experimental prototypes were designed to map the induced electric fields. The first prototype was constructed to measure the induced voltages within a spherical volume while the second was assembled to capture the voltages within a cartesian volume.

Resembling the size and shape of the head, the first model consists of three nested bell jars, stacked inside each other with adjustable rings to align their position (Figure 4.7). Three arrays of surface mount inductors (LQS66C3R3M04 - muRata company) were assembled and positioned inside the jars. Each array, which consists of five pairs of orthogonal inductors separated by equal distances of 2cm, was placed from the sphere center to its perimeter. Further, the array was attached to a ribbon cable with each pair of inductors soldered to three wires (one wire per inductor and the third is common for both). The ribbon cables, which extend outside the jars, are terminated by 15 pin connectors. These connectors are the interface between the measuring apparatus and the data acquisition card. Considering the distance between the inductors is known and by measuring the induced voltages, the electric field and its spatial (axial) distribution can be determined. More details regarding the measuring apparatus and the mapped electric field can be found in Chapter 5.

The second prototype is based on the same concept of the previous one; however, the volume of interest is a set of two dimensional planes (Figure 4.8). It should be noted that the main advantage of assembling the inductors in this arrangement is the ability to readily improve the spatial resolution of the measured data. For instance, the resolution can be doubled by shifting the entire assembly 1 centimeter from its original position.

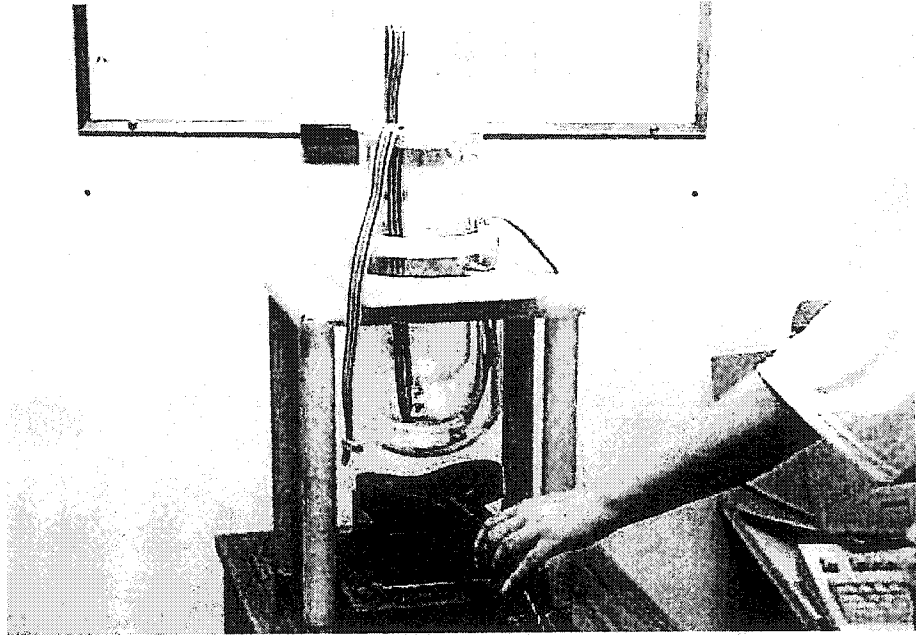


**Figure 4.7**  
Experiment setup - spherical volume.

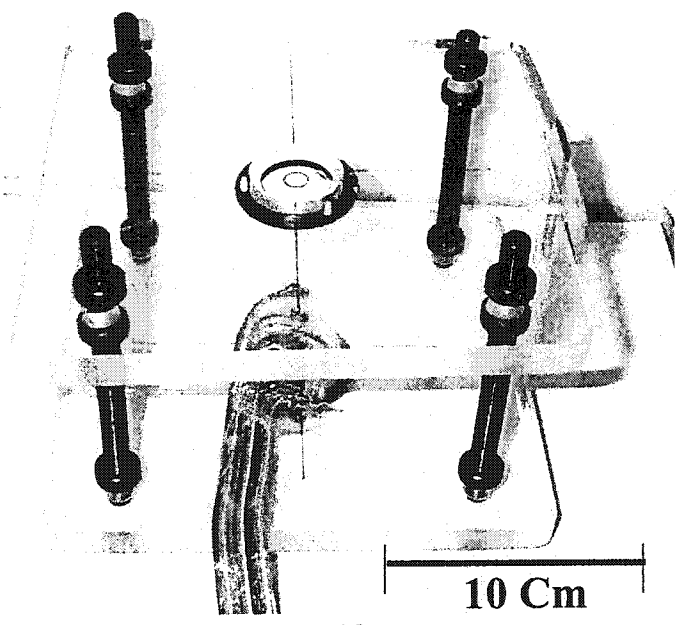


**Figure 4.8**  
Experiment setup - cartesian volume.

### 4.2.3 Experimental Hardware and Software

The influence of coil type, coil current rate of change, current direction, and media conductivity were examined for different stimuli intensities. A magnetic stimulator (Dantec MagPro) with a Figure-8 coil (outer diameter 10cm with 2x10 windings) and a circular coil (outer diameter 12cm with 13 windings) were used for this study [84]. The stimulus intensities were increased in steps of 10% from 20 to 100% of the maximum system output. For each step, ten consecutive signals were collected and averaged. To ensure that the same energy was supplied for all stimuli within one step the  $di/dt$  value, displayed on the front panel, was monitored throughout the experiment. The induced voltages were captured in two dimensions and their resultants were calculated from the orthogonal data. These resultants vary between 0.2 and 1.5 V ( $V_{peak}$ ) corresponding to 20-100% of the stimulation intensity. All measurements were taken directly from the inductors (no filtering was required) and collected by a data acquisition board guaranteed for 200 kS/sec (PCI-6024E a 12-bit data acquisition board - National Instruments). The common mode rejection ratio (CMMR) of the board is 85 dB for a gain of 100. The captured voltages, from a two dimensional plane, were sampled at 100 kHz and acquired by a stand-alone algorithm created using **LabVIEW** software (ver. 5.1 National Instruments) and **Matlab** software (ver. 5.2 Math Works Inc.) The algorithm enables the user to acquire a train of signals, calculate the area and the peak to peak amplitude of each pulse, and store the data in ASCII and spreadsheet formats. The algorithm also allows the user to retrieve or re-read the data from the stored files, average and post-process the data. Figure 4.9 captures the software front panel.

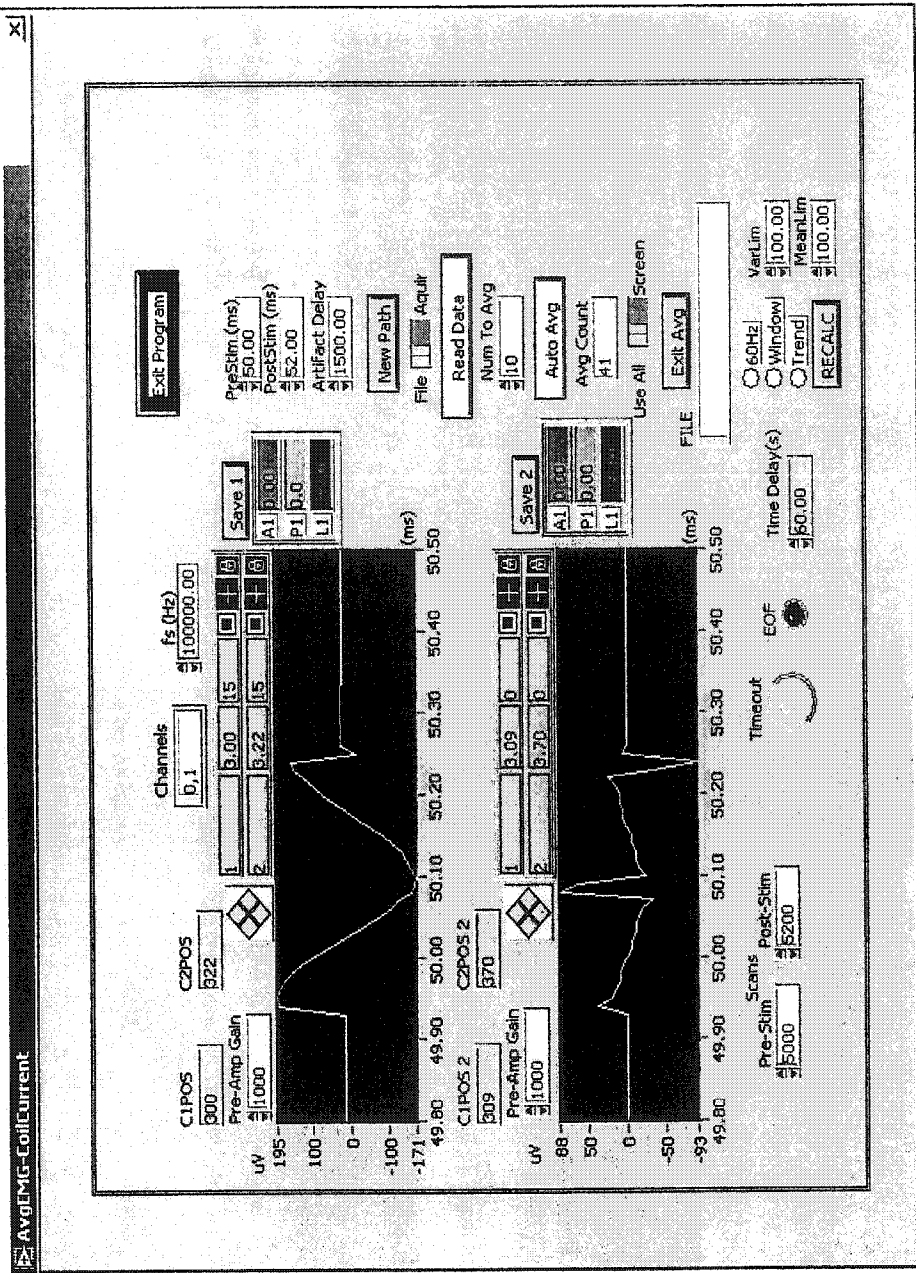


Figure 4.9 Front panel display of the software showing the induced voltages in each of the inductor pairs.

#### 4.2.4 Evaluating the Testing Apparatus

To evaluate the accuracy and precision of the testing apparatus, experiments were conducted. Using circular and Figure-8 coils, it was determined that the induced voltage waveforms were similar in shape, while their amplitudes were dependent on the position of the measuring coil. For the circular coil, the maximum induced voltage was measured above the coil edge, while for the Figure-8, it was measured above the coil center. Figures 4.10 and 4.11 show the induced voltages generated by a circular coil for bi-phasic and mono-phasic pulses respectively. Figure 4.12 shows a comparison between the induced voltages for circular and Figure-8 coils with the amplitudes normalized to the maximum bi-phasic voltage generated by each coil. For the figures below, the data were captured in two dimensions with the measuring device positioned at the sites generating maximum induced voltages.

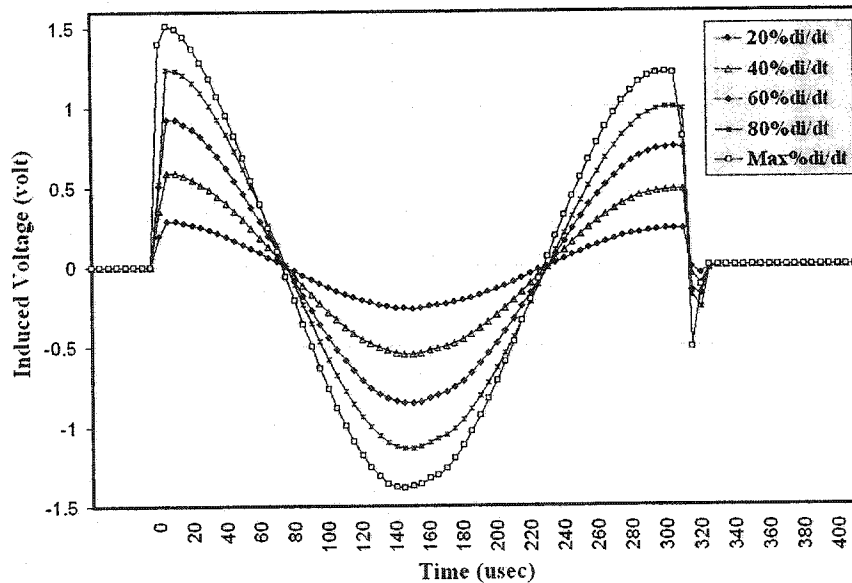


Figure 4.10  
Induced voltages generated by a circular coil when using bi-phasic waveforms.

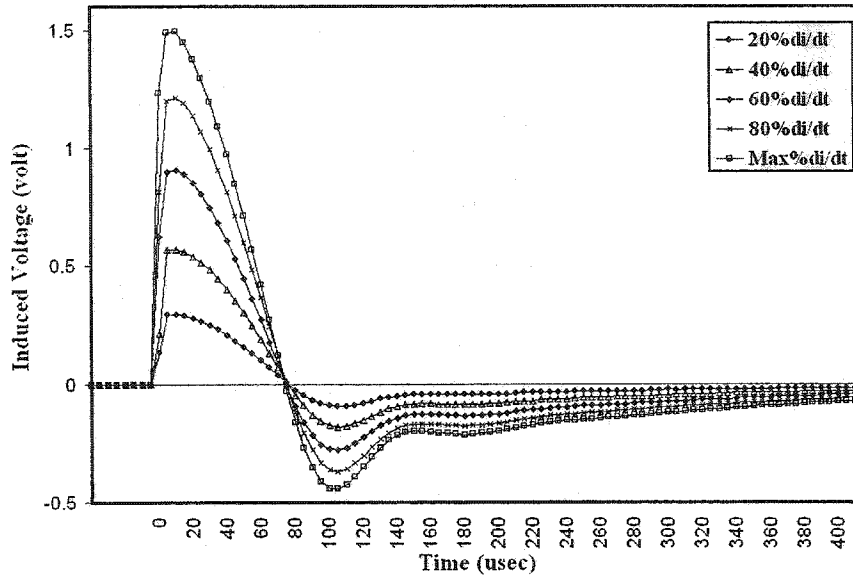


Figure 4.11  
Induced voltages generated by a circular coil when using mono-phasic waveforms.

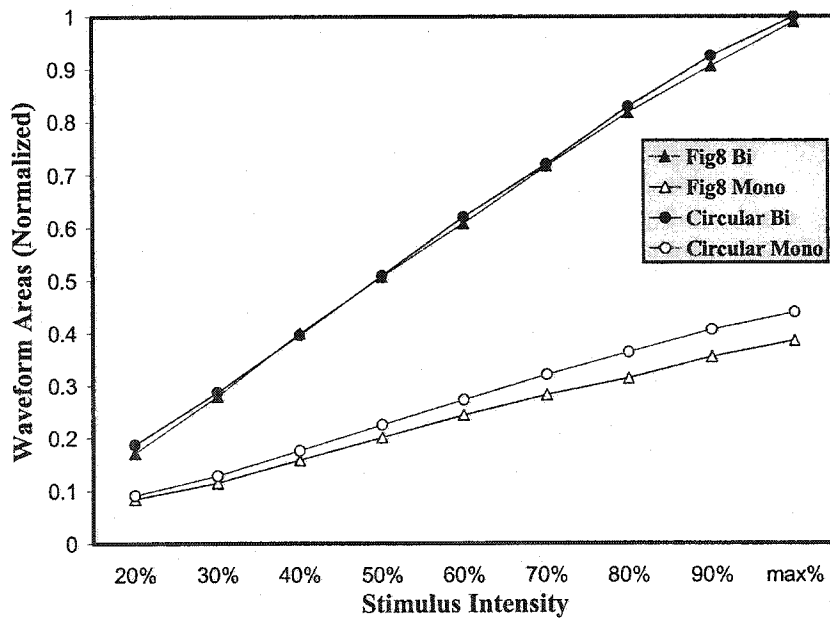


Figure 4.12  
The areas of the induced voltages for circular and Figure-8 coils using two waveforms.

#### 4.2.5 Discussion of the Experimental Results

From the experiments conducted to evaluate the measuring apparatuses, the following key findings can be extracted.

1. The results shown above are identical to the findings of Niehaus et al. [85] and Kammer et al. [40] in which a “pick up coil” was used to measure the waveform of a Dantec MagPro stimulator. However, the proposed apparatus provides additional advantages as the size of the measuring device (surface mounted inductor) is relatively small, which allows for a higher resolution and minimum interruption in the field pattern. In addition to the efficient process and minimum effort when using the proposed apparatus, this system consists of standard components that can be easily modified to accommodate various experimental set-ups.
2. Bi-phasic stimuli are more effective and result in higher induced fields when compared to mono-phasic. Further, the areas and the peaks of the induced voltage for both types of waveforms are linearly proportional to the coil current rate of change ( $di/dt$ ).
3. The maximum induced voltages generated by the circular and Figure-8 coils are similar in shape and are slightly different in amplitude (less than 5% variation with the circular coil generating higher induced voltages). This applies to both pulse configurations and for all stimulation intensities.
4. All the results presented in the previous figures were collected using empty spheres. The addition of saline solutions with different concentration levels (0.9% NaCl, 1.8% NaCL) increased the electric field gradient (for more details see Chapter 5).



These results agree with Maccabee et al. findings [37] in which various saline solutions were used.

5. With respect to coil current direction, it was found that reversing the current direction has no effect on the measurements. This was an expected result since the experiment was conducted using linear hardware within a homogeneous media.
6. It is important to reiterate that the measured results are very sensitive to the coil position and orientation. When the coil is properly positioned and maintained, the proposed prototypes ensure minimal movement, consistency in position and orientation of the measuring inductors, and consequently accurate measurements can be achieved.

## Chapter 5 Experimental Results

This chapter covers the experiments conducted to evaluate the theoretical aspects of this thesis and presents the results in two sections. The first section covers the testing and evaluation of various coils (commercial vs. proposed), while the second addresses the effects of coil orientation and media conductivities on the induced electric field generated by magnetic stimulation. The main objective of the second section is to evaluate and discuss Roth's hypothesis by using various coils positioned in different orientations.

### 5.1 Calculating the Induced electric field

As outlined in Chapter 3, the proposed coils consist of windings embedded in planes which are non-horizontal to the region of interest. Thus, the effect of the normal magnetic field component is to be considered and included in the simulation process as well as the experimental measurements.

Based on the discussion presented in Chapter 2, the effect of the normal component can be determined through the static field component ( $\zeta_\theta$ ). To calculate  $\zeta_\theta$ , the starting point is Maxwell's equation that governs the magnetic field:

$$\nabla \times \mathbf{H} = \mathbf{J} + \frac{\partial \mathbf{D}}{\partial t} \quad (5.1)$$

where  $H$  is the magnetic field,  $J$  is the electric current density,  $D$  is the electric flux density, and  $\nabla \times$  is the curl operator. Considering that the region of interest (biological tissues) is a conducting medium and the current density is  $J = \sigma E$ , equation (5.1) can be modified to:

$$\nabla \times H = \sigma E + \frac{\partial D}{\partial t} \quad (5.2)$$

where  $\sigma$  is the tissue conductivity and  $E$  is the electric field intensity. Figure 5.1 illustrates the interaction between the applied magnetic field and the resultant induced electric field. From this figure it can be seen that the magnetic field traveling along the  $x$  axis toward the region of interest induces an electric field along the  $y$  axis ( $H$  normal to  $E$ ).

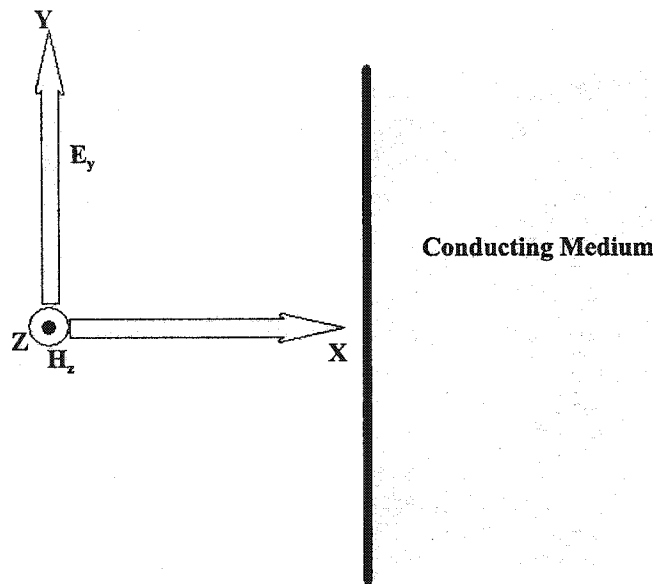


**Figure 5.1**  
Plane wave entering conducting medium at normal incidence.

By substituting the vector ( $D = \epsilon E$ ), equation (5.2) reduces to the following scalar equation:

$$-\frac{\partial H_z}{\partial x} = \sigma E_y + \varepsilon \frac{E_y}{\partial t} \quad (5.3)$$

where  $\varepsilon$  is electrical permittivity. Considering that  $E_y$  is a time harmonic variable and can be represented as  $E_y = E_0 e^{j\omega t}$ , equation (5.3) becomes:

$$-\frac{\partial H_z}{\partial x} = \sigma E_y + j\omega \varepsilon E_y \quad (5.4)$$

where  $\omega$  is radian frequency. Equation (5.4) is defined in terms of current density where  $\sigma E_y$  and  $j\omega \varepsilon E_y$  represent the *conduction* and *displacement current densities* respectively. As the parameters in equation (5.4) pertain to a wide range of media, it can be seen that this equation can be applied to dielectric, quasi conductor or conductor problems. For magnetic stimulation, the operating frequency ranges between 2-10 kHz [86]. The conductivity of the tissues varies between 0.01-1 Siemens, while the relative permittivity of the tissues ranges from 1-7 [81]. Accordingly, the term representing the displacement current density ( $j\omega \varepsilon E_y$ ) adds less than 0.1%. Thus, this term can be eliminated from equation (5.4) and the problem can be simplified.

The above argument can also be analyzed in terms of which part of the magnetic waveform is responsible for initiating neural excitation. Based on initial investigations conducted by Barker et al. [87], it was believed that the stimulation response depends on the current pulse rate of change within the first quarter of the waveform (rising edge). However, as suggested by Maccabee et al. [38] and discussed in Chapter 4, the effects of the stimuli depend primarily on the current pulse rate of change within the second and third quarters and

not the first. This means that charge accumulation during the pulse initial phase, is not applicable. This simplification leads to an elimination of the static field component, as the conduction time is negligible compared to that required for charge build up. Therefore, equation (2.17) can be simplified to:

$$\bar{\zeta} = -\frac{\partial \bar{A}}{\partial t} \quad (5.5)$$

## 5.2 Measuring the Induced electric field

Figure 5.2 illustrates a model using a surface mount inductor to measure the electric field<sup>1</sup>. In this model, which is a simplistic representation of the measuring apparatus, the electric field  $E_{(y)} \hat{a}_z$  and magnetic field  $B_{(y)} \hat{a}_x$  have transverse components that vary along the direction normal to both fields (y-axis).

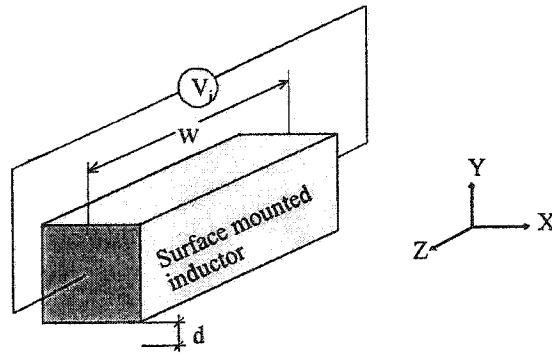


**Figure 5.2**

A model illustrating the measurement of electric field using an inductor.

<sup>1</sup>

For this model, axis orientations were defined to match that of the median nerve computer model (see Chapter 3).

For the above model, the measured induced voltage is found from the time rate of change of the flux linking the inductor and the stimulating coil, thus:

$$V_i = kw \int_d^\infty \frac{\partial B_x}{\partial t} dy \quad (5.6)$$

where  $V_i$  is the induced voltage,  $k$  is a scaling factor that depends on the inductor value,  $w$  is the inductor length, and  $d$  is the approximate distance separating the inductor from the stimulating coil (as the inductor thickness is negligible compared to the distance  $d$ ). However, according to Maxwell's equation, the electric field is related to magnetic flux density by:

$$\nabla \times E = -\frac{\partial B}{\partial t} \quad (5.7)$$

According to the discussion related to Figure 5.2, equation (5.7) can be simplified to:

$$\frac{\partial E_z}{\partial y} = \frac{\partial B_x}{\partial t} \quad (5.8)$$

By substituting equation (5.8) in equation (5.6) and integrating both sides, the induced voltage in the inductor can be represented in terms of  $E$  and  $B$ . Assuming that the flux density ( $B_x$ ) and the induced voltage ( $V_i$ ) diminish at distant regions (infinity) from the targeted area, the electric field measured by the inductor can be represented as:

$$E_z = \frac{V_i}{kw} \quad (5.9)$$

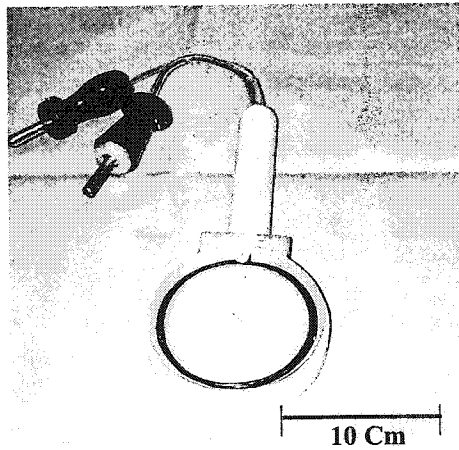
Equation (5.9) illustrates the calculation of the induced field in one direction ( $z$  axis) and for a specific depth ( $d$ ). Ultimately, by measuring the field at the same depth for another direction ( $x$  axis), the induced field within a two dimensional plane can be calculated (Chapter 4).

### 5.3 Testing and Evaluating the Stimulating Coils

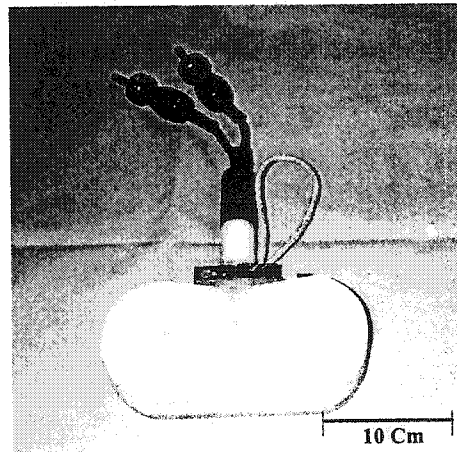
As described in Chapter 3, the parameters for the proposed and standard coils were defined and implemented using computer models. To verify the simulation results and confirm the coils' effectiveness, a set of coils (Figure-8, circular, and proposed the coils) was assembled. Using a magnetic stimulator system combined with a measuring apparatus, the constructed coils were tested. The resulting induced voltages, within the targeted region, were measured and mapped to their respective electric fields. It should be noted that the stimulator used was the simple type while the measuring apparatus was the prototype that captures the field in a two dimensional plane (see Chapter 4 for more details). All coils were fabricated from solid square copper wire (AWG #12) with their total DC resistances varying from 15 m $\Omega$  to 22 m $\Omega$ , while their inductances varied from 12 $\mu$ H to 25 $\mu$ H. The voltage used to test these coils was set to 500V during the entire experiment while the capacitor bank implemented was 200  $\mu$ F. This translates to an energy of 25 joules per pulse.

Figure 5.3 displays the constructed coils. This figure clearly illustrates the similarities between the air core and the slinky coils proposed by Lin et al.[73] and the resemblance between the magnetic core with that of Davey et al. [71] (see Chapter 3 for details). Also, it can be seen that the turns of the proposed coils are rectangular since this presumably

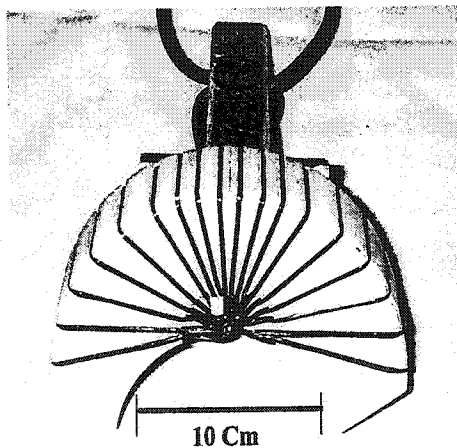
improves the induced electric field gradient. This assumption was based on the experimental results of Lin et al. [73] in which they show that the electric field produced by a rectangular coil is higher (approximately 18%) than the electric field produced by a round coil.



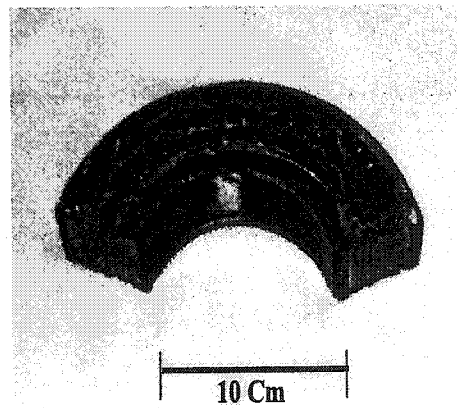
(a)  
Basic circular coil



(b)  
Figure-8 coil



(c)  
Air core coil (similar shape for magnetic)



(d)  
The embedded magnetic core

**Figure 5.3**  
Various types of assembled coils.



## 5.4 Experimental Results

With the objectives of evaluating the fabricated coils, an experiment similar to that outlined in Chapter 4 was conducted. During this experiment, the coils were placed below the testing apparatus with their axes projected against the transducer plane. To collect reliable and consistent data, the coils were manually maintained in their positions as precisely as possible. Further, to ensure that the same energy per pulse was supplied for all stimuli within one step, the high voltage of the discharging capacitor, displayed at the front panel, was maintained at 400V ( $\pm 1\%$ ) throughout the experiment.

For each transducer, five consecutive pulses were applied and their induced voltages were collected, sampled, and averaged. As there are five transducers on each axis, a total of nine steps are needed to capture the field within one quadrant. To ensure high accuracy ( $\pm 10 \mu\text{sec}$ ) for the measured data, a sampling rate of 100kS/sec was used. For more details regarding the measurement procedure see Chapter 4.

The coils evaluated for this experiment were: Figure-8, air core, and magnetic core coils. Figure 5.4 shows the waveforms of the induced fields generated by the three coils. From this figure it can be seen that the waveform duration of the magnetic core is longer than the other two coils. This is an expected result since the inductance of this coil is higher than that of the other two (due to the magnetic core). On the other hand, the pulse generated in the air core coil is lower than the Figure-8 indicating that the inductance of the former is lower than that of the latter. This result is different from that of the simulations in which air core and Figure-8 coils have equivalent inductances (approximately  $12\mu\text{H}$ ).

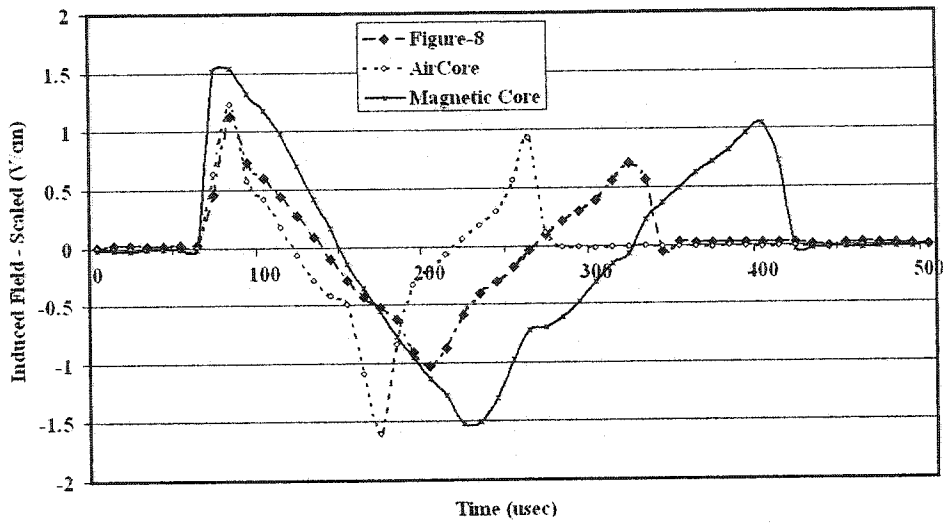


**Figure 5.4**  
Induced fields generated by various coils captured at 2cm below the coil centers.

Figures 5.5, 5.6, and 5.7 show the measured electric field in three dimensions for the Figure-8, air core, and magnetic core coils.

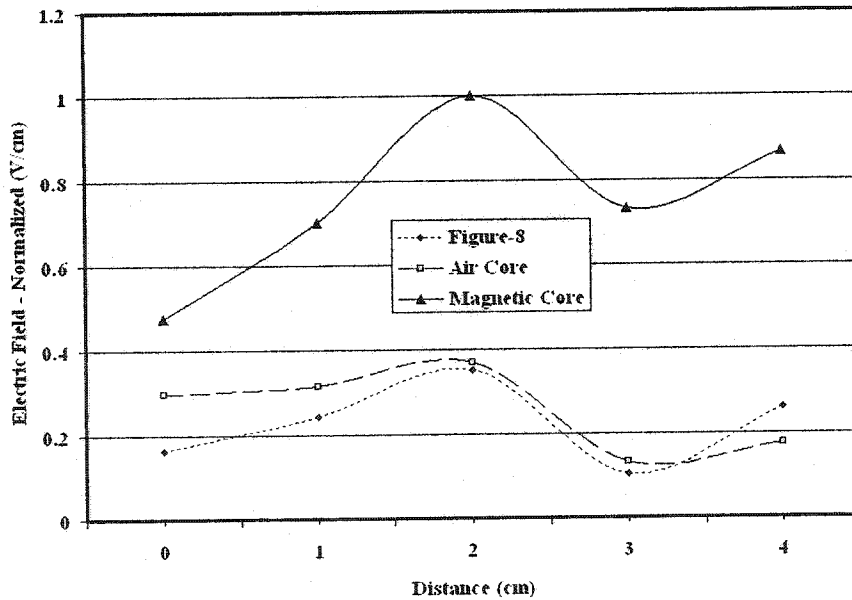


**Figure 5.5**  
The measured electric field (normalized) along the X-axis (field focality).

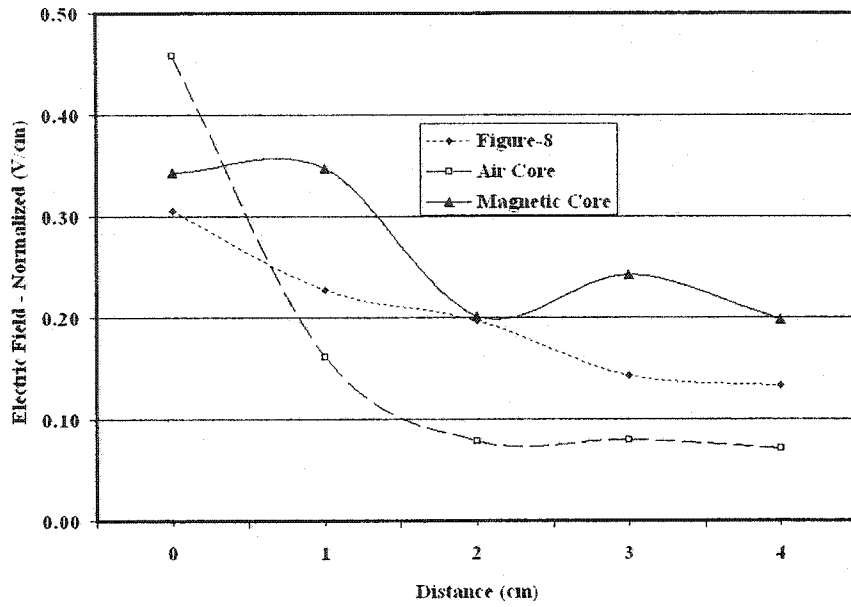


Figure 5.6

The measured electric field along the Y-axis (depth of field penetration).

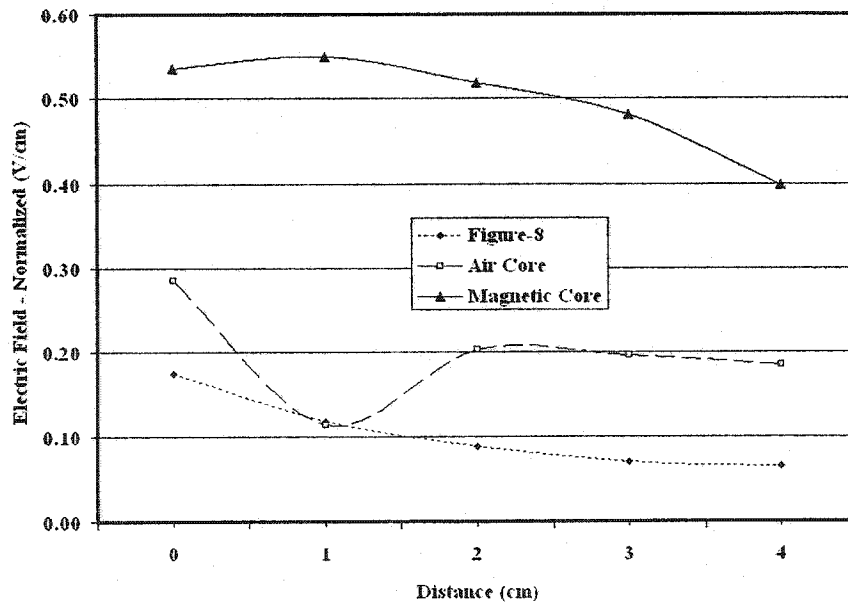


Figure 5.7

The measured electric field along the Z-axis (field focality).

## 5.5 Discussion of the Experimental Results

From Figure 5.4 it can be seen that the area below the waveform of the magnetic core coil is larger than for either of the other two coils. This is an indication that the energy stored by the magnetic core (and coupled to the targeted area) is higher than that in the other two coils. On the other hand, the waveform generated by the air core coil covers less area (shorter duration) and its associated field collapses faster. This indicates that the inductance of this coil is lower than the other coils which results in lower stored (and coupled) energy. To overcome this limitation, more coil turns could be added to increase the inductance of the air core coil, and thus improve its performance (field strength and coupled energy).

With respect to the electric field spatial distribution, the most critical criteria are the level of penetration ( $Y$ -axis) and its focality in the longitudinal direction ( $Z$ -axis). Figure 5.6, which illustrates the field level of penetration, shows that the magnetic core has the highest field gradient in the  $Y$  direction. This improvement can be utilized in rTMS as the current coils provide only 1-2cm of field penetration into the brain [32,33]. With respect to coil focality, Figure 5.7 illustrates the enhancement in field strength when using the magnetic core coil. This enhancement can be effectively implemented with the use of lower pulse energy (lower pulsing currents) to achieve the required stimulation. The reduction in energy and currents will decrease heat build up and consequently improve coil thermal performance.

In conclusion, despite the few errors in the collected data (Figure 5.6-magnetic core at 2 centimeter, Figure 5.7- air core at 1 centimeter), the experimental results confirmed that the magnetic core coil provides a tremendous improvement in field strength, penetration, distribution, and focality.

## 5.6 Measuring the Induced electric field within various media

With the objectives of investigating the impact of coil orientation (Roth's hypothesis) and the effect of media conductivity, an experiment similar to that outlined in Chapter 4 was performed. Using a Dantec magnetic stimulator combined with Figure-8 and circular coils [84], the induced electric fields were measured within various domains. The type of materials implemented to create these domains (targeted regions) were: air, saline, oil, and a mixture of saline-oil. Utilizing different combinations of these substances, target regions of both homogeneous and heterogeneous conductivities were created. The homogeneous set-up was created by covering an array of orthogonal inductors with a pool of one of the above materials, while the heterogeneous was developed by immersing an assembled probe into a similar pool. The probe was assembled from a pair of orthogonal inductors, placed in a sealed medium that is different from that of the pool. Figure 5.8 shows the probe.



**Figure 5.8**  
Two probes insulated and enclosed by a medium.

Figure 5.9 illustrates the experimental set up for homogeneous and heterogeneous media with the circular coil normal to the surface of the dominant media.

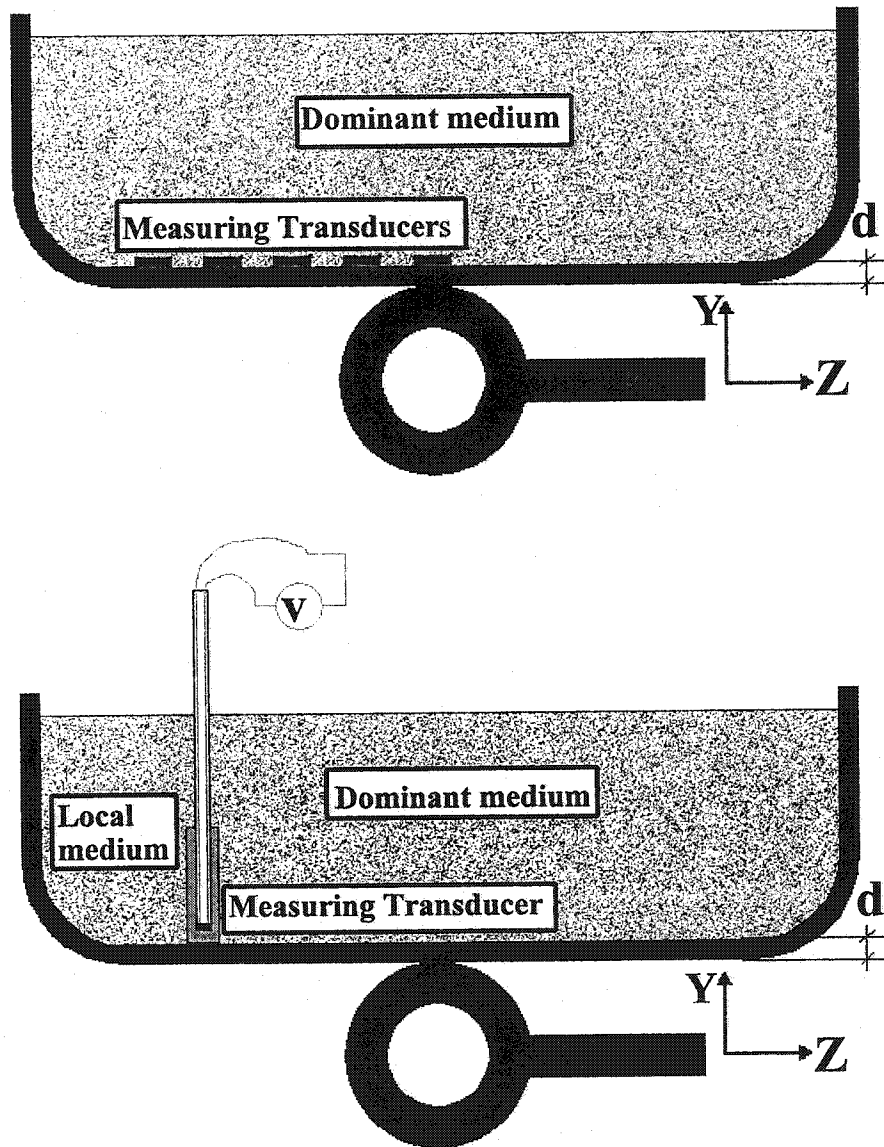


Figure 5.9  
Experiment setup - Top: homogeneous medium, Bottom: heterogeneous medium.

Some assumptions were considered for this experiment include:

1. The surface of the medium is planar and infinite in extent.
2. The media are uniform, isotropic volume conductors.
3. A quasi-static approximation is made when analyzing the electric field.

It should be noted that changing any of the above conditions may change the induced field pattern both horizontally and vertically.

## 5.7 Method and Results

During this experiment, the coils were positioned in two orientations (normal and horizontal) with respect to the targeted area. For each step, five consecutive pulses of a bi-phasic waveform with a 50% intensity were applied. The induced voltages were captured in two dimensions and their resultants were calculated from the orthogonal data. All measurements were taken directly from the inductors (no filtering was required) and collected by a data acquisition board guaranteed for 200 kS/sec (PCI-6024E a 12-bit data acquisition board - National Instruments). The captured voltages were sampled at 100 kHz and acquired by a stand alone algorithm created using **LabVIEW** software (ver. 5.1 National Instruments) and **Matlab** software (ver. 5.2 Math Works Inc.)

For each step, the measured voltages were normalized to the maximum collected voltage (see Chapter 4 for details). Figure 5.10 shows the normalized induced fields generated by a circular coil placed perpendicular to the pool surface with the inductors' leads insulated. For the same coil orientation and non-insulated inductors, Figures 5.11 and 5.12 show the normalized induced fields generated within homogenous and heterogeneous

volumes respectively. For the heterogeneous volumes, the measuring probe (the inductor assembly) was covered with oil while the media of the dominant region (pool) was alternated.

The procedure described above was repeated with the circular coil positioned horizontally. Next, the same steps were applied to the Figure-8 coil both in horizontal and vertical orientation. Since the focus of this part of the work was to determine the field distribution for a coil normal to the surface, the results of these steps are not presented. However, some of the key findings are qualitatively discussed at the end of this chapter.

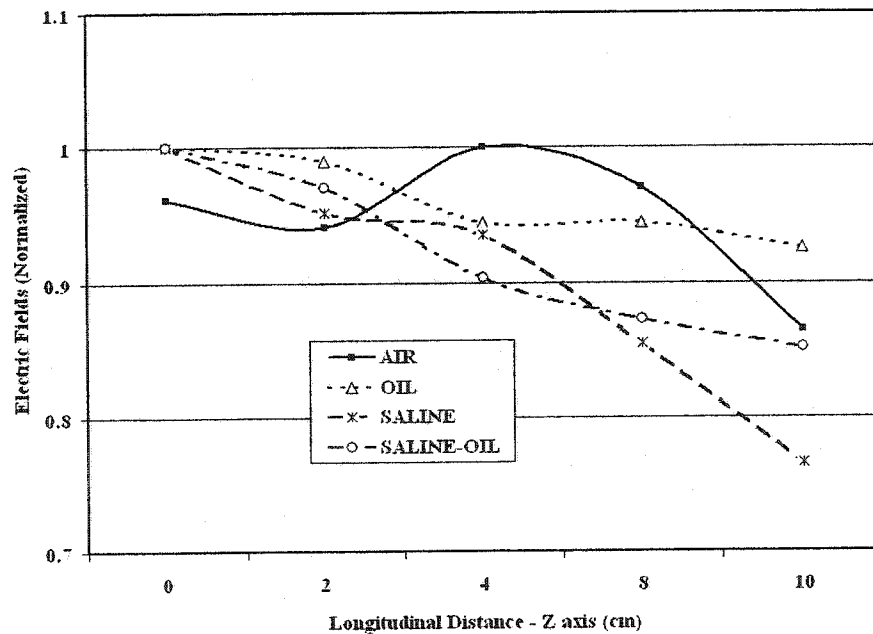


Figure 5.10  
Normalized electric fields captured by insulated inductors (circular coil normal to the surface).



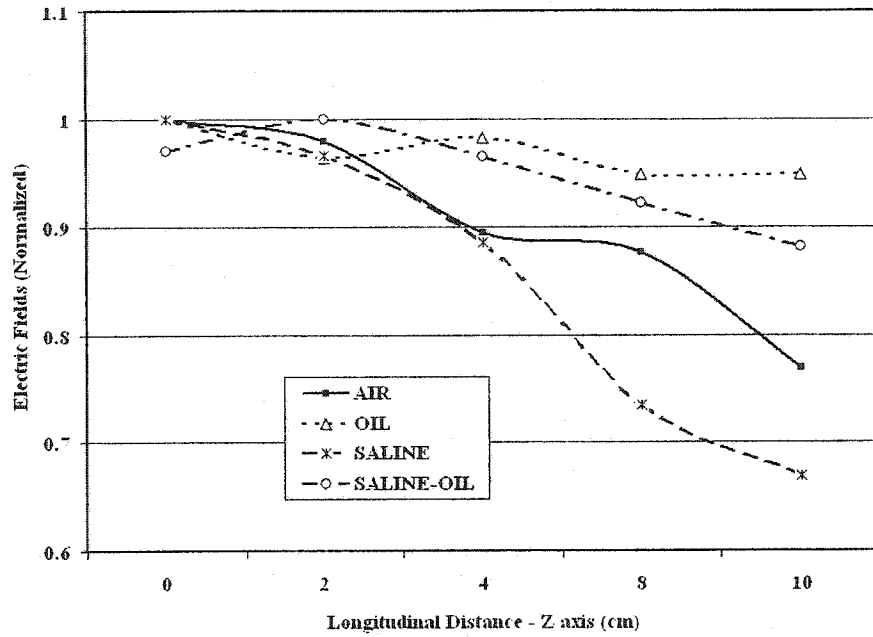


Figure 5.11

Normalized electric fields captured in homogeneous medium (circular coil normal to the surface).

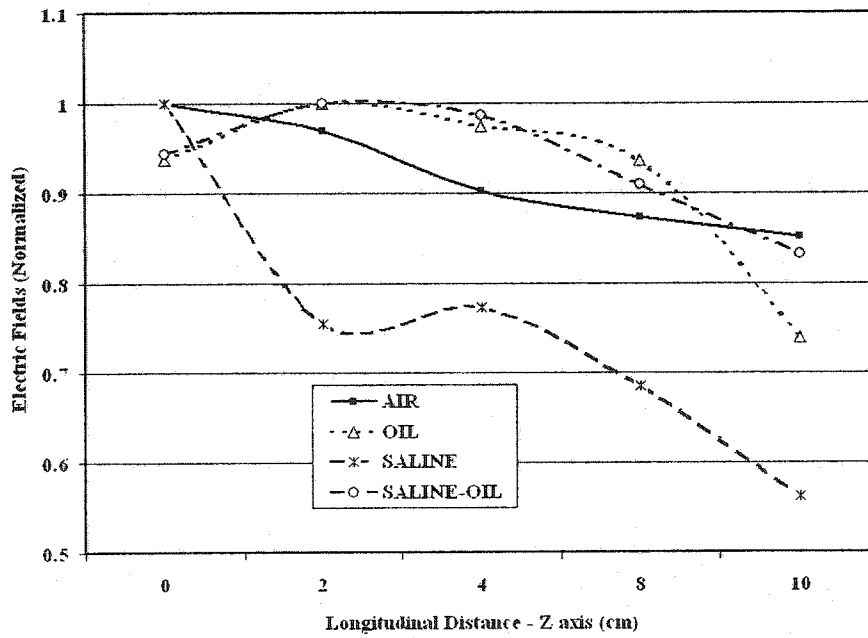


Figure 5.12

Normalized electric fields captured in heterogeneous medium (circular coil normal to the surface).

With respect to the above figures, some key points should be clarified:

1. The calculation of the induced voltages was based on the averaged area below the curves of the second and third quarters of the waveform (Chapter 4), while the calculation for the electric fields was based on the derived formula presented in the previous section.
2. When using the area or the slope to calculate the induced voltages for the previous point, the results were slightly different (< 5% variation with higher values resulting from calculating the area). This was expected as it was proved in Chapter 4.
3. Although not listed, it is critical to mention that the highest induced fields (non normalized) were measured in a pool of oil. These fields were not influenced by the type of medium filling the probe assembly.

## 5.8 Discussion of the Experimental Results

From the above experiment, the following key findings can be extracted.

1. Coils placed in a horizontal orientation with respect to the targeted area generate higher voltages (electric field) compared to those produced by coils in a normal orientation. These results agree with the published literature. Tofts [78] calculated the current densities resulting from coils placed in both directions (parallel, normal)<sup>2</sup>.

Based on his findings, he suggested that nerve fibers running parallel to the skin

---

<sup>2</sup>

His model consisted of a one-turn 10cm diameter coil which was placed parallel to the target and spaced 1cm from its surface. The target was modeled as a tissue with a conductivity of 0.2 Siemens. By applying a pulse with a current rate of change =  $10^8$  A/s, the calculated current densities were  $J_{parallel} = 6.8$  A/m<sup>2</sup> while  $J_{perpendicular} = 4.1$  A/m<sup>2</sup>.

surface are more likely to be stimulated than those running obliquely. Accordingly, he concluded that it is extremely difficult to stimulate nerve fibers running perpendicularly. Subsequently, coils in normal positions have been implemented in rTMS therapy as an option for sham treatment<sup>3</sup>.

2. The maximum voltages for the circular coil in horizontal and normal positions were measured above its outer edge. For the Figure-8 in a horizontal position the maximum voltage was measured above its center while in a normal position it was measured above its edge. With respect to depth, the maximum induced voltages, regardless of coil type or orientation, are located at the surface of the targeted region.
3. Increased conductivity of the dominant medium within the targeted region results in an increase in the electric field gradient. For the collected data, the highest gradient was obtained using a pool of saline solution. This applies for both coils regardless of orientation (data not shown due to its large size).
4. The question that might arise at this point: what is the validity of Roth's hypothesis and what is the impact of media conductivity on his model?

Recalling from Chapter 2, Roth's approach [60,63] states that the static field component will appear due to ion accumulation between the surface separating the two media (regions). However, there was no explanation for the source of these ions.

Further, the experimental results presented in this chapter clearly show that the

---

<sup>3</sup>

For rTMS sham protocol, a typical procedure is to apply stimulation with the coil positioned perpendicular to the head. This practice normally gives the patient the impression of receiving a genuine treatment yet in reality no cortical stimulation is taking place.

conductivity of the media (dominating the region of interest during magnetic stimulation) is the primary factor in improving the stimulation efficacy (increasing the electric field gradient). This concept was also observed during the *in vivo* study (Chapter 6).

## **Chapter 6      Magnetic Stimulation: The Effects of Pulse Configuration**

### **6.1 Introduction**

When applying magnetic stimulation two types of pulses are utilized: bi-phasic and mono-phasic. The former are used for therapeutic purposes and usually applied to nerves lying deep or with high thresholds of depolarization, while the latter are mostly used in the diagnosis of peripheral nerves. Despite the fact that both waves are implemented in various clinical applications, many key questions related to their effects are still not answered. For instance, there is still controversy regarding the impact of the pulse shape in defining the site of stimulation [38-41]. Also, to our knowledge, there isn't a well established method (especially with cranial stimulation) which quantifies the effects of waveform shapes and their responses.

Considering the above and after reviewing previous studies [36-41], it was decided to conduct a study with the objectives of determining the stimulation site and establishing a quantitative relation between pulse configuration and the resulting neurological responses. Subsequently, the study findings will be implemented to improve rTMS technique in treating neuropsychiatric illness.

Although the primary focus of this chapter is the design aspects and the results of this

study, it also includes a brief background of skeletal muscles' electro-physiology and their behavior during stimulation as well as a short review of other related studies.

## 6.2 The Organization and Function of Skeletal Muscle Tissues

Skeletal muscle fibers are single threadlike cells with diameters that range between 50-100  $\mu\text{m}$  and lengths that vary from a few millimeters to tens of centimeters. The activities of these muscles are controlled by bundles of axons which extend from the spinal cord and include descending motor axons and ascending sensory axons (peripheral nerve). Each motor axon is part of a motor neuron (nerve cell) that is connected to a number of muscle fibers. The combination of the motor neuron and the muscle fibers is called a motor unit. Figure 6.1 illustrates a motor unit consisting of a neuron cell body, a long conductive axon, and a group of muscle fibers innervated by axonal branches.

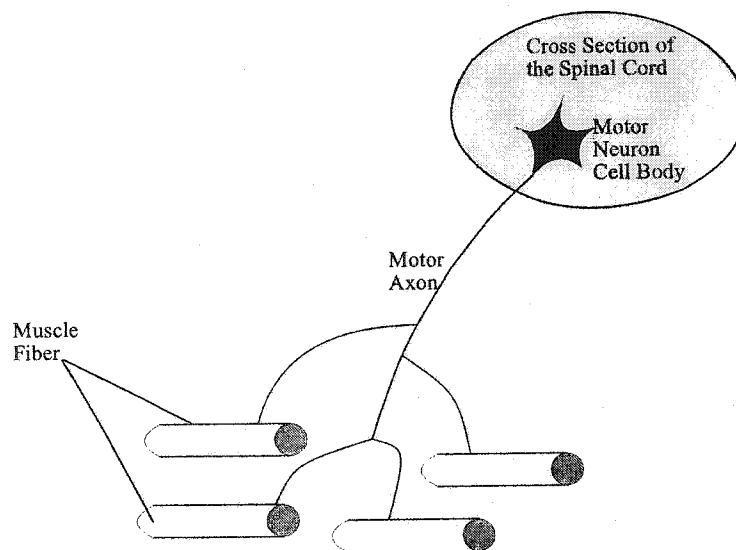


**Figure 6.1**  
An anatomical structure of a motor unit.

It should be noted that motor units have different sizes (within each muscle), and the number of muscle fibers in a motor unit is dependent on the type of activity assigned to that muscle. For instance, to achieve fine control for eye movement, the number of muscle fibers in a single motor unit could be in the order of tens of fibers. However, for a large muscle, such as the biceps brachii, this number may increase to several thousand fibers driven by a single motor neuron.

When recruited by the motor neuron, the muscle fibers contract as a group. The contraction process starts with the motor neuron initiating an electrical signal that propagates along the nerve fiber or axon. When this signal reaches the end of the neuron branch, a neurotransmitter, acetylcholine, is released into the synaptic cleft (a region between the pre synaptic neuron membrane and the muscle fiber post synaptic membrane). Proceeding toward the muscle fiber membrane under the branch terminus, the neurotransmitter binds with a group of protein receptors activating gates and allowing the flow of Sodium ions into the cell. By activating a sufficient number of protein gates, the muscle fibers are recruited and an electrical action potential propagates down the length of the muscle. The recorded amplitude of the motor unit action potential (which depends on the motor unit size and its distance from the electrodes) is in the order of hundreds of  $\mu\text{V}$  and increases for larger motor units.

The arrival of the action potential at the muscle fiber starts a chain of activities, such as the release of calcium ions from the sarcoplasmic reticulum into the cell interior. The release of these ions initiates forces of attraction between the actin and myosin (muscle fiber filaments) and ultimately results in muscle contraction which may last for several hundred

milliseconds. Following the contraction, the calcium ions are then pumped back into the sarcoplasmic reticulum and remain there until the arrival of another action potential.

Studies have revealed that the time required for a muscle fiber to contract and relax varies from a few milliseconds to approximately 200 milliseconds [48,88]. While the potential developed by a motor unit takes 5 to 12 milliseconds, the recorded potentials from individual fibers is approximately 1 to 2 milliseconds. The significant difference between these two durations is attributed to the fact that the sites of the axon innervation are spatially distributed (scattered) and there are different distances between the fibers and the recording electrode.

### 6.3 Modeling the M-wave

In order to model the M-wave, which is the sum of the motor unit action potentials, and discuss its properties, it is essential to consider the following assumptions.

1. The region between the motor unit and recording electrodes is homogeneous, isotropic, and purely resistive.
2. The duration of the action potential is shorter than the time required for its propagation along the axon. Hence, the action potential can be implemented as a Dirac Delta function ( $\delta(t)$ ).
3. The recorded motor unit action potentials are different in shape, duration, and amplitude. These differences are dependent on: the size of the motor unit, the spatial dispersion of the axon branches within the innervation zone, as well as the distance and orientation of the muscle fibers relative to the recording electrodes. To ensure



that the recorded signals are independent of electrode positions, all the above effects are incorporated in the transfer function  $h_n(t)$ .

Based on the above assumptions, the neuron action potential ( $\delta_n(t)$ ) that arrives at the muscle fiber  $n$ , can be defined as:

$$\delta_n(t) = \delta(t - t_{\text{delay}(n)}) \quad (6.1)$$

where  $t_{\text{delay}(n)}$  is the time delay resulting from the traveled distance.

The convolution of the motor unit impulse response ( $h_n$ ) with the delayed delta function (from equation (6.2)) results in:

$$m_n(t) = h_n(t - t_{\text{delay}(n)}) \quad (6.2)$$

where  $m_n(t)$  represents the motor unit action potentials recorded by the electrodes.

By summing the action potentials of all the activated individual motor units, the resultant is an M-wave that can be represented as:

$$M(t) = \sum_{n=1}^N h_n(t - t_{\text{delay}(n)}) \quad (6.3)$$

where  $M(t)$  is the summation of the motor unit responses as a result of nerve excitation/stimulation.

Figure 6.2 is a graphical model illustrating the generation of the M-wave (adapted from [88]).

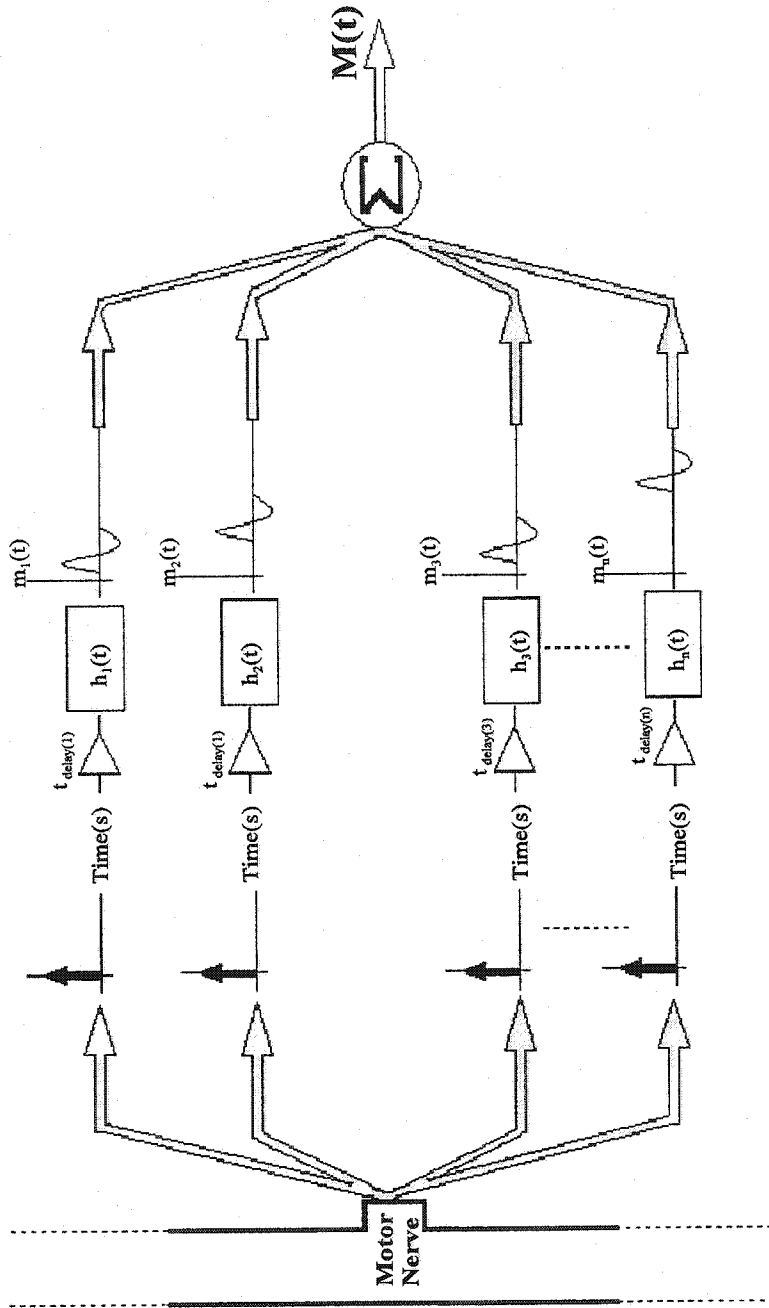


Figure 6.2

A model illustrating the generation of the M-wave from superimposed motor unit action potentials. This model includes: the motor neuron action potentials (represented by delta functions), a block of propagation time delays, and a block of motor unit impulse responses.

## 6.4 The Effect of Pulse Shape on Neural Stimulation

Many researchers have investigated the effect of pulse configuration during magnetic stimulation. Their studies addressed the following critical issues:

### 1. Evaluating the neurological responses resulting from changing pulse configuration

To our knowledge, the first group to investigate the effects of pulse configuration during magnetic stimulation was McRobbie et al. [36]. They suggested that a “damped sinusoid” pulse (bi-phasic) is more effective than a pulse with a “slow decay” (mono-phasic) and that the threshold of stimuli increased with decreased rate of pulse decay. Maccabee et al. [38] used a special magnetic stimulator (Cadwell laboratories) which generated mono-phasic and poly-phasic pulses with identical initial phases and different rates of decay. Their results showed that, both *in vivo* (median nerve) and *in vitro* (mammalian phrenic nerve), poly-phasic pulses can elicit higher responses than those produced by mono-phasic pulses regardless of the initial polarity of the pulse waveform. Furthermore, this group confirmed that both *in vivo* and *in vitro* the maximum elicited response was achieved from the pulse with the highest rate of change. Recently, Niehaus et al. [85], and Kammer et al. [40] investigated motor threshold amplitudes of M-waves for different stimulus intensities. Their findings agreed with that of previous groups.

### 2. The roles of pulse configuration and coil current direction in defining the site of stimulation (virtual cathode)

Nilsson et al. [39] investigated the relation between electrical and magnetic stimulations of the median nerve at the cubital fossa using mono-phasic electrical and bi-phasic magnetic pulses. They determined, using latency and amplitude measurements, that

the virtual cathode (believed to be the site of greatest neuronal activation) for a Figure-8 coil was approximately 3 cm from the coil center junction. Maccabee et al. [38] also noticed a similar shift of stimulus site in their study. However, Mathis et al. [89] noticed different shifts when stimulating the median or ulnar nerves just proximal to the wrist. Their conclusion indicated that tissue in-homogeneity plays a major factor in determining the induced electrical field. Contrary to Mathis et al. findings, Niehaus et al. [85] showed no significant effect for current direction on the virtual cathode position when stimulating the median nerve at the cubital fossa. Further, when stimulating the motor cortex, this group found no difference in latency of the M-wave for the First Dorsal Interosseus (FDI) muscle.

The effect of reversing coil current direction on the virtual cathode position was investigated by Nilsson et al. [39], Kammer et al.[40] and Niehaus et al. [85]. The findings of these groups contradict each other. While Nilsson and Kammer observed changes, Neihaus did not report any. In conjunction with these studies, Maccabee et al. [38] investigated the effect of current reversal both *in vivo* and *in vitro*. Their results showed significant differences in the neural responses when reversing current direction. It should be noted that although there is some agreement regarding the shift in the virtual cathode position, it is only conceptual and not quantitative as the reported shifts varied.

In summary, the results from the above studies agree that bi-phasic pulses are more effective in stimulating both the motor cortex and peripheral nerves. However, considerable controversy still exists regarding the effect of reversing current direction, the position of the virtual cathode (especially within inhomogeneous tissues), and its dependency on the waveform configuration.

## 6.5 Experimental Study

Given the conflicting results mentioned above, a study was conducted to investigate the influence of pulse configuration and current direction when applying magnetic stimulation. This study was approved by the ethics committee at St. Joseph's Hospital (Hamilton, Ontario). Ten healthy subjects (8 males and 2 females ages ranging between 19 and 46 years with a mean age of 27.7) were recruited and gave informed consent. The hypotheses considered for this study were:

1. Bi-phasic waveforms are more effective than mono-phasic waveforms.
2. The stimulus site is not at the junction of the two coils (Figure-8).
3. Coil orientation is critical in neurophysiological responses.
4. Current reversal alters the population of the excited neurons but doesn't introduce any shift to the stimulus site.

The study objectives can be summarized by the following:

1. To quantify the effectiveness of different waveform configurations during magnetic stimulation.
2. To determine the stimulus site (virtual cathode) using different waveforms and coils.
3. To determine the most effective coil (field) orientation.
4. To determine the effects of current reversal when using different coils.

As the median nerve is well defined, easy to access and its response is simple to evaluate, it was chosen as the targeted area for this experiment. The variables considered for this study were: pulse shape (mono-phasic and bi-phasic), coil current rate of change ( $di/dt$ ), coil type (Figure-8 and circular coils), and coil current direction.

## 6.6 Experiment Hardware and Software

In this study, the median nerve of each subject was stimulated at the wrist and cubital fossa using electric followed by magnetic stimulation. For electric stimulation, an electrical stimulator (Dantec-Cantata Inc.) was used to produce single pulses of 200  $\mu\text{sec}$ . The stimulating pulses were delivered by a pair of 8 mm diameter silver electrodes mounted 2.5 cm apart on a plastic bar. To collect the EMG data, pre-gelled disposable surface electrodes were used (Medtronic Inc.). The first electrode was positioned over the thenar eminence crossing the first metacarpal bone perpendicularly at the junction of its proximal and middle thirds. The second electrode was attached over the proximal phalanx of the thumb while the third was attached to the dorsum of the hand. Figure 6.3 illustrates the positions of the three electrodes as well as the sites of stimulation.

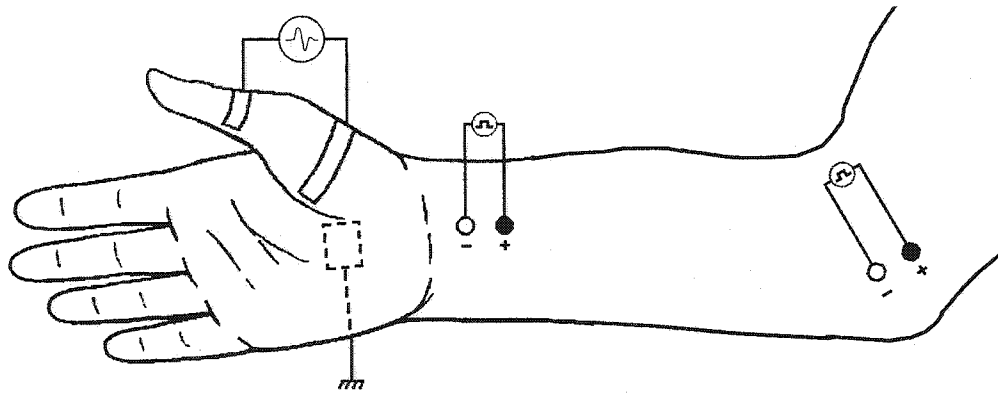


Figure 6.3  
The positions of the recording electrodes and the sites of stimulation.

For magnetic stimulation, a magnetic stimulator (Dantec MagPro) combined with a Figure-8 coil (outer diameter 10 cm consisting of 2x10 windings) and a circular coil (outer diameter 13 cm consisting of 10 windings) was used [84]. The advantage in using the Dantec

system is the flexibility in changing the current direction by a switch located at the front panel, without rotating the coil.

The measured M-waves were amplified to a gain of 2mv/div, bandpass filtered between 20 Hz and 2 kHz, sampled at 10 kHz, and collected via a data acquisition board (PCI-6024E, a 12-bit board guaranteed for 200kS/sec-National Instruments). To ensure high precision ( $\pm 10 \mu\text{sec}$ ) for the M-wave latency studies, the data were also sampled at 100 kHz. All the signals were captured by a stand alone algorithm created using **LabVIEW** software (National Instruments) and **Matlab** software (Math Works Inc.). The algorithm enables the user to acquire a train of signals, calculate the area and the peak to peak amplitude of each pulse, and store the data in ASCII and spreadsheet formats. It also allows the user to retrieve or re-read the data from the stored files, average, and post-process the data (see Figure 6.4).

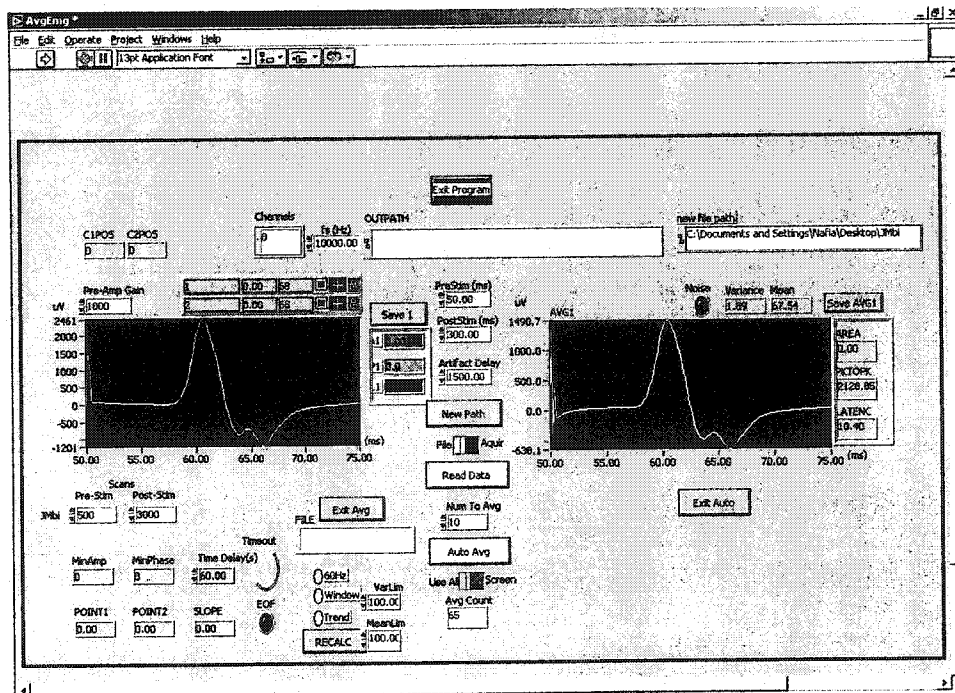


Figure 6-4  
Front panel display of the software capturing the M-wave of a subject.

## 6.7 Method

The subjects were comfortably seated with their arms fully extended and supported by foam and sand bags. Considering that each session lasted one to two hours, it was crucial that the subject be relaxed throughout the experiment to ensure successful and reliable recorded data.

Following a few trials, it was concluded that defining the coil's most effective position and maintaining it throughout the experiment were critical factors during magnetic stimulation. To precisely determine these positions, it was decided to perform electric stimulation prior to magnetic stimulation.

During electric stimulation, at both the elbow and the wrist, the most effective position of the stimulating electrodes was defined according to the cathode placement that gave the lowest stimulus threshold of the thenar muscle [39]. Next, the optimum cathode position was marked at each stimulating site and the distance between the two positions, along the forearm, was measured. Using the measured distance and the difference in the latencies of the captured M-wave, the nerve conduction velocity was calculated. This value was used during magnetic stimulation to define the stimulation site (the position of the virtual cathode) and to calculate any shift in its location. A self adhesive tape was used to mark the exact placement of the cathode (cross mark). In addition to defining the cathode sites, the electric stimulation was utilized to map the path of the median nerve at the elbow.

During magnetic stimulation, the coils were superimposed over the marked cathode while their axes were oriented to generate maximum stimulation for a given current. This was done, with the help of a laser pen projecting the marked electrical cathode position on



the internal perimeter of the circular coil and the center of the Figure-8 coil. The handles for both coils were pointed toward the subject's shoulder and aligned along the mapped median nerve. With the aim of collecting reliable measurements, the coil positions were manually maintained as precisely as possible throughout the experiment.

## 6.8 Results

### 1. Determining stimulation site

Electric stimulation was applied to the median nerve at two sites: wrist and cubital fossa. Five pulses were applied at each site and their recruited M-waves were measured and averaged. Figure 6.5 shows the averaged M-waves when electrical stimulation was applied to the median nerve at the elbow and the wrist of a subject.

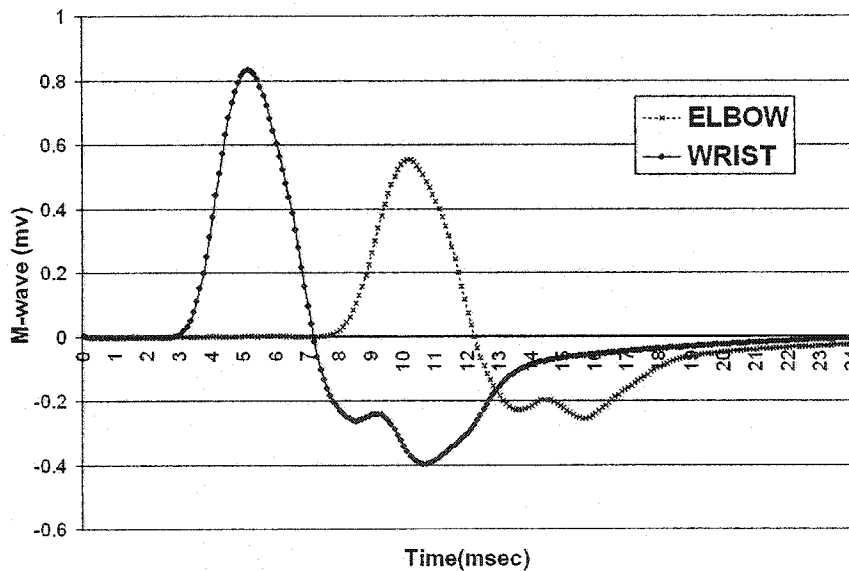
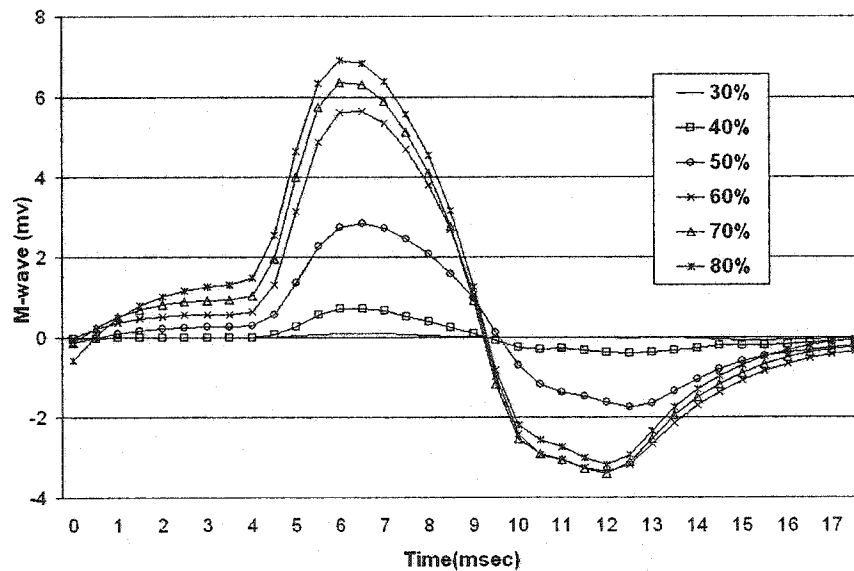


Figure 6.5  
M-wave responses using electrical stimulation.

## 2. The effect of pulse configuration

Using Figure-8 and circular coils, magnetic stimulation was applied to the median nerve at two sites: wrist and cubital fossa. The influence of pulse configuration (bi-phasic, mono-phasic) was investigated for different stimulus intensities. The intensities were varied from 30% to 80% of the maximum stimulator output with a 10% step increase. At each step, ten consecutive stimuli were applied and their responses were collected, sampled at 10kHz, and averaged. To ensure that the same energy was supplied for all stimuli within one step, the  $di/dt$  value, displayed at the front panel, was monitored throughout the experiment. Figures 6.6 and 6.7 show M-wave responses of bi-phasic and mono-phasic waveforms respectively, when placing a Figure-8 coil at the elbow of a subject.



**Figure 6.6**

M-wave responses for bi-phasic pulses using a Figure-8 coil at the elbow. The starting point of the time axis was selected to accommodate the figure size.

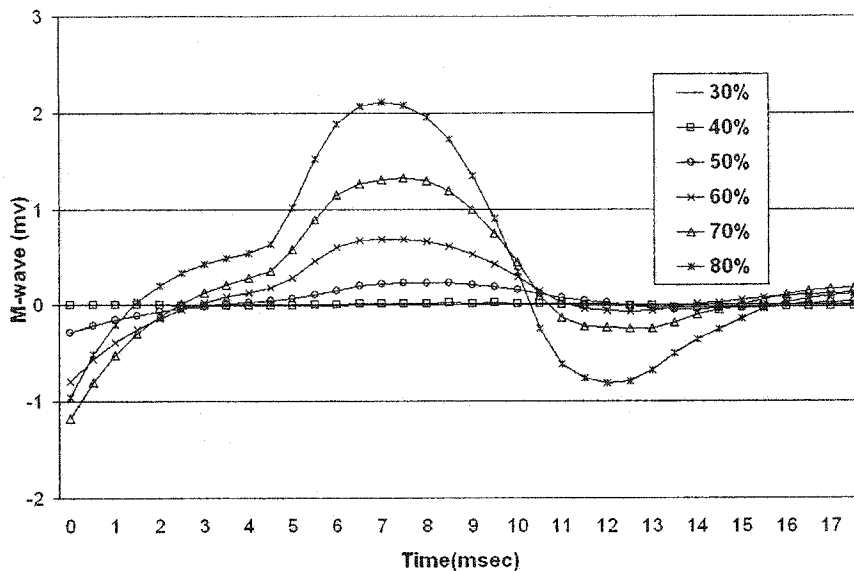


**Figure 6.7**

M-wave responses for mono-phasic pulses using a Figure-8 coil at the elbow. The starting point of the time axis was selected to accommodate the figure size.

From Figures 6.6 and 6.7, it is apparent that bi-phasic stimuli result in higher responses compared to that of mono-phasic. Further, Figure 6.6 clearly shows that the rate of change of the M-waves decreases at higher stimulating intensities (an indication that the number of motor units recruited approaches its maximum at these intensities). It should be noted that the responses obtained from stimulating the nerve at the wrist resulted in lower (amplitude) responses with shorter latencies.

### 3. The effect of changing current direction

In this section, the procedure outlined above was repeated using normal and reversed stimulating current pulses. The variables considered in this section are: stimulus intensities

(50%, 60%), pulse configuration (bi-phasic, mono-phasic), coil type (Figure-8, circular), and stimulating sites (wrist and cubital fossa). These variables were applied for both normal and reverse current directions. For each subject, the procedure starts with normal bi-phasic stimulation at the elbow using the Figure-8 coil. Five consecutive stimuli were applied for each intensity (50%, 60%) and their responses were collected and averaged. To ensure that the same energy was supplied for all stimuli within one step, the  $di/dt$  value, displayed at the front panel, was monitored constantly. While maintaining the coil position, the current direction was reversed and the stimulation was repeated (at the elbow) for both intensities. Next, mono-phasic stimulation was applied using 50% and 60% for both current directions. Five consecutive stimuli were applied for each intensity and their responses were collected and averaged. Figure 6.8 shows M-wave responses of normal and reversed current pulses when placing a Figure-8 coil at the elbow of a subject.

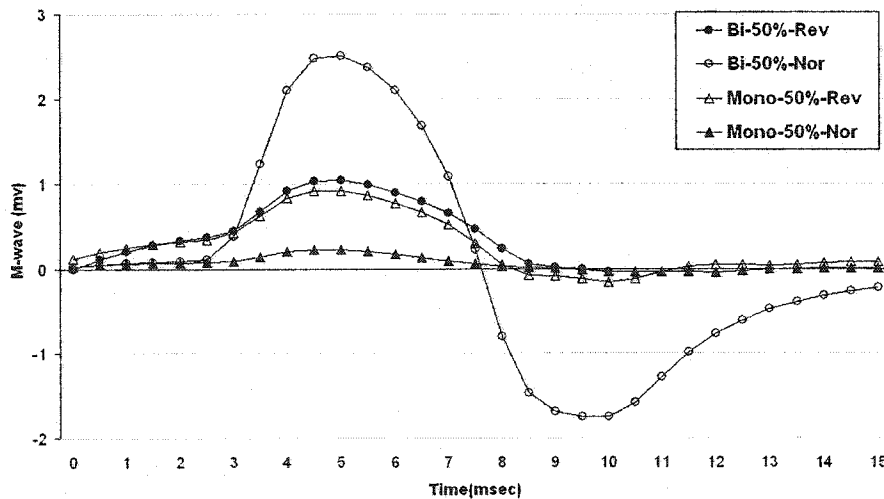


**Figure 6.8**  
M-wave responses for various waveforms and current directions using a Figure-8 coil.

The above steps were also performed at the wrist and the entire procedure was repeated using the circular coil.

It is important to clarify a few critical points related to the results presented in this section. First, all the latencies were calculated using the peak of the M-waves and not the initial point of their rising edge. This procedure was followed to minimize the effect of the artifact which is dominant at the M-wave base line. Second, the data for the “normal” current direction were collected while the coil was placed along the arm with its handle pointing toward the subject’s shoulder. Third, the “normal” direction represents the default output of the Dantec MagPro stimulator, while “reverse” direction should be set by the user. Fourth, to ensure high precision ( $\pm 10 \mu\text{sec}$ ) when measuring the M-wave latencies, the collected data in this section (also used in the next section) were sampled at a rate of 100kS/sec.

#### 4. The effects of pulse configuration and current direction on the M-wave latency

In this study, the shift in the virtual cathode position (the site of stimulation) was determined using precise measurements of the M-wave latencies (at the wrist and the elbow) combined with the nerve conduction velocity (calculated from electric stimulation).

During electrical stimulation, the difference between the M-wave latencies (elbow vs wrist) was calculated for each subject using the following formula:

$$\text{Latency}(n) = \frac{\left[ \sum_{i=1}^{K_e} (\tau_{\text{elbow}}(i) - \tau_{\text{wrist}}(i)) \right]}{K_e} \quad (6.4)$$

where  $n$  and  $i$  are notations for the subject and electric pulses respectively,  $K_e$  is the

total number of applied pulses,  $\tau_{elbow}$  and  $\tau_{wrist}$  are the M-wave latencies when stimulating the elbow and the wrist respectively. Considering that the distance between the two stimulating positions is known, the nerve conduction velocity ( $CV$ ) can be calculated for each subject using:

$$CV(n) = \frac{d_{elbow}(n) - d_{wrist}(n)}{\text{Latency}(n)} \quad (6.5)$$

where  $d_{elbow}$  and  $d_{wrist}$  are the distances between the measuring electrodes and the sites of electrical stimulation at the elbow and wrist respectively.

The calculated conduction velocity was implemented during magnetic stimulation to determine the shift in cathode placement using the following equation:

$$\text{Shift}(n) = CV(n) \times \left( \left[ \frac{\sum_{i=1}^{K_m} \tau_{magnetic}(i)}{K_m} \right] - \tau_{electric}(n) \right) \quad (6.6)$$

where  $n$  and  $i$  are notations for the subject and magnetic pulses respectively,  $K_m$  is the total number of magnetic pulses applied (using the same stimulation intensity),  $\tau_{magnetic}$  and  $\tau_{electric}$  are the latencies due to magnetic and electric stimulation respectively. Using equation 6.6, if the calculated shift is positive it implies cathode movement toward the shoulder, however, if it is negative it indicates cathode shift toward the hand.

Finally, to calculate the average shift for all of the subjects ( $N$ ) the following equation was used:

$$\text{Average Shift} = \frac{\left[ \sum_{n=1}^N \text{Shift}(n) \right]}{N} \quad (6.7)$$

## 6.9 Analyses of the Results

### 1. The effect of pulse configuration

Table 6.1 illustrates the averaged M-waves resulting from stimulating the cubital fossa by various coils. It should be noted that prior to averaging the presented data they were normalized (per subject) to their maximum responses (bi-phasic stimuli at 80% intensity).

Table 6.1  
Summary of the M-waves resulting from using different coils at the elbow

Stimulus Intensity % of Max.O/P	Average ( $di/dt$ ) (A/ $\mu$ s)	Figure-8 coil Peak $\pm$ s.d.(normalized)		Circular coil Peak $\pm$ s.d.(normalized)	
		Bi	Mono	Bi	Mono
30%	46.3	0.05 $\pm$ 0.04	0.03 $\pm$ 0.02	0.08 $\pm$ 0.06	0.02 $\pm$ 0.04
40%	62.5	0.18 $\pm$ 0.19	0.04 $\pm$ 0.04	0.16 $\pm$ 0.14	0.06 $\pm$ 0.08
50%	77.7	0.39 $\pm$ 0.25	0.12 $\pm$ 0.07	0.24 $\pm$ 0.16	0.08 $\pm$ 0.10
60%	90.8	0.64 $\pm$ 0.24	0.26 $\pm$ 0.17	0.47 $\pm$ 0.27	0.10 $\pm$ 0.14
70%	106.6	0.86 $\pm$ 0.12	0.43 $\pm$ 0.28	0.65 $\pm$ 0.57	0.12 $\pm$ 0.16
80%	121.5	1.00 $\pm$ 0.00	0.62 $\pm$ 0.36	1.00 $\pm$ 0.00	0.16 $\pm$ 0.22

To determine if the above results have any statistical significance with respect to the effect of pulse configuration, the software Statistica was used (StatSoft Inc., ver. 5.5). Considering an alpha of 0.01, coil type and phase as independent variables, M-wave peaks as the dependent variable, and the stimulus intensity as the repeated measure, the analysis conducted was repeated measures ANOVA (Analysis of variance) combined with the Bonferroni test. The advantage of applying this protocol is that it prevents any over-correction that might result when comparing the variables of interest more than once [90].

The results of the analysis indicated significant statistical relation between stimulation intensity vs M-wave amplitude ( $p=0.00003$ ) as well as a significant phase effect ( $p=0.0046$ ).

Figure 6.9 shows the effect of pulse configuration at different stimulation intensities.

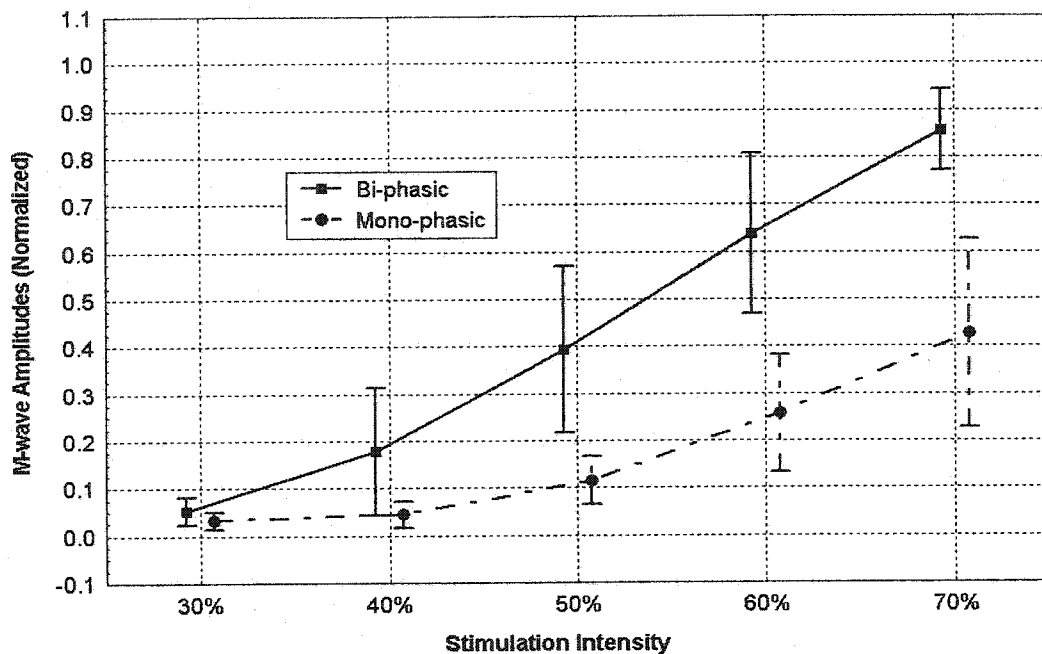


Figure 6.9

Normalized M-wave amplitudes (mean  $\pm$  S.D.) for bi and mono pulses (10 subjects, Figure-8 coil, elbow).

During the post-hoc testing, pre-planned paired t-tests were used with the Bonferroni correction to compare the effects of pulse configuration at different stimulation intensities (30% and 40%). For these intensities, the difference between the means was not statistically significant ( $p=0.17$  and  $p=0.07$  respectively). However, for stimulation intensities at or above 50% the results show significant mean differences between the effect of bi-phasic and mono-phasic waveforms (all  $p<0.01$ ). This conclusion is also applicable when using a circular coil.

## 2. The virtual cathode position

Both Figure-8 and circular coils were used to investigate the shift in the virtual



cathode position, however, the collected measurements from the latter were not considered for statistical analysis as they showed large variances. The results for the circular coil confirm the theoretical aspects of the unfocused magnetic field generated by this coil. Table 6.2 shows the effects of changing pulse configuration on the virtual cathode position when using a Figure-8 coil at the elbow.

Table 6.2  
Summary of the shift in the virtual cathode position

Stimulus Intensity % of Max. O/P	Average $di/dt$ (A/ $\mu$ s)	Bi-phasic Shift $\pm$ s.d.(cm)	Mono-phasic Shift $\pm$ s.d.(cm)
30%	46.3	1.93 $\pm$ 5.59	1.45 $\pm$ 4.39
40%	62.5	1.40 $\pm$ 4.33	1.98 $\pm$ 3.64
50%	77.7	0.43 $\pm$ 4.45	1.20 $\pm$ 2.28
60%	90.8	-0.31 $\pm$ 4.69	0.49 $\pm$ 2.43
70%	106.6	-0.64 $\pm$ 4.52	-0.67 $\pm$ 2.24
80%	121.5	-0.98 $\pm$ 4.44	-1.12 $\pm$ 2.66

To determine if the above results have any statistical significance, the software Statistica was used. Considering an alpha of 0.01, the analysis conducted was repeated measures ANOVA combined with the Bonferroni test. The analysis results showed that there is no significant shift ( $p > 0.05$ ) in the virtual cathode position when changing pulse configuration. However, the results indicate a significant relationship between the level of stimulation and the shift in the virtual cathode position ( $p < 0.01$ ). As well, when applying paired t-tests, a consistent shift in the virtual cathode (toward the hand) was noticed when increasing the stimulation level. This shift applies to both waveforms and for all intensities.

Table 6-3 presents the shift of the virtual cathode for nine subjects. Comparable to electrical stimulation, this trend is expected since more distal nodes will be stimulated at higher field intensities.

Table 6.3  
Shift of the virtual cathode (in centimeters) from the electrical cathode when using bi-phasic and mono-phasic pulses (9 subjects, Figure-8 coil at the elbow)<sup>1</sup>

Subject	30%B	40%B	50%B	60%B	70%B	80%B	30%M	40%M	50%M	60%M	70%M	80%M
GH	-6.76 <sup>2</sup>	4.16	-3.12	-4.16	-5.20	-5.72	-4.68	-4.68	-3.12	-3.12	-4.16	-4.68
GO	5.50	0.00	-0.50	-1.00	-1.50	-2.00	-0.50	0.00	-0.50	-1.50	-3.00	-4.50
JR	-2.27	-1.70	-1.14	-2.27	-2.27	-2.84	-0.57	-0.57	0.57	3.97	-1.14	-0.57
JL	-2.63	-2.63	-2.63	-2.10	-2.10	-3.15	-3.67	8.40 <sup>2</sup>	0.53	-2.10	-2.10	-3.67
JM	7.30 <sup>2</sup>	0.61	0.00	-0.61	-1.22	-1.83	0.61	0.61	0.61	0.61	0.61	0.61
NA	1.67	0.56	0.00	-2.23	0.00	0.56	1.67	1.67	1.11	1.67	1.67	2.23
RM	3.31	1.25	0.38	-0.76	-1.19	-1.46	4.34	3.80	3.80	1.63	-1.09	-2.17
SM	3.66	2.62	2.62	2.09	1.05	1.57	4.71	4.71	3.66	-1.05	-1.05	-1.05
TB	-2.46	-2.87	-3.28	-4.10	-4.92	-4.92	2.05	0.82	0.82	0.82	0.00	-0.41

<sup>1</sup> As shown in the above table, one subject was excluded from this analysis due to an error in the collected data.  
<sup>2</sup> The marked results are significantly high due to stimulation threshold effect or errors in the measured data.

Figure 6.10 shows the effect of pulse configuration on the virtual cathode position when using a Figure-8 coil at various stimulation intensities.

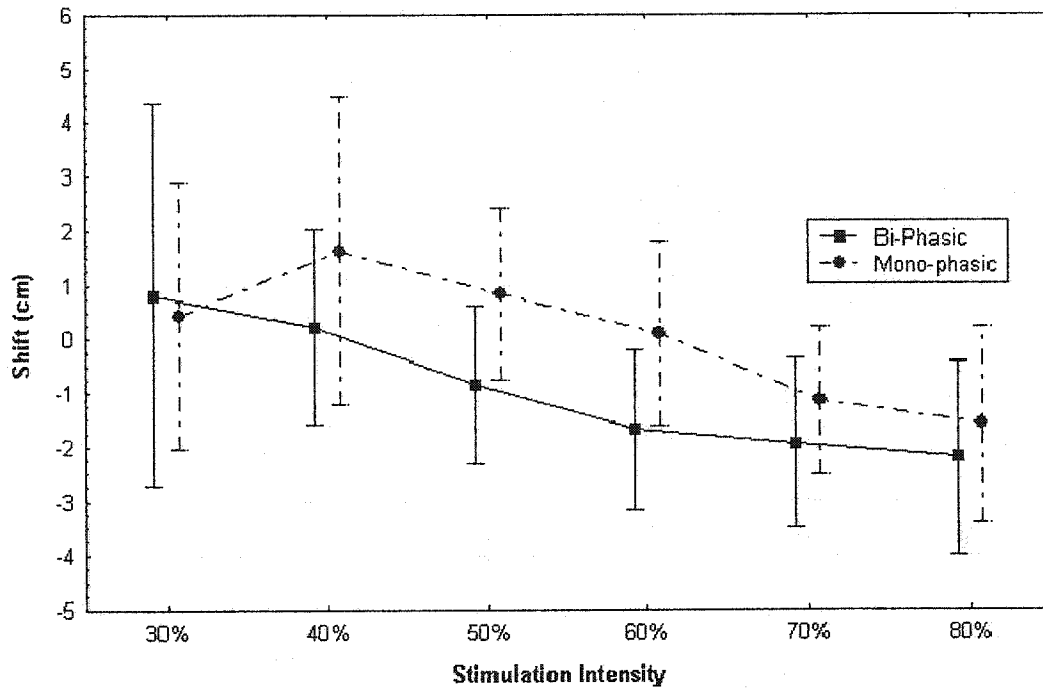


Figure 6.10

Shift (mean  $\pm$  S.D.) in the virtual cathode due to bi and mono waveforms (9 subjects, Figure-8 coil, elbow).

### 3. The effect of changing current direction

Table 6.4 shows averaged M-wave amplitudes resulting from stimulating the elbow and wrist with Figure-8 and circular coils. Sampled at a rate of 100kS/sec, the data was collected for both normal and reverse current directions using 50% and 60% intensities. Table 6.5 summarizes averaged shifts in the virtual cathode position for these experimental conditions. It should be noted that prior to averaging the results presented in Table 6.4 they were normalized (per subject) to their maximum responses (biphasic stimuli, 80% intensity).

Table 6.4  
Averaged M-wave responses (normalized) as a function of current direction (Fig8,elbow)

Site Coil type	Stimulation Intensity (%)	Bi-phasic Peak $\pm$ s.d.(normalized)		Mono-phasic Peak $\pm$ s.d.(normalized)	
		Normal	Reverse	Normal	Reverse
Wrist Figure-8	50%	0.27 $\pm$ 0.19	0.21 $\pm$ 0.16	0.16 $\pm$ 0.13	0.27 $\pm$ 0.18
	60%	0.48 $\pm$ 0.26	0.34 $\pm$ 0.25	0.23 $\pm$ 0.18	0.39 $\pm$ 0.24
Wrist Circular	50%	0.18 $\pm$ 0.20	0.07 $\pm$ 0.05	0.07 $\pm$ 0.08	0.22 $\pm$ 0.32
	60%	0.33 $\pm$ 0.38	0.16 $\pm$ 0.19	0.17 $\pm$ 0.19	0.33 $\pm$ 0.35
Elbow Figure-8	50%	0.50 $\pm$ 0.28	0.27 $\pm$ 0.12	0.05 $\pm$ 0.04	0.17 $\pm$ 0.07
	60%	0.66 $\pm$ 0.28	0.50 $\pm$ 0.17	0.12 $\pm$ 0.07	0.42 $\pm$ 0.18
Elbow Circular	50%	0.25 $\pm$ 0.19	0.18 $\pm$ 0.18	0.09 $\pm$ 0.14	0.06 $\pm$ 0.09
	60%	0.48 $\pm$ 0.28	0.31 $\pm$ 0.19	0.09 $\pm$ 0.08	0.16 $\pm$ 0.16

Table 6.5  
Averaged shifts of the virtual cathode (in centimeters) as a function of current direction

Site Coil type	Stimulation Intensity (%)	Bi-phasic		Mono-phasic	
		Normal	Reverse	Normal	Reverse
Wrist Figure-8	50%	3.79 $\pm$ 2.45	5.51 $\pm$ 2.46	5.11 $\pm$ 3.04	5.59 $\pm$ 3.83
	60%	4.03 $\pm$ 2.48	5.17 $\pm$ 2.73	5.17 $\pm$ 3.06	5.32 $\pm$ 2.79
Wrist Circular	50%	9.02 $\pm$ 3.91	7.94 $\pm$ 3.04	8.17 $\pm$ 4.48	7.98 $\pm$ 2.95
	60%	8.89 $\pm$ 0.91	6.81 $\pm$ 4.05	8.83 $\pm$ 3.89	8.51 $\pm$ 3.09
Elbow Figure-8	50%	0.21 $\pm$ 2.84	0.93 $\pm$ 2.95	0.53 $\pm$ 3.53	1.21 $\pm$ 3.05
	60%	-0.59 $\pm$ 2.54	0.46 $\pm$ 3.14	0.43 $\pm$ 3.33	0.51 $\pm$ 3.23
Elbow Circular	50%	2.15 $\pm$ 5.71	2.69 $\pm$ 9.81	2.57 $\pm$ 5.83	4.00 $\pm$ 7.78
	60%	3.36 $\pm$ 10.50	2.96 $\pm$ 10.05	1.16 $\pm$ 5.00	1.37 $\pm$ 4.89

To determine if the data presented in Table 6.4 has any statistical significance, a paired t-test (defined by Statistica software as “t-test for dependent samples”) was applied. For the cubital fossa, the results of the analysis show a significant difference in the effects of pulse configuration on the M-wave amplitudes ( $p < 0.05$ ). This conclusion is applicable for both current directions and coil types. However, for the wrist, no significant differences were found in the responses. This can be attributed to tissue in-homogeneity and the measurements are less precise because of the large artifacts embedded in the measured signals (especially with mono-phasic stimulation). These artifacts are due to the coil proximity to the measuring electrodes.

With respect to the shift in the virtual cathode, the analysis results show no significant effect when changing current directions. This holds true for both the cubital fossa and wrist stimulation.

## 6.10 Discussion

The key findings of this study can be summarized by the following:

1. Using the same stimulating intensity, bi-phasic stimuli result in higher M-wave amplitudes than those achieved with mono-phasic. This holds especially true for high stimulus intensities (at or above 50%) and applies for both coils. The different responses can be explained by either the nerve hyperpolarization-depolarization phenomena [91] or by the difference in current rate of change within the second and third phases of the two waveforms [38].

With respect to the first explanation, it is well established that the reversal of  $Na^+$

inactivation (through initial hyperpolarization) results in an increased number of the  $Na^+$  channels available for the subsequent depolarization phase [91]. This translates to an increase in fiber excitation as well as a decrease in the stimulation threshold required for activation. This mechanism was suggested by Maccabee et al. as a possible reason for the different pulse effects [38].

The second explanation, which is based on the outward charge transfer, depends primarily on the area (integration) of the stimulus depolarizing phase (second and third quarter of the pulse waveform). As well, this concept was adopted by Maccabee et al. with an attempt to explain the different effects due to pulse type [38].

From our perspectives and based on the findings of this study, the second suggestion is preferable as it has been proved both theoretically through computer simulations (Figures 3.11, 3.13) and experimentally (Figure 4.12). In fact, it is interesting to see that the results are quantitatively comparable to that of the clinical study (Figure 6.9).

2. The shift in position between the virtual and electrical cathodes is complicated as it depends on many variables. The variables include tissue in-homogeneity, distance of median nerve from the coil, median nerve pathway geometry, pulse intensity as well as coil type, position, and orientation. Although not included in the data, the experimental results qualitatively indicate that coil orientation has a tremendous influence on the elicited responses<sup>3</sup>. Some differences emerged when comparing the findings of this study with that of other researchers who defined the shift in the

---

<sup>3</sup>

It must be stressed that the Figure-8 coil axis was positioned as parallel as possible to the median nerve axis.

virtual cathode position as a fixed distance (ranging between 3 and 4cm) [38-41]. These differences can be attributed to the following. First, the outcomes of these experiments depended on the interaction of many complex variables which are not uniform including hardware (systems, coils), experimental protocols, and subject variability. Second, the studies presented in the literature (including this one) have quantified the stimulation responses based on measuring the electrical signal generated by muscles. Although this technique is not a direct precise measure for a single nerve fiber excitation, it is the only viable *in vivo* approach. Third, the mechanism for magnetic stimulation is not yet fully understood, and “the neurophysiology is still largely unknown” [92]. A confounding factor in all studies is the precise orientation of the median nerve with respect to the coil axis. Although considerable effort was made to map the median nerve at the elbow, its direction changes widely within the area of magnetically induced activation.

3. In conjunction with the above, an attempt was made in this study to accommodate subjects' variability by determining the median nerve conduction velocity for each subject independently. However, it should be noted that a slight variation within each subject still exists and can't be avoided. For instance, at threshold stimulation the tendency is to stimulate only large axons (greater inter nodal distance) which have a faster conduction velocity than the average. Conversely, with higher levels, smaller axons with a slower conduction velocity will also be excited. Thus, M-wave latencies and subsequently shifts in the virtual cathode position may vary depending on the average fiber size of the activated axons.

4. The study showed no significant effect either to the pulse type or the current direction in defining the position of the virtual cathode. This result agrees with Niehaus et al. findings [85] and disagrees with that of Kammer et al. [40]. Further, the study showed that the shift in the virtual cathode was substantial at the wrist compared to the elbow. This significant shift can be attributed to tissue in-homogeneity, large embedded artifacts, or other unknown factors. However, the contribution of any of these sources is difficult to assess from the experimental data.
5. With respect to tissue in-homogeneity, unique responses were observed in two particular subjects who had higher subcutaneous fat at the cubital fossa (TB in Table 6.3 and another subject whose results were rejected due to measurement error). It was noticed that the averaged M-wave responses in both subjects were lower and had a longer latency when compared to the group. These observations can be attributed to the increased distance of the median nerve from the coil and/or to tissue in-homogeneity in that region.
6. Changing current direction results in different responses for both pulse configurations with bi-phasic stimuli generating higher M-wave amplitudes than those achieved with mono-phasic. The outcomes of current reversal may be attributed to the change in the excited neuron population. This can be confirmed by reviewing the responses of each subject and comparing them to that of the group. The collected data (not presented due to its size) clearly indicates that the effects of changing current direction are not comparable within the group as each subject responds differently. The main reason for the different responses is the subjects' variability which may



result in potential miss-alignment between the median nerve and the coil axis.

7. For both pulse configurations, regardless of coil type or current direction, the increase of stimulus intensity ( $di/dt$ ) results in non-linear increases in the M-wave responses. This is expected as the same is true for electrical stimulation.

## **Chapter 7      Conclusions and Future Investigation**

### **7.1 Conclusions**

The primary objective of this thesis was to present new coil designs which can be implemented in magnetic nerve stimulation. Using computer simulations, the Finite Element Method in three dimensions combined with a transient analysis was applied to evaluate the proposed coils. The simulation results showed that the proposed coils improved the strength and focality of the induced fields. To verify these results, a set of coils (Figure-8, circular, and the proposed coils) was assembled based on specifications established with the aid of computer models. The findings of an experiment conducted to evaluate the constructed coils agree with the results of the simulations, confirming the advantages of the proposed coils.

The second objective of this work was to investigate the effect of different stimulus waveforms both theoretically and empirically. This was realized through computer simulations, performing an experiment, and conducting a study on stimulating lower motor neurons. With respect to the study, the goals were to establish a quantitative relation between the stimuli waveform parameters vs the responses and to investigate the effect of pulse configuration in determining the stimulation site.

Considering the above objectives, the key findings of this thesis can be summarized by the following conclusions.

### **Conclusion #1**

The simulation results confirm that the proposed coils enhance the field strength and focality within the targeted area. This improvement was achieved through better turn distribution as well as the addition of a third set of windings. Equally important is the introduction of the ferromagnetic core with its unique shape, which is determined so as to accommodate the width and depth of the target region. When evaluating the performance of various coils, the simulation results indicate that the coil with the magnetic core was superior. Further, when compared to the Figure-8 coil, the experimental results showed a 200% improvement in the induced electric field generated by the coil with the magnetic core. However, some of the advantages in using this coil might be offset by its weight, considering that the coil is manually placed and held.

### **Conclusion #2**

Based on the simulation results, the combination of the three sets of windings provides flexibility in delivering the required stimulus as it enhances the coil selectivity in stimulating one group of nerves whilst leaving another unaffected. For instance, if deep stimulation is required, the current supplied to the first and second sets of coils should be higher than the third (perpendicular) coil. However, if the targeted region is close to the skin surface, effective stimulation can be achieved by supplying current to the third coil only [76]. Although the measured induced fields are lower than those estimated by the simulations (one fold vs one order in

magnitude), the final outcome of the proposed coils can still be considered an improvement to current technology.

### **Conclusion #3**

In this work it has been shown, both mathematically and experimentally, that the first spatial derivative of the induced electric field is directly proportional to the conductivity of the medium dominating the region of interest. Subsequently, if the region of interest is heterogenous with subcutaneous fatty tissues, the electric field gradient will be lower than that within a region of highly conductive tissues (muscle, nerve fiber). This holds true regardless of coil orientation with respect to the targeted area (horizontal, normal).

However, this outcome doesn't totally agree with Roth's widely accepted model [60] which indicates that the total electric field ( $\zeta_{Total}$ ) is dependant on both transient magnetic field ( $\zeta_A$ ) and the electrostatic potential ( $\zeta_\phi$ ) with the latter depending on coil orientation.

### **Conclusion #4**

Bi-phasic stimuli result in higher responses than those achieved with mono-phasic. This conclusion is based on computer simulations (Figures 3.11, 3.13), experimental work (Figure 4.12), and a clinical study (Figure 6.9). In fact, it is interesting to see that the results of the three approaches are quantitatively comparable. This outcome qualitatively agrees with the findings of other researchers [36-41]. However, the

approach introduced to minimize the effects of subjects' variability provides a critical enhancement to realize more reliable results from *in-vivo* studies.

Corresponding to the above, it is important to discuss the mechanism utilized by magnetic stimulators in displaying current rates of change. Typically, these systems capture the waveform rate of change at the first quarter (rising edge). Thus, the displayed reading is the same for mono-phasic and bi-phasic waveforms. However, as have been outlined in Chapters 4 and 6, neural excitation is defined primarily by the current rate of change within the pulse second and third quarters. Thus, capturing and displaying this rate of change, as an indication for pulse effectiveness, is more logical and informative.

#### **Conclusion #5**

Defining the site of stimulation (virtual cathode) during magnetic stimulation is complicated as it depends on many variables. The variables include tissue inhomogeneity, distance between the nerve and the coil, pulse intensity as well as coil type, position, and orientation. Some differences emerged when comparing this conclusion to that of other researchers who defined the shift in virtual cathode as a fixed distance (ranging between 3 and 4cm) [38-41]. These differences can be attributed to the following. First, the outcomes of this type of experiment depend on the interaction of many complex variables that are not uniform such as hardware (systems, coils), protocols, and subject variability. Second, the studies presented in the literature (including the one presented in this thesis) have quantified the

stimulation responses based on measuring the electrical signal generated by muscles. Although, this technique may not give a precise estimate of a single nerve fiber excitation, it is the only viable approach in *in vivo* studies. Third, the mechanism for magnetic stimulation is not yet fully understood, and “the neurophysiology is still largely unknown” [92].

### **Conclusion #6**

The measuring apparatuses designed for this study proved to be effective as the collected data is comparable to that published in the literature [37,40,73,85]. While the attempts by other researchers to measure the electric field are not to be minimized, it may be said that the novel approach introduced in the proposed apparatus provides additional advantages. The main advantage is the reduction in the size of the measuring device (surface mounted inductor) which subsequently results in higher resolution and minimum distortion to the field pattern. As well, the proposed measuring apparatuses can be used as the basis for the development of an automated system to determine the coil's most effective position and orientation within a three dimensional volume.

## 7.2 Future Investigations

### 1) Designing coils for animal studies

Studies in animals indicate that rTMS can produce behavioral and biological effects which are qualitatively similar to those seen after electroconvulsive shock (70-72). Nevertheless, there are several issues that have to be addressed in order to achieve meaningful results. For instance, standard coils are currently used to stimulate the brain of a rat which consequently stimulate the targeted area (left frontal region) as well as the entire body. Considering the importance of animal models in elucidating the potential mechanisms and optimizing stimulus parameters for rTMS, it is critical to design suitable coils for these types of studies. Recently, Post and Keck (157) have developed and tested a 5.7 cm circular coil for their studies and concluded that it can provide the expected focal stimulation of a rat brain. However, even this relatively small coil is still too large for this type of investigations.

In a continuation to this research, a coil prototype will be designed and constructed to be used on animals. As the effectiveness of magnetic stimulation depends on the brain/coil size ratio, the target size of this coil will not exceed 2cm diameter. However, designing such a coil poses many challenges such as large stimulating currents and high accumulated thermal energy (due to coil compact size).

### 2) Head and Coil Positioning System (Frameless stereotactic system)

Despite the critical implication of coil positioning, it has not been thoroughly investigated. For rTMS, the current practice is to place the coil on the head 5 cm anterior to

the site on the motor cortex for activation of the abductor pollicis brevis muscle, irrespective of the size and shape of the subject's head. This technique potentially results in a coil placement over widely different brain regions across subjects with different head sizes.

The few studies analyzing the effect of coil placement have shown that coil position (including tilting and orientation [41]) plays a major role in neurophysiology responses [93,94]. Also, these studies confirmed that maintaining coil position, especially in extended clinical trials, is essential to achieve consistence results. Accordingly, a more precise mechanism (stereotactic system) is needed even for CMAP studies. However, the current clinical stereotactic frameless systems are prohibitively expensive, costing from \$50,000 to over \$100,000. Also, these systems are over-designed for the relatively simple task of monitoring the position of the cranium and the coil during rTMS.

As part of future investigations, a project has been proposed to design and build an inexpensive frameless stereotactic system. The system will allow the operator to place the coil on the target and accurately maintain its position. Furthermore, the system will store the target information for each patient as well as the parameters for each treatment session.

### 3) Improving coil thermal performance

One of the problems related to rTMS is heat accumulation within the coil. This heat buildup, which is proportional to stimulation intensity and rate of repetition, results in using the coil for limited length of time. Thus, more than one coil is required during each treatment session which subsequently results in a coil shifting position from the targeted area.

To overcome heat buildup within the coil, manufactures adapted various solutions



including the circulation of water for cooling or filling the enclosure with gel to absorb generated heat. These solutions, however, add complexity and excessive weight to the coil assembly, therefore, a more practical solution is needed. Such a solution can be implemented by fabricating the enclosure with a special insulating material with high thermal conductivity.

#### 4) Investigating the effect of pulse configuration by applying cranial stimulation

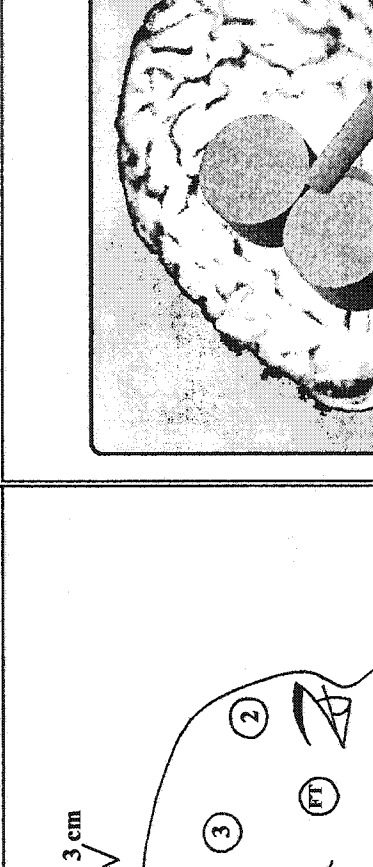
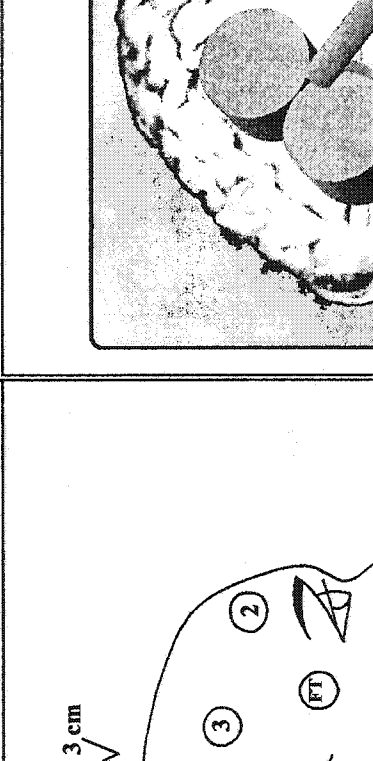
In this thesis a study was conducted to investigate the effect of pulse configuration when stimulating lower motor neurons. Proceeding with the same objectives, a new study examining the effect of pulse configuration on upper motor neurons should be conducted with special consideration given to coil orientation. The outcomes of both studies can then be analyzed and compared.

## Appendix A

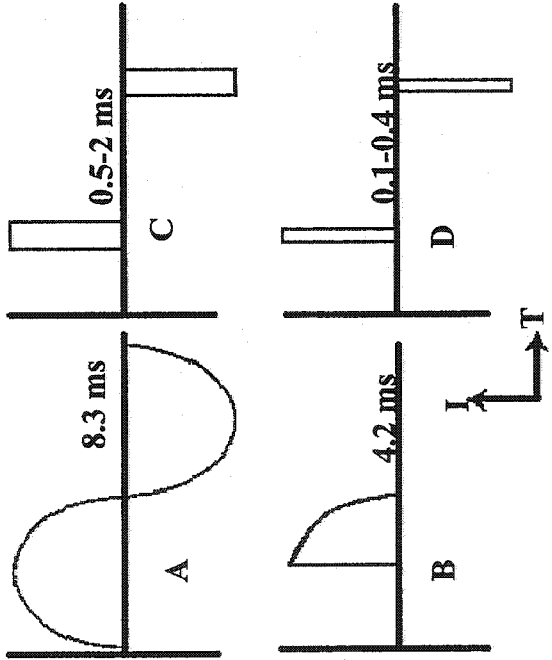
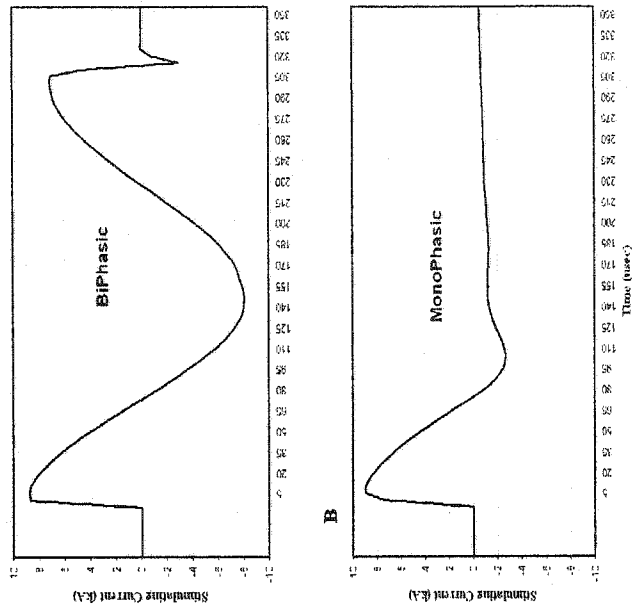
The data and information in this appendix focus on comparing ECT to rTMS in treating depression. As some of this data overlaps, it was decided not to list the references, which include [5,31,84,95-99], within the table.

	ECT	rTMS
<b>Background</b>		
<b>General Aspects</b>	<ul style="list-style-type: none"> <li>● a non-pharmacological treatment that is based on the deliberate induction of seizures under anaesthesia</li> </ul>	<ul style="list-style-type: none"> <li>● a non-pharmacological treatment that does not require anaesthesia nor induces seizures</li> </ul>
<b>History</b>	<ul style="list-style-type: none"> <li>● a well established therapy started in 1938; since then, it was used to treat mania, catatonia, Parkinson's disease, as well as schizophrenia and it is still considered a "gold standard" in treating depression</li> </ul>	<ul style="list-style-type: none"> <li>● a new investigative therapy started in the early 1990s, which requires regulatory agency approval in Canada and USA, to treat major depression and other neuropsychiatric disorders</li> </ul>
<b>Clinical Aspects</b>	<ul style="list-style-type: none"> <li>● convulsive treatment with short lived therapeutic effects</li> <li>● applied to inpatients and conditionally to outpatients</li> <li>● treatment dosage is 2-3 treatments per week for a total of 3-4 weeks</li> <li>● maintenance includes pharmacological treatment and/or ECT sessions</li> <li>● side effects include headaches, nausea, and memory/ cognitive loss or impairment</li> </ul>	<ul style="list-style-type: none"> <li>● non-convulsive treatment with therapeutic effects that may be shorted lived</li> <li>● primarily applied in outpatient settings</li> <li>● treatment dosage is 5 treatments per week for a total of 1-4 weeks★</li> <li>● maintenance includes pharmacological treatment and/or rTMS sessions★</li> <li>● see Appendix B for side effects</li> </ul>
<b>Electrodes and coil positions</b>	<ul style="list-style-type: none"> <li>● both bilateral and unilateral electrode positioning are used; bilateral ECT is probably more effective but causes greater memory impairment</li> </ul>	<ul style="list-style-type: none"> <li>● the coil is primarily positioned above the left dorsal lateral pre-frontal cortex (DLPFC), however, recent studies suggest coil positioning on the right DLPFC</li> </ul>

\* Note: the parameters for these points are not fully defined and still under investigation

Electrodes and coil positions	ECT	rTMS
 <p data-bbox="373 961 743 1669"><b>Figure A.1 (taken from [95])</b> An illustration of various placement of unilateral electrodes with the reference electrode being at the vertex. FT=frontotemporal, 1=d'Elia; 2=Muller; 3=Lancaster; 4=Zinkin and Birtchnell; 5=McAndrew et al; 6=Impastato and Karlner; 7=Halliday et al.</p>	 <p data-bbox="373 961 1291 1669"><b>Figure A.2 (taken from [97])</b> The common practice is to place the coil on the head 5 cm anterior to the site on the motor cortex for activation of the abductor pollicis brevis muscle.</p>	

Physiological Aspects	ECT	rTMS
<p><b>Stimulating mechanisms</b></p>	<ul style="list-style-type: none"> <li>● ECT is based on injecting current via electrodes using a constant current source</li> <li>● due to the skull high resistivity, only a fraction of the current passes to the tissues with the neural response depending primarily on the stimulating current</li> <li>● peak current density induced in the brain is substantially greater with ECT</li> <li>● stimulus intensity is based on seizure induction which is a clear and relevant end-point to guide stimulation</li> </ul>	<ul style="list-style-type: none"> <li>● rTMS is based on inducing current via a magnetic coil using a transient magnetic field</li> <li>● the cranial structure contributes no attenuation to the magnetic field while the induced currents in neural tissues depend on coil shape, orientation and position as well as current rate of change</li> <li>● peak current density in the brain is substantially lower with rTMS</li> <li>● stimulus intensity is based on motor evoked potential (MEP) threshold which doesn't present a precise measure of the stimulating effect and involves more uncertainty at different coil locations</li> </ul>
<p><b>Stimulation depth, focality, and efficacy</b></p>	<ul style="list-style-type: none"> <li>● relatively deeper stimulation due to the high current density throughout the brain as a result of shunting tissue impedances</li> <li>● relatively less focused</li> <li>● the most potent antidepressant treatment available and is superior when compared to rTMS</li> </ul>	<ul style="list-style-type: none"> <li>● depth of penetration is relatively low and limited to the cortex and the grey-white junction as the magnetic field decreases exponentially with respect to the distance from the coil</li> <li>● more focal resulting in greater spatial specificity of stimulation</li> <li>● although the optimum parameters of rTMS are not well established, preliminary studies indicate promising results</li> </ul>

Technical Aspects	ECT	rTMS
Pulse shape 		<p data-bbox="1112 541 1136 661">Figure A.4</p> <p data-bbox="1161 317 1226 919">Different waveforms used in rTMS; A=BiPhasic, B=MonoPhasic (after [99]).</p>

Technical Aspects	ECT	rTMS
<b>Pulse configuration</b>	<ul style="list-style-type: none"> <li>● square pulses are commonly used as they may initiate a seizure with lower energy compared to that required by sine waves</li> </ul>	<ul style="list-style-type: none"> <li>● bi-phasic waveforms are dominantly used due to their high efficacy when compared to mono-phasic</li> </ul>
<b>Pulse parameters</b>	<ul style="list-style-type: none"> <li>● although an effective pulse width of 0.1-0.2ms may initiate excitation, the current practice is to use a range of 0.5-2.0ms (see Figure A.3)</li> <li>● the frequency for most ECT systems range between 40-90 Hz with 90 Hz as a preset value for some devices</li> <li>● pulse current amplitude ranges between 0.55-0.8 A with 0.8A as a preset value for some devices</li> <li>● pulse train duration ranges between 0.5-8sec</li> </ul>	<ul style="list-style-type: none"> <li>● the pulse width varies from system to system and ranges between 0.2-1ms with the effective energy of the bi-phasic pulse being longer in duration than that of the mono-phasic (see Figure A.4)</li> <li>● the frequency ranges between 1-30Hz with low frequency (1Hz) applied to right DLPPFC, and high frequency (20 Hz) applied to left DLPPFC</li> <li>● pulse current rate of change (<math>di/dt</math>) ranges between 30-150 A/<math>\mu</math>s</li> <li>● pulse train duration ranges between 0.2-10sec</li> </ul>

## Appendix B

### rTMS: Risks and Safety Guidelines

Despite its potential benefits, rTMS may produce undesirable and serious side effects with the most critical listed below.

#### 1. Seizure induction

Although rTMS is a non-convulsive therapy, it should be noted that it has the potential to introduce epileptic seizures [100]. This side effect requires significant attention even though the systems currently available appear to be capable of producing seizures only when safety guidelines are exceeded. In contrast to single-pulse TMS, where seizures have not been reported in healthy individuals, at least eight seizures have been reported during rTMS [101]. Based on these events and some additional studies, guidelines have been established to ensure safe practice when applying TMS or rTMS. For single pulse TMS, the guidelines are given in the International Federation of Clinical Neurophysiology publication [102]. The guidelines for rTMS have been developed by the International Society of Transcranial Magnetic Stimulation (ISTS) [101,103]. These guidelines include stimulation intensity, train duration-frequency, and the interval between stimulation trains (see tables at the end of this appendix).

To minimize or eliminate the possibility of seizures, subjects with a history of

seizures should not be treated, drugs that lower the seizure threshold should be discontinued and stimulus-dose guidelines should be considered [101-103].

## 2. Cognitive side effects

Recent studies suggest that rTMS may have long-wearing deleterious effects on cognition (at least 1-2 hours following stimulation) [according to 101]. Although, there are many critical parameters which influence this side effect, they are either unknown or not fully understood. For instance, the stimulation threshold that produces cognitive effects is not known and the causes of these side effects and their potential are not fully determined. Nonetheless, in order to prevent cognitive side effects during rTMS, it is critical to avoid (as often as possible) protocols with high stimulating intensities [101].

## 3. Health effects of long-term exposure to magnetic fields

The American National Research Council (1996) has stated that there are no proven health risks associated with long term exposure to low-intensity low-frequency magnetic fields such as those produced by 60 Hz sources [quoted in 101]. The same conclusions were extended covering people, such as MRI technicians, who are exposed to high-intensity low-frequency magnetic fields. With respect to TMS safety, these affirmations are somewhat reassuring considering that magnetic stimulators produce field peaks comparable to the static fields of MRI machines.

Histological studies in animals<sup>1</sup> [104] and specimens of two humans<sup>2</sup> [105] following

---

<sup>1</sup> Using Cadwell MES-10 stimulator and a 5cm circular coil, the stimulation was delivered at: 100% intensity, 1,000 stimuli per week for a period of 4-12 months.

<sup>2</sup> Using Cadwell stimulator and an 11cm circular coil, the stimulation was delivered at: 60% intensity for a total of ~2,000 stimuli.



TMS exposure have failed to show any pathological changes. Additionally, Nahas et al. [106] presented images from MRI scans obtained from patients before and after rTMS sessions which showed no changes. In summary, the conclusions of the animal studies suggest that even with prolonged exposure to high intensities of magnetic stimulation, there is very little likelihood of structural brain damage [101]. Nonetheless, the long-term adverse effects of rTMS, especially on staff regularly administering it, are extremely important and can not be fully defined until large and systematic studies are undertaken.

#### 4. Frequency effects

The frequencies associated with rTMS can be clustered into two sections: stimulating frequency which can be adjusted by the operator, and the stimulator ringing frequency which is fixed and defined by the system hardware.

With regard to the stimulating frequency, studies showed that high frequency rTMS (5-20 Hz) temporarily increases the excitability of the motor cortex [107,108], whereas low-frequency rTMS (1 Hz or less) appears to temporarily decrease corticospinal excitability [109]. The conclusion of these studies is that frequency plays a critical role in rTMS outcomes with its most distinct impact evident in two complementary effects: “kindling” (as a result of high frequency) and “quenching” (as a result of low frequency) [110]. Though the kindling phenomenon has not been described in humans, animal studies suggest that high frequency magnetic pulses could induce a seizure [101]. Fortunately, the frequency required to induce kindling is approximately 60Hz which is higher than the operating frequency (typically 10-20 Hz) currently used during rTMS [101].

With respect to the ringing frequency, which varies between 2 and 10 kHz depending

on the system hardware [86], the resultant effects other than tissue stimulation are primarily related to tissue heating. As will be discussed in chapter two, a multi-cellular tissue can be modeled as a combination of resistors and capacitors in parallel. These circuit elements yield an overall tissue impedance with a resistive to reactance ratio of:

$$\frac{R}{X_c} = \frac{2\pi f \epsilon_0 \epsilon_r}{\sigma} \quad (\text{B.1})$$

where  $\epsilon_0$  is the dielectric constant for a vacuum,  $8.85 \times 10^{-12}$  F/m,  $\epsilon_r$  is the tissue relative dielectric constant, and  $\sigma$  is the tissue conductance S/m. At a frequency of 10 kHz, the relative dielectric constant of many tissues is in the order of  $10^4$  while the average conductivity is 0.5 S/m [81]. Accordingly, the ratio of resistive to capacitive parts of the tissue impedance is approximately 0.01. This implies that the tissue can be considered purely resistive with resulting ohmic heating due to the induced currents within the tissue. However, these currents are extremely low [31] and their heating effect can be considered of no significant hazard [111].

##### 5. Cardiac effects

To evaluate the effects of rTMS on cardiac activities, many studies were conducted with the most important conducted by Foerster et al. [112]. By monitoring blood pressure, pulse, and electrocardiograms while delivering rTMS, this group reported clear physiological responses with no significant cardiovascular side effects. The results of the other studies agree with that of [112] as they found no significant cardiovascular effects during rTMS [101,113].

## 6. Headaches

Depending on the stimulation intensity, frequency, and duration, subjects under rTMS treatment may experience mild headaches and local pain especially at the front of the head. This pain could be the result of muscle tension which may be triggered by stimulating peripheral facial and scalp nerves.

## 7. Hearing damage

The loud clicking noise generated by the magnetic stimulator may cause an increase in the auditory threshold or even hearing damage. Using foam ear plugs, for both the subject and the operator, are essential to prevent any hearing damage [113,114].

## 8. Burns

Due to the magnetic transient field, eddy currents are induced in the metal surface EEG electrodes located near the stimulating coil [115]. These currents may cause heat build up which could theoretically result in minor burns. However, studies in our TMS laboratory showed very low heat accumulation within the electrodes even at high stimulation intensity. Nonetheless, reduction of eddy currents (and thermal accumulation) can be achieved either by notching the electrodes or using conductive plastic electrodes.

### Current rTMS Safety Guidelines

Tables B1, B2 show the safety guidelines for TMS and rTMS as documented by [101] and [116] respectively. It is readily apparent that the parameters included in these tables may be traded off against each other in order to form a large number of combinations that are likely to be safe. However, depending on the individual, it should be noted that none of these combinations can be considered risk free.

**Table - B1** (taken from [101])

Maximum safe duration for single trains of rTMS based on the National Institute of Neurological Disorders and Stroke Experience

Freq. (Hz)	Intensity (% of MEP threshold) -rTMS												
	100	110	120	130	140	150	160	170	180	190	200	210	220
1	<1800	<1800	360	<50	<50	<50	<50	27	11	11	8	7	6
5	<10	<10	<10	<10	7.6	5.2	3.6	2.6	2.4	1.6	1.4	1.6	1.2
10	<5	<5	4.2	2.9	1.3	0.8	0.9	0.8	0.5	0.6	0.4	0.3	0.3
20	2.05	1.6	1.0	0.55	0.35	0.25	0.25	0.15	0.2	0.25	0.2	0.1	0.1
25	1.28	0.84	0.4	0.24	0.2	0.24	0.2	0.12	0.08	0.12	0.12	0.08	0.08

Note: Numbers preceded by < are the largest train of pulses tested [101].

**Table - B2** (Adapted from [116])  
 Current rTMS safety guidelines: safe intertrain intervals

Frequency (Hz)	rTMS intensity	
	≤110% motor threshold	> 110% motor threshold
≤20 Hz	5sec. (Perhaps less; definitely >1s)	60sec. (Probably less)
> 20 Hz	60sec. (Probably less)	60sec. (Probably less)

## Appendix C

### Mono-phasic and Bi-phasic Pulses in Magnetic Stimulation

#### C.1 The effect of L, R, C on current pulse configuration

The current pulse in a magnetic stimulator is governed by three elements: coil inductance ( $L$ ), circuit equivalent resistance ( $R$ ), and circuit discharging capacitance ( $C$ ). For an  $LRC$  circuit with the three elements in series, the inductance and the capacitance determine the pulse current magnitude (peak) and duration while the inductance combined with the resistance sets the pulse damping rate. Depending on the values of  $L$ ,  $R$ , and  $C$ , three types of pulse currents can be generated: over damped, under damped, and critically damped [117]. These pulse configurations can be defined as:

$$\text{if } \alpha > \omega_0 \quad i(t) = A_1 e^{s_1 t} + A_2 e^{s_2 t} \quad \text{over damped} \quad (\text{C.1})$$

$$\text{if } \alpha = \omega_0 \quad i(t) = (A_1 + A_2 t) e^{s_1 t} \quad \text{critically damped} \quad (\text{C.2})$$

$$\text{if } \alpha < \omega_0 \quad i(t) = (A_1 \cos \omega_r t + A_2 \sin \omega_r t) e^{-\alpha t} \quad \text{under damped} \quad (\text{C.3})$$

where  $i(t)$  is the coil current,  $A_1$  and  $A_2$  are constants that can be determined from the initial conditions,  $\alpha$  is a damping factor,  $s_1$  and  $s_2$  are two quadratic roots,  $\omega_0$  and  $\omega_r$  are the resonant and ringing frequencies respectively. The above variables can be defined as:

$$s_1, s_2 = -\alpha \pm \sqrt{\alpha^2 - \omega_0^2} \quad \text{over damped} \quad (\text{C.4})$$

$$s_1 = s_2 = -\alpha \quad \text{critically damped} \quad (\text{C.5})$$

$$s_1, s_2 = -\alpha \pm j\omega_r \quad \text{under damped} \quad (\text{C.6})$$

$$\text{where } \alpha = \frac{R}{2L}, \quad \omega_0 = \sqrt{\frac{1}{LC}}, \quad \omega_r = \sqrt{\omega_0^2 - \alpha^2} \quad (\text{C.7})$$

## C.2 The current pulses during magnetic stimulation

When applying magnetic stimulation, the three pulses described above result in two primary waveforms: bi-phasic and mono-phasic. To illustrate the process of generating these waveforms a circuit model of a typical magnetic stimulator is illustrated in Figure C.1.

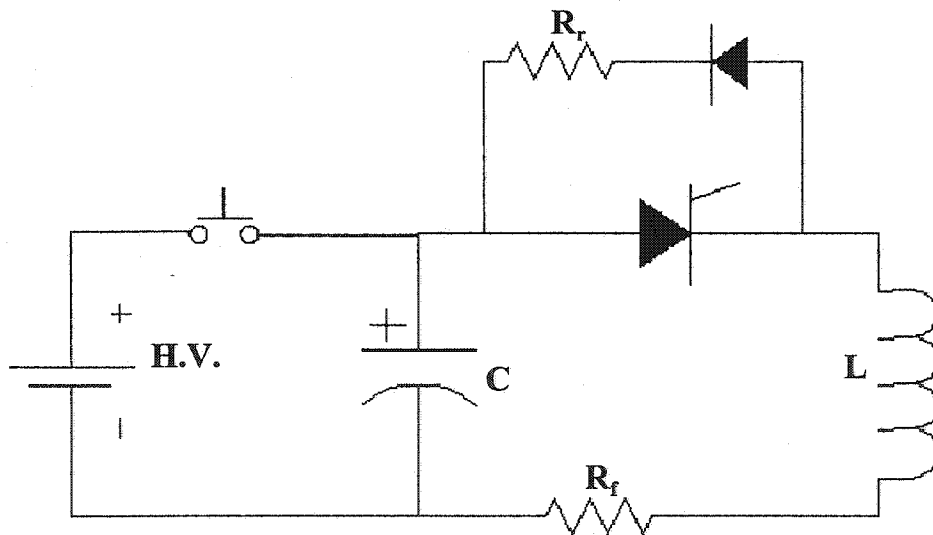
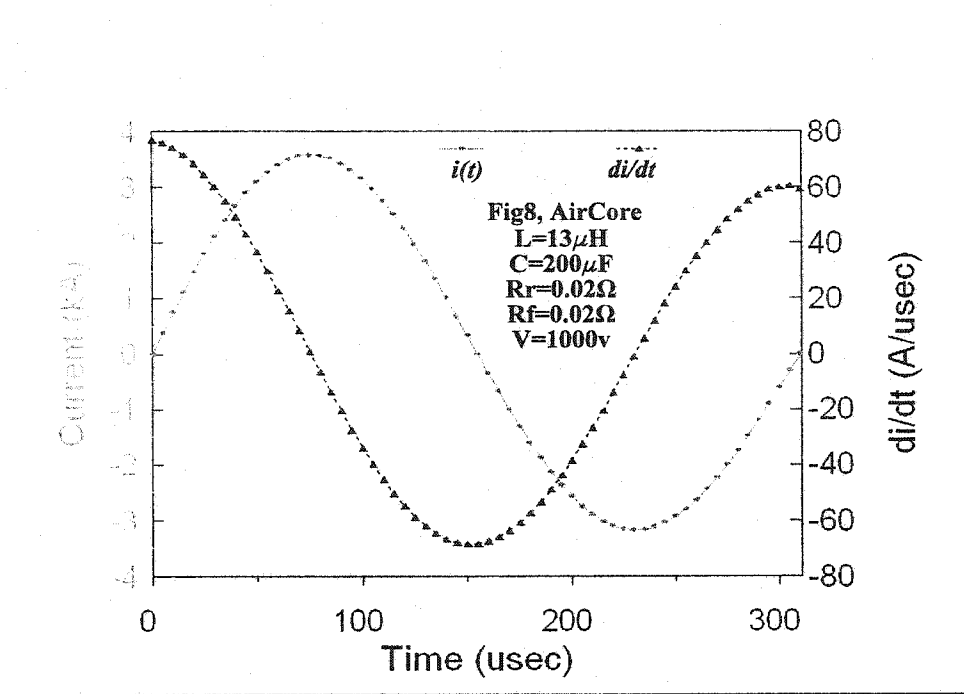


**Figure C.1**  
A circuit model of a typical magnetic stimulator.

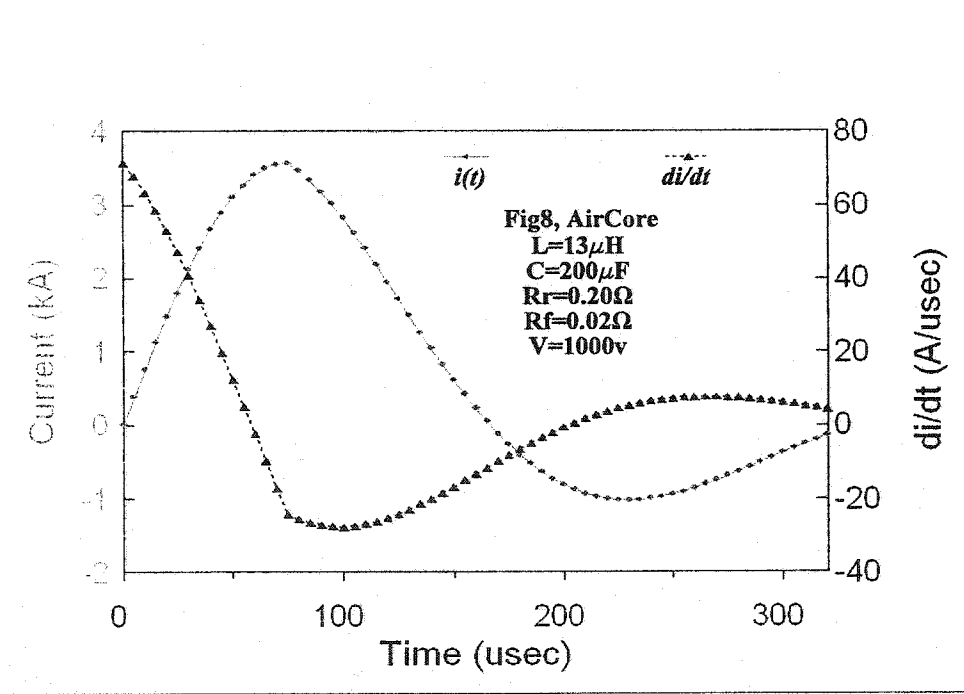
From Figure C.1,  $R_f$  represents the pathway resistance of the current which flows from the capacitor to the coil while  $R_r$  is the pathway resistance of the current that flows from the coil to the capacitor. For a bi-phasic waveform the current damping ratio is defined by the coil inductance and  $R_f$  ( $R_r$  is treated as a short circuit). For a mono-phasic, the damping ratio of the current pulse first half is defined by the coil inductance and  $R_f$  while the current damping ratio of the second half is defined by the coil inductance and the summation of  $R_r$  and  $R_f$ . It should be noted that these waveforms as well as the described components are based on measurements conducted using a Dantec stimulator (MagPro).

Based on the circuit components included in Figure C.1, two **Matlab** algorithms were written to generate the pulses required for **Magnet** (see chapter 3). Figure C.2 shows the current pulses (bi-phasic, mono-phasic) generated to supply Figure-8 and air core coils while Figure C.3 shows the current pulses generated to supply the magnetic core coil. Both figures also include the current rate of change for each waveform respectively. It can be noticed that the circuit capacitance and its initial charging voltage have been modified in Figure C.3 from that used in Figure C.2. This modification compensates for the increased inductance of the magnetic core coil (compared to that of Figure-8 and air core coils) and ensures an equivalent energy per pulse.



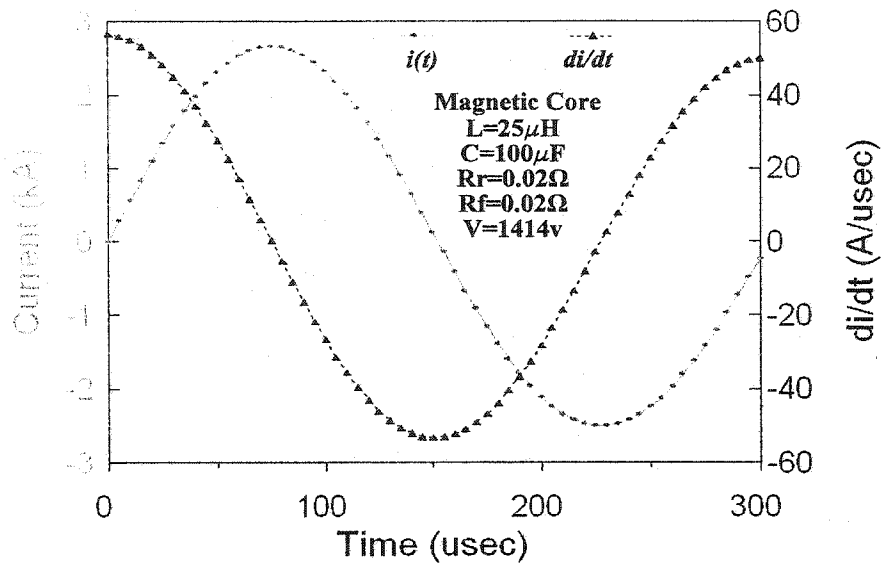


A bi-phasic current pulse and current rate of change.

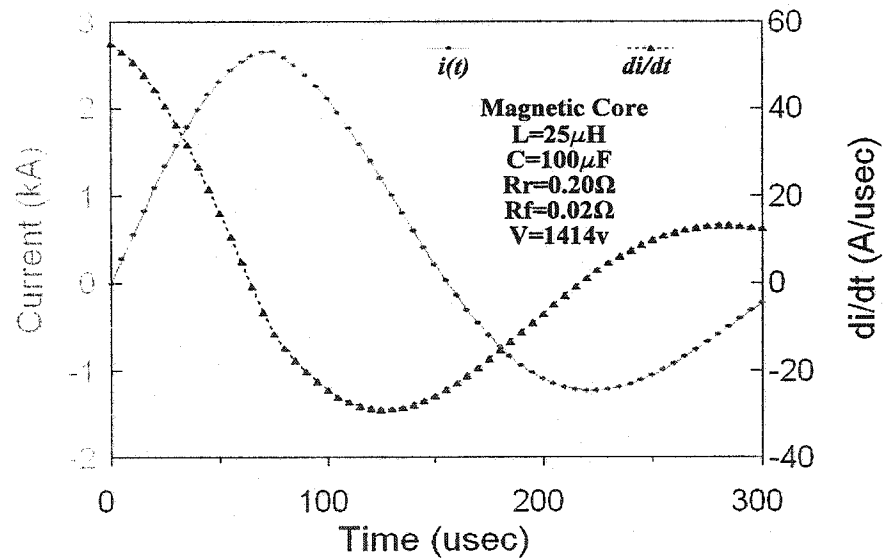


A mono-phasic current pulse and current rate of change.

**Figure C.2**  
Waveforms generated for Figure-8 and air core coils.



A bi-phasic current pulse and current rate of change.



A mono-phasic current pulse and current rate of change.

Figure C.3  
Waveforms generated for a magnetic core coil.

# Appendix D

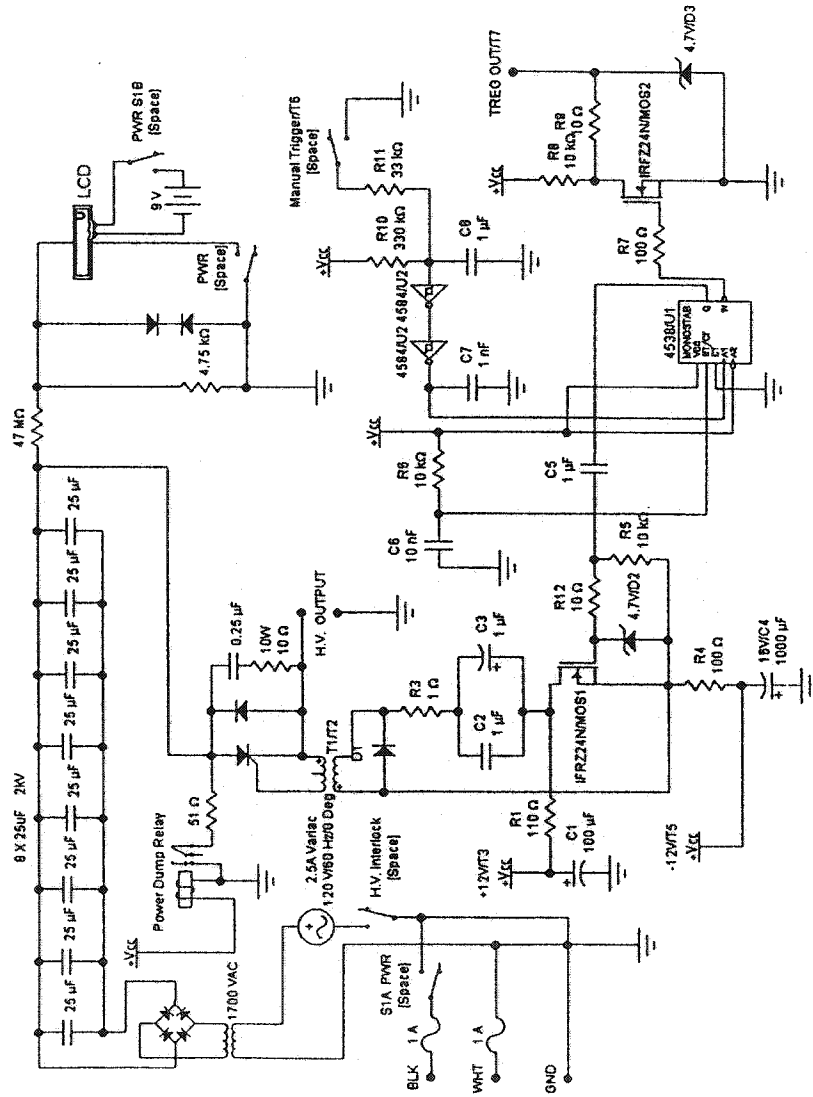
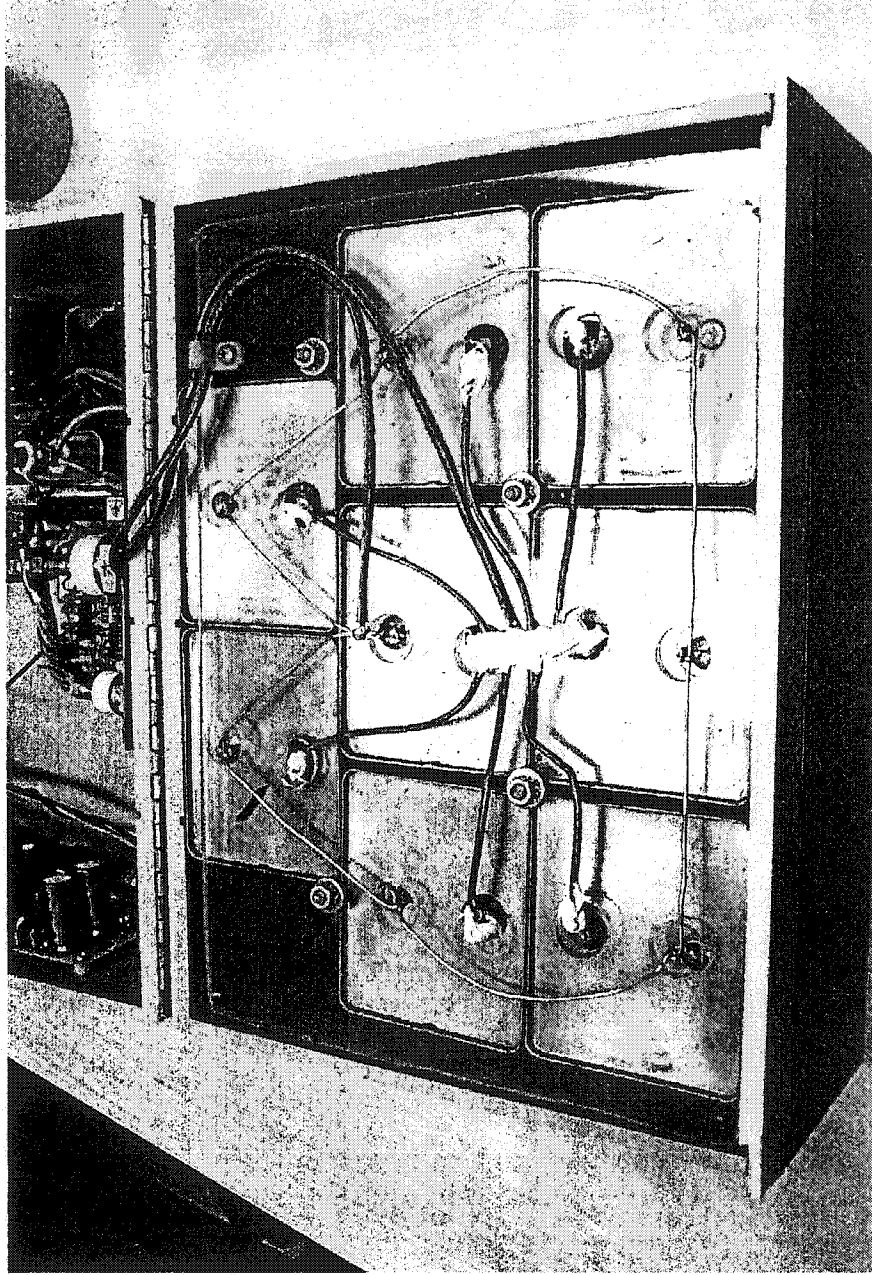
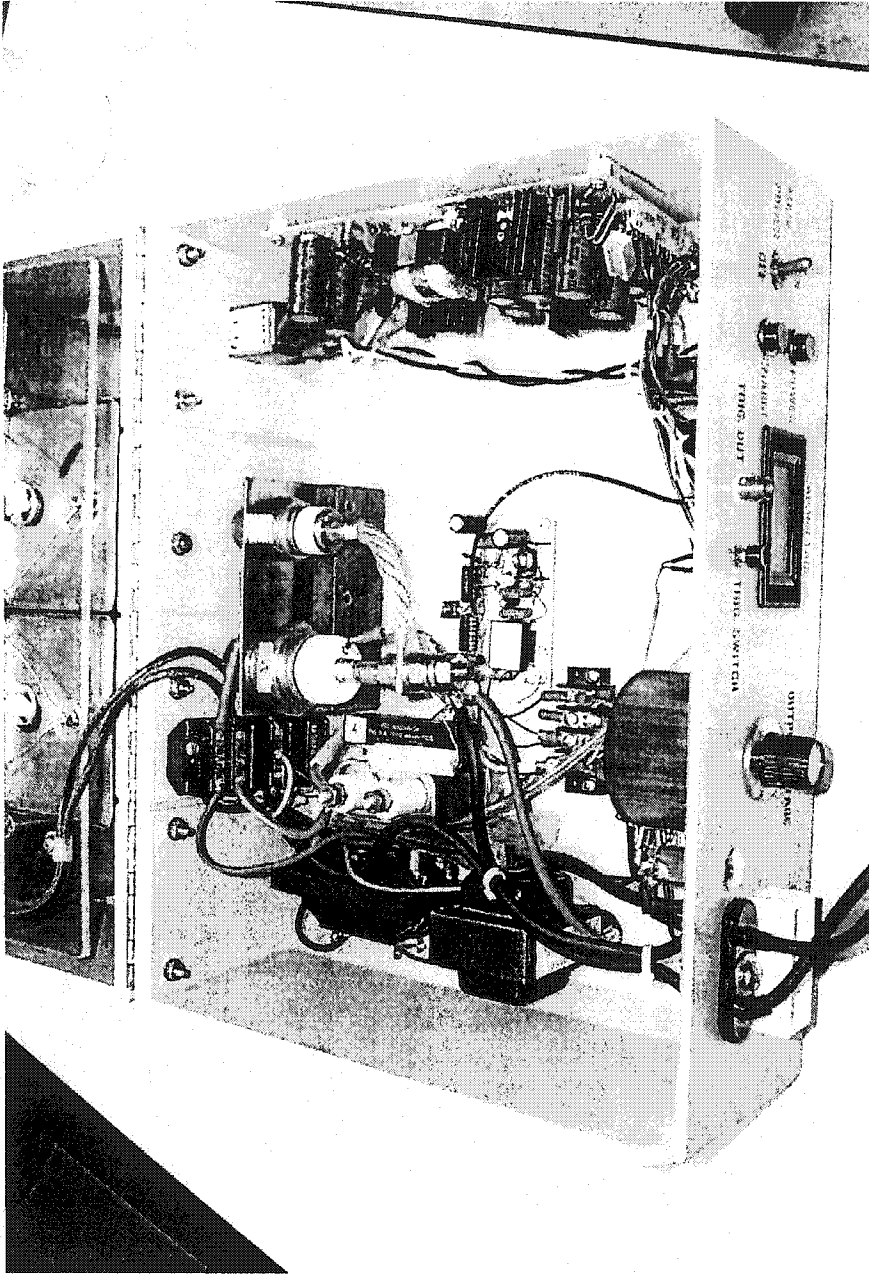


Figure D.1  
A schematic diagram of the simple magnetic stimulator.



**Figure D.2**  
The high voltage capacitor bank.



**Figure D.3**  
The hardware circuitry of the simple magnetic stimulator.

## REFERENCES

- [1] Rattay F, *Electrical Nerve Stimulation: Theory, Experiments and Applications*, Springer-Verlag Wien, 1990.
- [2] Endler NS, Persad E, *Electroconvulsive Therapy, The Myths and the Realities*, Hans Huber Publishers, 1988.
- [3] Barker AT, "The history and basic principles of magnetic nerve stimulation", *Electroencephalography and Clinical Neurophysiology Supplement*, vol. 51, pp. 3-21, 1999.
- [4] Barker AT, Jalinous R, Freeston IL, "Non-invasive magnetic stimulation of the human motor cortex", *Lancet*, pp.1106-7, 1985.
- [5] Hasey G, "Transcranial magnetic stimulation in the treatment of mood disorder: a review and comparison with electroconvulsive therapy", *Canadian Journal of Psychiatry*, vol. 46, pp. 720-7, 2001.
- [6] Triggs WJ, Menkes D, Onorato J, et al., "Transcranial magnetic stimulation identifies upper motor neuron involvement in motor neuron disease", *Neurology*, vol.53(3), pp. 605-11, 1999.
- [7] Miscio G, Pisano F, Mora G, Mazzini L, "Motor neuron disease: usefulness of transcranial magnetic stimulation in improving the diagnosis", *Clinical Neurophysiology*, vol. 110(5), pp. 975-81, 1999.
- [8] Cicinelli P, Traversa R, Bassi A, et al., "Interhemispheric differences of hand muscle representation in human motor cortex", *Muscle and Nerve*, vol. 20(5), pp.535-42, 1997.
- [9] Lin VW, Wolfe V, Frost FS, Perkash I, "Micturition by functional magnetic stimulation", *Journal of Spinal Cord Medicine*, vol. 20(2), pp. 218-26, 1997.
- [10] Lin VW, Nino-Murcia M, Frost F, et al., "Functional magnetic stimulation of the colon in persons with spinal cord injury", *Archives of physical medicine and rehabilitation*, vol. 82(2), pp.167-73, 2001.

- [11] Yamanishi T, Yasuda K, Suda S, et al., "Effect of functional continuous magnetic stimulation for urinary incontinence", *Journal of Urology*, vol.163(2), pp. 456-9, 2000.
- [12] Fujishiro T, Enomoto H, Ugawa Y, et al., "Magnetic stimulation of the sacral roots for the treatment of stress incontinence: an investigational study and placebo controlled trial", *Journal of Urology*, vol. 164(4), pp.1277-9, 2000.
- [13] Polkey M.I, Luo Y, Guleria R, et al., "Functional magnetic stimulation of the abdominal muscles in humans", *American Journal of Respiratory and Critical Care Medicine*, vol. 160(2), pp. 513-22, 1999.
- [14] Singh H, Magruder M, Bushnik T, Lin VW, "Expiratory muscle activation by functional magnetic stimulation of thoracic and lumbar spinal nerves", *Critical Care Medicine*, vol. 27(10), pp. 2201-5, 1999.
- [15] Jalinous R, *Guide to Magnetic Stimulation*, Jali Medical, Inc.1996.
- [16] Baldwin JC, Jolley DJ, "The prognosis of depression in old age", *British Journal of Psychiatry*, vol. 149, pp. 574-83, 1986.
- [17] Koenig HG, Goli V, Shelp F, et al., "Major depression in hospitalized medically ill older patients: documentation, management, and prognosis", *International Journal of Geriatric Psychiatry*, vol. 7, pp. 25-34, 1992a.
- [18] Calabrese JR, Shelton MD, Bowden CL, et al., "Bipolar rapid cycling: focus on depression as its hallmark", *Journal of Clinical Psychiatry*, vol. 62, Suppl 14, pp. 34-41, 2001.
- [19] Ciaparelli A, Dell'Osso L, Tundo A, et al., "Electroconvulsive therapy in medication-non-responsive patients with mixed mania and bipolar depression", *Journal of Clinical Psychiatry*, vol. 62, pp. 552-5, 2001.
- [20] Pascual-Leone A, Rubio B, Pallardo F, Catala MD, "Rapid-rate transcranial magnetic stimulation of left dorsolateral prefrontal cortex in drug resistant depression", *Lancet*, vol. 348, pp. 233-7, 1996.
- [21] George MS, Wassermann E, Kimbrell T, et al., "Mood improvement following daily left prefrontal repetitive transcranial magnetic stimulation in patients with depression: a placebo-controlled crossover trial", *American Journal of Psychiatry*, vol. 154, pp.1752-6, 1997.

- [22] Hoflich G, Kasper S, Hufnagel A, et al., "Application of transcranial magnetic stimulation in treatment of drug-resistant major depression: A report of two cases", *Human Psychopharmacology*, vol. 8, pp. 361-5, 1993.
- [23] Zyss T, "Will electroconvulsive therapy induce seizures: magnetic brain stimulation as hypothesis of a new psychiatric therapy", *Psychiatria Polska*, vol. 26, pp. 531-41, 1992.
- [24] Fleischmann A, Prolov K, Abarbanel J, Belmaker RH, "The effect of transcranial magnetic stimulation of rat brain on behavioural models of depression", *Brain Research*, vol. 699, pp.130-2, 1995.
- [25] Zyss T, Gorka Z, Kowalska M, Vetulani J, "Preliminary comparison of behavioral and biochemical effects of chronic transcranial magnetic stimulation and electroconvulsive shock in rats", *Biological Psychiatry*, vol. 42, pp. 920-4, 1997.
- [26] Lisanby SH, Belmaker RH, "Animal models of the mechanism of action of repetitive transcranial magnetic stimulation (RTMS): comparisons with electroconvulsive shock (ECS)", *Depression and Anxiety*, vol. 12, pp. 178-87, 2000.
- [27] Grunhaus L, Dannon P, Schreiber S, "Repetitive transcranial magnetic stimulation is as effective as electroconvulsive therapy in the treatment of non-delusional major depressive disorder: an open study", *Biological Psychiatry*, vol. 47, pp. 314-24, 2000.
- [28] Pridmore S, "Substitution of rapid transcranial magnetic stimulation treatments for electroconvulsive therapy in a course of electroconvulsive therapy", *Depression and Anxiety*, vol.12, pp. 118-23, 2000.
- [29] Puri BK, "The use of transcranial magnetic stimulation in major psychiatric disorders", *Handbook of Transcranial Magnetic Stimulation*, edited by Pascual-Leone A, Davey NJ, Rothwell J, et al., pp. 396-9, Arnold publication, 2002.
- [30] Post RM, Speer AM, "Speculations on the future of rTMS and related therapeutic modalities", *Transcranial Magnetic Stimulation in Neuropsychiatry*, edited by George M, Belmaker R, pp. 269-87, American Psychiatric Press, Inc., 2000.
- [31] Lisanby SH, Sackeim HA, "Transcranial magnetic stimulation and electroconvulsive therapy: similarities and differences", *Handbook of Transcranial Magnetic Stimulation*, edited by Pascual-Leone A, Davey NJ, Rothwell J, et al., pp. 376-95, Arnold publication, 2002.
- [32] Epstein CM, Schwartzberg DG, Davey KR, Sudderth DB, "Localizing the site of magnetic brain stimulation in humans", *Neurology*, vol. 40, pp. 666-70, 1990.



- [33] Marg E, Rudiak D, "Phosphenes produced by magnetic stimulation over the occipital brain: description and probable site of stimulation", *Optomum of Vision Science*, vol. 71, pp. 301-11, 1994.
- [34] Davidson RJ, "Anterior electrophysiological asymmetries, emotion, and depression: conceptual and methodological conundrums", *Psychophysiology*, vol. 35, pp. 607-14, 1998.
- [35] Speer AM, Kimbrell TA, Wassermann EM, "Opposite effects of high and low frequency rTMS on regional brain activity in depressed patients", *Biological Psychiatry*, vol. 48, pp. 1133-41, 2000.
- [36] McRobbie D, Foster MA, "Thresholds for biological effects of time-varying magnetic fields," *Clinical Physics and Physiological Measurements*, vol. 5(2), pp. 67-78, 1984.
- [37] Maccabee PJ, Amassian VE, Eberle LP, et al., "Magnetic coil stimulation of straight and bent amphibian and mammalian peripheral nerve in vitro: locus of excitation," *Journal of Physiology*, vol. 460, pp 201-19, 1993.
- [38] Maccabee PJ, Nagarajan SS, Amassian VE, et al., "Influence of pulse sequence, polarity and amplitude on magnetic stimulation of human and porcine peripheral nerve", *Journal of Physiology*, vol. 513(2), pp.571-85, 1998.
- [39] Nilsson J, Panizza M, Roth BJ, et al., "Determining the sight of stimulation during magnetic stimulation of a peripheral nerve", *Electroencephalography and Clinical Neurophysiology*, vol. 85, pp. 253-64, 1992.
- [40] Kammer T, Beck S, Thielscher A, et al., "Motor thresholds in humans: a transcranial magnetic stimulation study comparing different pulse waveforms, current directions and stimulators types", *Clinical Neurophysiology*, vol. 112, pp.250\258, 2001, Elsevier Scientific Publishers.
- [41] Mills KR, Boniface SJ, Schubert M, "Magnetic brain stimulation with a double coil: the importance of coil orientation", *Electroencephalography and Clinical Neurophysiology*, vol. 85, pp.17-21, 1992.
- [42] Begley CE, Annegers JF, Swann AC, et al., "The Lifetime Cost of Bipolar Disorder in the US: An Estimate for New Cases in 1998", *PharmacoEconomics*, vol.19 (5), pp. 483-95, 2001.
- [43] Woods SW, "The economic burden of bipolar disease", *Journal of Clinical Psychiatry*, vol. 61, Suppl 13, pp. 38-41, 2000.

- [44] Druss BG, Rosenheck RA, Sledge WH, "Health and disability costs of depressive illness in a major US corporation", *American Journal of Psychiatry*, vol. 157, pp. 1274-8, 2000.
- [45] Weiss TF, "*Cellular Biophysics Electrical Properties*", MIT press, 1996.
- [46] Guyton AC, Hall JE, "*Textbook of Medical Physiology*", W.B. Saunders Co., 1996.
- [47] Kandel ER, Schwartz JH, Jessell TM, "*Principles of neural science*", 4<sup>th</sup> edition, McGraw-Hill, New York, 2000.
- [48] Szlavik RB, "*In Vivo Electrical Stimulation of Motor Nerves*", A PhD Thesis, McMaster University - Hamilton, 1999.
- [49] McNeal DR, "Analysis of a model for excitation of myelinated nerve", *IEEE Transactions on Biomedical Engineering*, vol. 23, pp. 329-37, July 1976.
- [50] Gorman PH, Mortimer JT, "The effect of stimulus parameters on the recruitment characteristics of direct nerve stimulation", *IEEE Transactions on Biomedical Engineering*, vol. 30, pp. 407-14, July 1983.
- [51] Grill WM, Mortimer JT, "Stimulus waveforms for selective neural stimulation", *IEEE Engineering in Medicine and Biology*, vol. 14, pp. 375-85, August 1995.
- [52] Ganong WF, *Review of Medical Physiology*, Appleton and Lange, 1997.
- [53] Katz B., *Nerve, Muscle, and Synapse*, McGraw-Hill, 1966.
- [54] Roth, BJ, Basser PJ, "A Model of the Stimulation of a Nerve Fiber by Electromagnetic Induction", *IEEE Transactions on Biomedical Engineering*, vol. 37, pp. 588-97, June 1990.
- [55] Basser PJ, Roth BJ, "Stimulation of a myelinated nerve axon by electromagnetic induction", *Medical and Biomedical Engineering and Computing*, vol. 29, pp. 261-8, May 1991.
- [56] Nagarajan SS, Durand DM, Warman EN, "Effects of induced electric fields on finite neuronal structures: a stimulation study", *IEEE Transactions on Biomedical Engineering*, vol. 40 (11), pp. 1175-87, November 1993.
- [57] Reilly JP, "Peripheral nerve stimulation by induced electric currents: exposure to time-varying magnetic fields", *Medical and Biological Engineering and Computing*, vol. 27, pp. 101-10, March 1989.

- [58] Kraus JD, Carver KR, *Electromagnetics*, McGraw-Hill, New York, 1973.
- [59] Chari MVK, Silvester PP, *Finite Elements in Electrical and Magnetic Field Problems*, John Wiley and Sons, 1980.
- [60] Roth BJ, Cohen LG, Hallett M, "The electric field induced during magnetic stimulation", *Magnetic Motor Stimulation: Basic Principles and Clinical Experience, (EEG Suppl. 43)*, edited by: Levy WJ, Cracco RO, Barker AT, Rothwell J, pp. 268-78, Elsevier Science Publishers, 1991.
- [61] Mouchawar GA, Nyenhuis JA, Bourland JD, Geddes LA, "Influence of coil geometry on localization of the induced electric field in magnetic (eddy-current) stimulation of excitable tissue", *IEEE Transactions on Magnetics*, vol. 26(5), pp. 1545-7, September 1990.
- [62] Nyenhuis JA, Mouchawar GA, Bourland JD, Geddes LA, "Energy considerations in the magnetic (eddy-current) stimulation of tissues", *IEEE Transactions on Magnetics*, vol. 27(1), pp. 680-7, January 1991.
- [63] Roth BJ, Saypol JM, Hallett M, et al., "A theoretical calculation of the electric field induced in the cortex during magnetic stimulation", *Electroencephalography and Clinical Neurophysiology*, vol. 81, pp. 47-56, 1992.
- [64] Ueno S, Tashiro T, Harda K, "Localized stimulation of neural tissues in the brain by means of a paired configuration of time-varying magnetic fields", *Journal of Applied Physics*, vol. 64 (10), pp. 5862-4, November 1988.
- [65] Mouchawar GA, Nyenhuis JA, Bourland JD, et al., "Guidelines for Energy-Efficient Coils: Coils Designed for Magnetic Stimulation of the Heart" *Magnetic Motor Stimulation: Basic Principles and Clinical Experience, (EEG Suppl. 43)*, edited by: Levy WJ, Cracco RO, Barker AT, Rothwell J, pp. 255-67, Elsevier Science Publishers, 1991.
- [66] Hosono A, Andoh T, Goto T, et al., "Effective Combination of Stimulating Coils for Magnetic Heart Stimulation", *Japan, Applied Physics*, vol. 31 (I-11), pp. 3759-62, November 1992.
- [67] Roth BJ, Turner R, Cohen LG, Hallett M, "New coil design for magnetic stimulation with improved focality", *Movement Disability*, vol. 5 (Suppl.1:32), 1990.
- [68] Roth BJ, Maccabee PJ, Eberle LP, et al., "In vitro evaluation of a 4-leaf coil design for magnetic stimulation of peripheral nerve", *Electroencephalography and Clinical Neurophysiology*, vol.93, pp. 68-74, 1994.

- [69] Ren C, Tarjan P, Popovic DD, "A Novel Electric Design for Electromagnetic Stimulation - The Slinky Coil", *IEEE Transactions on Biomedical Engineering*, vol. 42 (9), pp. 918-25, September 1995.
- [70] Knaulein R, Weyh TH, "Minimization of Energy Stored in the Magnetic Field of Air Coils for Medical Application", *Technische Universitat, Munchen Germany*, pp.477-83,1996.
- [71] Davey K, Epstien CM, "Magnetic Stimulation Coil and Circuit Design", *IEEE Transactions on Biomedical Engineering*, vol. 47 (11), pp. 1493-99, November 2000.
- [72] Carburaru R, Durand DM, "Toroidal Coil Models for Transcutaneous Magnetic Stimulation of Nerves", *IEEE Transactions on Biomedical Engineering*, vol. 48 (4), pp.434-41, April 2001.
- [73] Lin VW, Hsiao IN, Dhaka V, "Magnetic Coil Design Considerations for Functional Magnetic Stimulations", *IEEE Transactions on Biomedical Engineering*, vol. 47 (5), pp.600-10, May 2000.
- [74] Hsiao IN, Lin VW, "Improved Coil Design for Functional Magnetic Stimulation of Expiratory Muscles", *IEEE Transactions on Biomedical Engineering*, vol. 48 (6), pp.684-94, June 2001.
- [75] Hsu K, Durand DM, "A 3-D Differential Coil Design for Localized Magnetic Stimulation", *IEEE Transactions on Biomedical Engineering*, vol. 48 (10), pp.1162-68, October 2001.
- [76] Al-Mutawaly N, "A Novel Coil Design for Magnetic Nerve Stimulation", Master's Degree Thesis, McMaster University - Hamilton, September 1998.
- [77] Cohen LG, Roth BJ, Nilsson J, et al., "Effect of coil design on delivery of focal magnetic stimulation. Technical considerations", *Electroencephalography and Clinical Neurophysiology*, vol. 75, pp. 350-7, 1990.
- [78] Tofts PS, "The distribution of induced currents in magnetic stimulation of the nervous system", *Physiology and Medical Biology*, vol. 35 (8), pp. 1119-28, 1990.
- [79] Infolytica Corporation, "Magnet 5.1a User manual", © Copyright Infolytica Corporation, Part Number 5T0302, Revised November 4, 1994.
- [80] Zienkiwwicz OC, "The Finite Element Method", McGraw-Hill Company, 1977.

- [81] Foster KR, Schwan HP, "Dielectric properties of tissues and biological materials: a critical review", *CRC Critical Review in Biomedical Engineering*, vol.17(1), pp. 25-104, 1989.
- [82] Geddes LA, "Optimal Stimulus Duration for Extracranial Cortical Stimulation", *Neurosurgery*, vol. 20 (1), pp. 94-9,1987.
- [83] Weissman JD, Epstein CM, Davey KR, "Magnetic brain stimulation and brain size: relevance to animal studies", *Electroencephalography and Clinical Neurophysiology*, vol. 85, pp. 215-9, 1992.
- [84] Dantec Inc., "*DANTEC Magnetic Stimulator MagPro*", Service Manual and Technical Data, Denmark, 1993.
- [85] Niehaus L, Meyer B-U, Weyh T, "Influence of pulse configuration and direction of coil current on excitatory effects of magnetic motor cortex and nerve stimulation," *Clinical Neurophysiology*, vol. 111, pp.75-80, 2000.
- [86] Al-Mutawaly N, de Bruin H, "Designing and constructing a magnetic stimulator: theoretical and practical considerations", *Proc 23rd Ann Int Conf IEEE EMBS*, Oct 2001, Istanbul, CD-ROM ISBN: 0-7803-7213-1.
- [87] Barker AT, Garnham CW, Freeston IL, "Magnetic nerve stimulation: the effect of waveform on efficiency, determination of neural membrane time constants and the measurement of stimulator output", *Magnetic Motor Stimulation: Basic Principles and Clinical Experience, (EEG Suppl. 43)*, edited by: Levy WJ, Cracco RO, Barker AT, Rothwell J, pp. 227-37, Elsevier Science Publishers, 1991.
- [88] Basmajian JV, *Muscles Alive*, Baltimore: Williams & Wilkins Company, 1978.
- [89] Mathis J, Seemann U, Weyh T, Jakob C, Struppler A, "The boundary effect in Magnetic stimulation: analysis at the peripheral nerve", *Electroencephalography and Clinical Neurophysiology*, vol. 97, pp. 238-45, 1995.
- [90] Norman GR, Streiner DL, *Biostatistics The Bare Essentials*, B.C. Decker Inc., 2000.
- [91] Hodgkin AL, Huxley AF, "The dual effect of membrane potential on sodium conductance in the giant axon of *Loligo*", *Journal of Physiology*, vol. 116, pp. 497-506, 1952.
- [92] Corthout E, Barker AT, Cowey A, "Transcranial magnetic stimulation which part of the current waveform causes the stimulation?", *Experimental Brain Research*, vol. 141, :pp.128-132, 2001.

- [93] Gugino LD, Romero JR, Aglio L, et al., Transcranial magnetic stimulation coregistered with MRI: a comparison of a guided versus a blind stimulation technique and its effect on evoked compound muscle action potentials, *Journal of Clinical Neurophysiology*, vol. 112, pp.1781-92, 2001.
- [94] Herwig U, Padberg F, Unger J, et al., Transcranial magnetic stimulation in therapy studies: examination of the reliability of "standard" coil positioning by neuronavigation, *Biological Psychiatry*, vol. 50, pp. 58-61, 2001.
- [95] Mecta Corporation, "*Instructional manual of SR and JR models*", 1985.
- [96] Kiloh LG, Smith JS, Johnson GF, "*Physical treatments in psychiatry*", Chapter 3, Blackwell Scientific Publication, 1988.
- [97] Hasey G, "Transcranial magnetic stimulation in the treatment of mood disorder", *Lecture Notes*, 2001.
- [98] Bohning DE, "Introduction and overview of TMS physics", *Transcranial Magnetic Stimulation in Neuropsychiatry*, edited by George M, Belmaker R, pp. 13-44, American Psychiatric Press, Inc., 2000.
- [99] Al-Mutawaly N, de Bruin H: "Measuring the induced electrical fields in 3-dimensions when applying magnetic stimulation to a spherical target.", *Proc 24th Annual Meeting of Bioelectromagnetic Society*, June 2002, Montreal, Canada.
- [100] Wassermann EM, "Safety and side-effects of transcranial magnetic stimulation and repetitive transcranial magnetic stimulation", *Handbook of Transcranial Magnetic Stimulation*, edited by Pascual-Leone A, Davey, NJ, Rothwell J, et al., pp.39-49, Arnold publication, 2002.
- [101] Lorberbaum JP, Wassermann, E.M, "Safety concerns of rTMS", *Transcranial Magnetic Stimulation in Neuropsychiatry*, edited by George M, Belmaker R, pp. 141-61, American Psychiatric Press, Inc., 2000.
- [102] Rossini PM, Barker AT, Berardelli A, et al., "Non-invasive electrical and magnetic stimulation of the brain, spinal cord and roots: basic principles and procedures for routine clinical application", *Electroencephalography and Clinical Neurophysiology*, vol. 91, pp. 79-92, 1994
- [103] Wassermann EM, "Risk and safety of repetitive transcranial magnetic stimulation: report and suggested guidelines from the International Workshop on the Safety of Repetitive Transcranial Magnetic Stimulation", June 5-7, 1996. *Electroencephalography and Clinical Neurophysiology*, vol. 108, pp.1-16, 1998.

- [104] Counter SA, "Neurobiological effects of extensive transcranial electromagnetic stimulation in an animal model", *Electroencephalography and Clinical Neurophysiology*, vol. 89, pp. 341-8, 1993.
- [105] Gates JR, Dhuna A, Pascual-Leone A, "Lack of Pathologic changes in human temporal lobes after transcranial magnetic stimulation", *Epilepsia*, vol. 33, pp. 504-8, 1992.
- [106] Nahas Z, Speer AM, Lorberbaum JP, et al., "Safety of rTMS: MRI scans before and after 2 weeks of daily left prefrontal rTMS for depression", *Biological Psychiatry*, 43(95s):#316, 1998.
- [107] Berardelli A, Inghilleri M, Rothwell JC, et al., "Facilitation of muscles evoked responses after cortical stimulation in man", *Exp Brain Research*, vol. 122, pp. 79-84, 1998.
- [108] Pascual-Leone A, Valls-Sole J, Brasil\_Neto JP, et al., "Akinesia in Parkinson's disease, I: shortening of simple reaction time with focal, single-pulse transcranial magnetic stimulation", *Neurology*, vol. 44, pp. 884-91, 1994.
- [109] Chen R, Classen J, Gerloff C, et al., "Depression of motor cortex excitability by low-frequency transcranial magnetic stimulation", *Neurology*, vol. 48, pp. 1398-403, 1997.
- [110] Weiss S, Li X, Heynen T, et al., "Kindling and quenching: conceptual links to rTMS", *CNS Spectrums*, vol. 2, pp. 32-35, 1997.
- [111] Barker AT, Freeston IL, Jalinous R, et al., "Magnetic stimulation of the human brain and peripheral nervous system: an introduction and the results of an initial clinical evaluation", *Neurosurgery*, vol. 20 (1), pp. 100-9, 1987.
- [112] Foerster A, Schmitz JM, Nouri S, et al., "Safety of rapid-rate transcranial magnetic stimulation: heart rate and blood pressure changes", *Electroencephalography and Clinical Neurophysiology*, vol. 104, pp. 207-12, 1997.
- [113] Pascual-Leone A, Houser CM, Reese K, et al., "Safety of rapid-rate transcranial magnetic stimulation in normal volunteers", *Electroencephalography and Clinical Neurophysiology*, vol. 89, pp. 120-30, 1993.
- [114] Pascual-Leone A, Cohen, LG, Shotland LI, et al., "No evidence of hearing loss in humans due to transcranial magnetic stimulation", *Neurology*, vol. 42, pp. 647-51, 1992.

- [115] Roth BJ, Pascual-Leone A, Cohen LG, et al., "The heating of metal electrodes during rapid-rate magnetic stimulation: a possible safety hazard" *Electroencephalography and Clinical Neurophysiology*, vol. 85, pp.116-123, 1992.
- [116] Chen R, Gerloff C, Classen J, et al., "Safety of different inter-train intervals for repetitive transcranial magnetic stimulation and recommendations for safe ranges of stimulation parameters", *Electroencephalography and Clinical Neurophysiology*, vol. 105, pp. 415-21, 1997.
- [117] Rashid MH, *Power Electronics Circuits, Devices, and Applications*, 2<sup>nd</sup> Edition, Prentice Hall, Englewood Cliffs, New Jersey 07632, 1998.



## List of Publications

- [1] Al-Mutawaly N, de Bruin H, "A coil design for magnetic nerve stimulation: three dimensional Analysis", *Proceedings of the 25<sup>th</sup> Conference of the Canadian Medical and Biological Engineering Society*, June 1999, London, Ontario, Canada.
- [2] Al-Mutawaly N, de Bruin H, Findlay R, "Magnetic nerve stimulation: field focality and depth of penetration", *Proceedings of the 23<sup>rd</sup> Annual international Conference of the IEEE Engineering in Medicine and Biology Society*, October 2001, Istanbul, Turkey.
- [3] Al-Mutawaly N, de Bruin H, "Designing and constructing a magnetic stimulator: theoretical and practical considerations", *Proceedings of the 23<sup>rd</sup> Annual international Conference of the IEEE Engineering in Medicine and Biology Society*, October 2001, Istanbul, Turkey.
- [4] Al-Mutawaly N, de Bruin H, Findlay R, "Magnetic nerve stimulation: a comparison between mono-phasic and bi-phasic waveforms", *Proc 24<sup>th</sup> Annual Meeting of Bioelectromagnetic Society*, June 2002, Montreal, Canada.
- [5] Al-Mutawaly N, de Bruin H: "Measuring the induced electrical fields in 3-dimensions when applying magnetic stimulation to a spherical target", *Proc 24<sup>th</sup> Annual Meeting of Bioelectromagnetic Society*, June 2002, Montreal, Canada.
- [6] Al-Mutawaly N, de Bruin H, "Design and construction of an electrical nerve stimulator", *Proceedings of the 27<sup>th</sup> Conference of the Canadian Medical and Biological Engineering*

*Society*, November 2002, Ottawa, Ontario, Canada.

- [7] Al-Mutawaly N, de Bruin H, Hasey, G, “The effect of pulse configuration on the compound muscle action potentials (CMAPs) during magnetic stimulation”, *Proceedings of the 27<sup>th</sup> Conference of the Canadian Medical and Biological Engineering Society*, November 2002, Ottawa, Ontario, Canada.